Doctoral Dissertation (Shinshu University)

Studies of silk protein nanofibers from different origins of silkworms and their physical properties

September 2012

Zhang Xianhua

CONTENTS

Chapter 1 General introduction

1.0 Introduction 1
1.1 Electrospinning technology 2
1.2. Silk sericin 8
1.3. Tussah silk fibroin 11
1.4. The purpose, method and significance of our research 13
1.5 Organization of this dissertation 14
References 14

Chapter 2: The surface morphologies of electrospun silk sericin nanofibers and analyzed the characteristics

2.0. Introduction 21
2.1. Experiment 23
2.1.1. Materials 23
2.1.2. Sample solution 23
2.1.3. Electrospinning setup and process 24
2.1.4. Characterizations of SS nanofibers 24
2.2. Results and discussion 25
2.2.1. Electrospinning of SS nanofibers from SS-water solution 25
2.2.2. Electrospinning of SS nanofibers from SS TFA solution 27
2.3. Conclusions 35
References 36

Chapter 3: Fabrication of silk sericin nanofibers from a silk sericin-hope cocoon with electrospinning method

3.0. Introduction 38
3.1. Experimental 41
3.1.1. Materials 41
3.1.2. Preparation of SC solution 41
3.1.3. Electrospinning 41
3.1.4. Characterization 42
3.2. Results and discussion 42
3.2.1. Electrospinning processing parameters 42

3.2.2. Structural features of electrospun SC nanofibers 53
3.2.3. Thermal behavior of electrospun SC nanofibers 54
3.3. Conclusions 57
References 57
Chapter 4: Fabrication and physical properties of electrospun tussah silk fibroin nanofibers
4.0. Introduction 60
4.1. Experiments 62
4.1.1. Materials 62
4.1.2. Preparation of the TSF solution 62
4.1.3. Electrospinning 63
4.1.4. Characterization 63
4.2. Results and discussion 64
4.2.1. Morphologies and standard deviation of TSF nanofibers 64
4.2.2. Effect of the dissolution time 69
4.2.3. Thermal behavior of electrospun TSF nanofibers 71
4.2.4. FTIR spectra of the electrospun TSF nanofibers 73
4.3. Conclusions 76
References 76

Chapter 5: Preparation and characterization of ultrafine composite SC/TSF fibers
5.0. Introduction 79
5.1. Experiment 80
5.1.1. Solution preparation 80
5.1.2. Electrospinning setup and process 80
5.1.3. Characterization 81
5.2. Results and discussion 82
5.2.1. Morphologies of SC/TSF composite nanofibers 82
5.2.2. Distribution of SC/TSF composite nanofibers 83
5.2.3. Effect on dissolution time 84
5.2.4. Structural features of SC/T composite nanofibers 87
5.2.5. Thermal behavior 88
5.3. Conclusions 91
References 91

Chapter 6: Conclusions 93

List of publications 96

Acknowledgments 97

Chapter 1

General introduction

Chapter 1: General introduction

1.0. Introduction

The term 'silk' refers to a wide range of filaments spun by several species of Lepidoptera and Arthropoda to build structures external to the body such as cocoons and webs. However, only silk threads spun by the larvae of domestic silkworms from Bombyx mori and wild silkworms from various Antheraea species such as pernyi, yamamai, mylitta, assamensis, etc. are of practical importance as a textile fiber source. Sericulture, the practice of breeding silkworms for the production of raw silk, has been underway for at least 5000 years in China [1]. Silkworms were first domesticated during the Han Dynasty in china 2000 years ago.

Among natural and synthetic fibers, silk occupies a leading position for its outstanding properties, such as water absorption, heat retention, handling, luster, comfort, brilliant color shades obtained by dyeing and printing, etc. However, the textile performances of silk also include a few weak points [2] i.e. crease recovery, rub resistance, color fastness, wash and wear properties, photoyellowing, which seriously limit its general use. Furthermore, the increasing attractiveness of clothing articles having superior easy care and wear properties, as well as the need to expand silk consumption by developing new textile products have given a strong emphasis on the study of new finishing techniques.

Silk protein polymers that are produced by silkworms are classified into two general groups: domestic type (Bombyx mori) and wild type (Antheraea pernyi etc.) silkworms. Silk cocoon filaments from the Bombyx mori silkworm consists of fibrous protein, fibroin and a sticky protein, sericin, which envelops fibroin threads to glue them together [2-3]. The cocoon is made of a thread of raw silk from 300 to 900 meters long. The fibers are very fine and lustrous, about 10 micrometers in diameter [4]. The B. mori silk fibroin (SF) has been widely studied as a source of biomaterials to be used in biotechnological and biomedical fields because it has good blood compatibility, oxygen permeability, and so on [5]. Silk Sericin (SS) is a family of

adhesive silk proteins that are synthesized exclusively in the middle silk gland of silkworm, and contributes about 20-30% of total cocoon weight [6]. SS is anti-bacterial, biocompatible, UV resistant, absorbs and releases moisture easily, consists high serine content and so on [7]. Sericin's physicochemical properties are not sufficiently elucidated because SS is easily degraded by heat or alkaline treatment during processing for separation from fibroin threads. Yamamoto and colleagues developed a new strain of fibroin-deficient mutant silkworm [8-9]. The Sericin-hope silkworm secrets sericin almost exclusively.

Among the wild silks, the silk produced by Antheraea pernyi, tussah silk, is the most popular for production and use. Tussah silk is an excellent clothing material with an inherent elegant sheen, soft and smooth handing, beautiful appearance, moisture absorption, sweet exclusion, and affinity to to human skin. While SF has been studied extensively, the research on tussah silk fibroin (TSF) is only at an early stage. Study on the chemical structure, molecular conformation and physical properties of TSF showed that it has more Ala, Asp, and Arg, and less Gly than SF [10]. There are many crystalline region of domestic SF; however, there are many -(Ala)n- sequences in the crystalline region of TSF. In addition, considering the presence of Arg-Gly-Asp, commonly named RGD sequence in TSF may act as a biological recognition signal, which is helpful to promoting cell adhesion [11-12], TSF might be a better new biomaterials for tissue engineering.

Electrospinning has been explioted for almost one century to process polymers and related materials into nanofibers with controllable compositions, diameters, porosities, and porous structures for a variety of applications [13]. Electrospinning is a relatively simple and inexpensive method to produce fibers with diameter in nanometer range.

1.1. Electrospinning technology

1.1.1. Basic principle

Electrospinning provides a simple and versatile way to fabricate very fine continuous polymer fibers that form a nonwoven structure. Electrospinning,

previously known as 'electrostatic spinning', was first studied by zeleny in 1914, and was found to be a feasible technique for spinning small-diameter polymer fibers [14]. But technical impeded development until 1934, when Formhals was issued the first US patent for the process of spinning synthetic fibers and an apparatus used in this procedure [15]. Following the initial patent, the process of developing nanofibers from a wide range of polymers using the electrospinning technique has ensued [16–21]. In 1969, Taylor published his work regarding the jet forming process [22], in which he described the phenomena of Taylor cone for the first time, which develops from the pendant droplet when the electrostatic forces are balanced by surface tension. Taylor also observed the emission of a fiber jet from the apex of the cone, which explained the generation of fibers with significantly smaller diameters compared to the spinneret [23]. Shortly after the discovery of the Taylor cone, interest in the field shifted to a more thorough understanding of the relationship between electrospinning processing/solution parameters and the structural characteristics of the resulting fibers. In 1971, Baumgarten studied the effects of solution and processing parameters on the structure of electrospun fibers using a polyacrylonitrile/dimethylformamide (PAN/DMF) solution. He discovered a positive relationship between fiber diameter and solution viscosity [20]. Concurrently, other researchers began to examine the potential of electrospun fibrous matrices for other applications. In 1978, Annis and Bornat evaluated the feasibility of electrospun polyurethane mats as vascular prostheses [24]. By 1985, Fisher and Annis had assessed the long-term in vivo performance of electrospun arterial prostheses [25].

It has been almost 1 century since the discovery of the electrospinning process. However, little of the process has changed since Formhals described it in his first patent. A typical electrospinning equipment consists of three components: a high voltage supplier, a capillary needle or pipette, and a grounded collector (Fig. 1). The polymer solution is applied into a syringe which is equipped with a piston and a stainless steel capillary serving as electrode and pushed by a pump with a defined flow rate. The spinneret is connected with the high-voltage source and applies high voltage to the polymer. Surface tension and viscoelastic forces of the polymer solution

retain the hemispherical shape of the suspended droplet, while the electric force pulls the droplet away from the capillary [26]. As the applied voltage is increased beyond a critical value, where the electrostatic forces balance out the surface tension of the droplet at the tip of the capillary, the development of the Taylor cone occurs [22, 27-30]. As a result, a fiber jet ejects from the apex of the cone and accelerates towards the grounded collector.

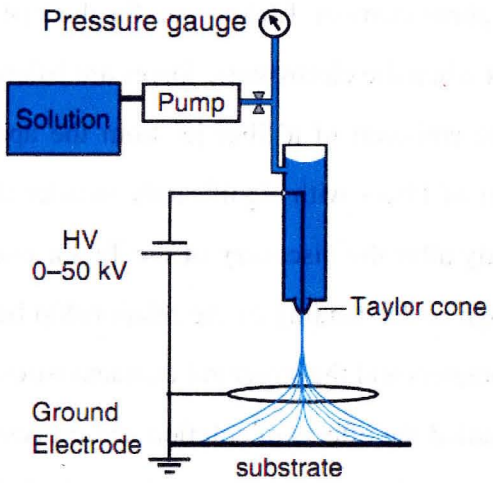

Fig. 1.1 Setup for electrospinning from polymer solutions [32].

Two different models were proposed to explain the nanofibers drawing process: single filament elongation or splitting of a fiber into several smaller fibers [32]. Many investigators supporting the single fiber theory reported that the fiber jet undergoes a chaotic whipping and bending trajectory while accelerating towards the collector due to repulsive interactions among like charges in the polymer jet [33-34]. This process aids in fiber thinning and solvent evaporation by increasing the transit time and path length to the collector. Doshi and Reneker hypothesized the occurrence of a different model involving the splitting of a fiber jet caused by the increase in charge repulsion during elongation [35]. However, recent studies have imaged the unstable zone of fiber jet with the aid of highspeed photography. These studies revealed that a whipping instability leads the single fiber to bend and turn rapidly, thereby resulting in the incorrect notion of fiber splitting [36-37].

With recent technical developments and a better understanding of the process, continuous fibers with diameters ranging from nanometers to a few micrometers have been generated by using a diversity of materials in various fibrous assemblies. Moreover, the simplicity of the setup makes the process highly attractive to both academia and industry [38]. In the basic process of electrospinning, a number of factors have been found to affect fiber formation and structure [39-40].

1.1.2. Process parameters

Factors that significantly affect the process of electrospinning have been widely investigated on a great number of polymers [41-44], and are summarized into three main categories:

1. Polymer properties such as molecular weight, structure and distribution of the polymer, and melting point and glass transition point; solution related parameters, such as concentration, viscosity, elasticity, conductivity, surface tension, and presence of other additives.

The relationship between polymer concentration and fiber diameter has been discussed in many studies [45-50]. Generally, increasing the concentration of a polymer solution results in increasing fiber diameter and decreasing in bead formation, though the applicable ranges vary depending on the solvent system, average molecular weight and molecular weight distribution of the polymers used [51-53]. Polymer concentration and molecular weight collectively determine the 'spinnability' of the solution through effects on solution viscosity and surface tension [39]. If the solution is too dilute, the fiber will break into microsize droplets before reaching the collector as a result of varicose jet instability and the phenomenon of "electrospray" will be observed instead of "electrospinning". Electrospray is also observed when a polymer solution with low molecular weight is used. However, if the solution is too concentrated, it will be difficult for the polymer solution to flow through the capillary due to high viscosity, therefore no fiber will form.

2. Process related parameters, such as hydrostatic pressure in the capillary tube, applied electrical potential, delivery volume, needle diameter, flow rate of the solution

and distance from tip to collector.

Among the electrospinning process parameters examined, the applied electric potential had an effect on electrospinning in terms of fiber jet formation, bead defects and fiber diameter [47, 54-56]. Increased electrostatic forces can overcome solution surface tension and further extract polymer chains. However, the tendency of the fiber jet to contract into droplets resulted in bead defects along the fiber extensions due to insufficient entanglement between polymer macromolecules. Generally, an increase in voltage results in an initial decrease followed by an increase in fiber diameter, while no significant effects were found when the increase of voltage was above a certain level [39]. The increased fiber diameters resulting from the increased electrostatic fields were attributed to an increase in mass throughput with an increased electric force.

The flow rate of polymer solution, determined by the gravity or use of a pump, can also affect the size and shape of electrospun fibers [33, 56-57]. The feed rate directly impacts the volume of solution suspended at the tip of the spinneret, which influences the shape of the Taylor cone. The maintenance of the cone shape at the tip of the capillary is important to obtain a continuous fiber jet [22]. Increases in fiber diameter, pore size, bead defects, and ribbon-shaped fiber formation have been demonstrated in response to increased flow rate. The optimal conditions can be achieved by controlling the shape of the Taylor cone without excess solution dripping. The distance between the capillary tip and the collector can also influence the fiber diameter and morphology, however to a lesser extent than other process factors, such as electric potential and flow rate. It has been found that a minimum distance is required for fibers to have sufficient time to dry before reaching the collector. Otherwise, 'electrospray' will occur instead of 'electrospinning'. Bead formation was observed at distances that were either too close or too far from capillary tip to collector [58-59].

3. ambient parameters such as solution temperature, humidity, atmosphere, air velocity in the electrospinning chamber.

An optimal combination of these electrospinning parameters should establish

conditions to generate fibers with narrow variations in diameter and absence of beads. The micro/nanometer scale bears helpful specialties, high aspect ratio, high-specific surface area and high porosity with very small pore size. Therefore, the micro/nanofibers can simulate the extracellular matrix (ECM) and enhance the cell migration and proliferation and be applied in biomedical domain, involving drug delivery, wound dressing, tissue engineering scaffolds and others [60-61].

1.1.3. Electrospun structures

Electrosinning can be used to produce novel fibers with the diameters in the range from 100 nm to 10um. As the solvent evaporating, the polymer molecules can come together by either a phase separation through a spinodal reaction or through classic nucleation and growth of the crystalline phase [62]. As a result, the structure in the polymer deposited on the collector can consist of a totally amorphous, an oriented, a spherulitic or a textured fibrillar structure. In electrospinning, jets are stretched along their axis by the external electrical field and are elongated further by the repulsive force between charges on adjacent segments. The results area reduction rate and the associated high longitudinal strain rate imply that the macromolecules in the fibers should be stretched and axially oriented [63]. It is generally recognized that electrospinning may lower the degree of crystallinity in the polymer [64-65]. The exact reasons for this behavior are not clear. It has been suggested that the development of structure in electrospinning occurs much more rapidly than other processes and this kinetic effect may result in low crystallinity [65]. A high degree of orientation may also be observed in the fibrils. The degree of orientation of the molecules in the amorphous regions is directly proportional to the amount of extensional flow. In summary, electrospinning is a novel technique that can be used to produced nano-scale porous structures with a variety of morphologies. The fiber size and distribution, and inter-fiber spacing (i.e. porosity) and distribution and be varied significantly by controlling the process parameters. Drugs and growth factors can be incorporated easily into the structure for biomedical applications.

1.2. Silk sericin

1.2.1. Structure and properties

Over the last few decades, research has widened interest for the use of silk beyond that of purely textile applications, it is a candidate for a range of possible uses, in particular for biomedical applications [66-67]. The raw silk produced by the B. mori silkworm, is composed of two fibers embedded into a sheath, all based on proteins. The contribution to mechanical properties of sericin has generally been considered as negligible [68]. However, Jauzein and Anthony showed the sericin sheath acts like a matrix in a composite material allowing stress sharing between the fibres and permitting properties to be improved and reducing their variability [69]. Sericin is glue protein produced specifically in the middle silk gland (MSG) of the silkworm B. mori. In presence of sericin the fibers are hard and tough and become soft and lustrous after its removal.

Sericin is a macromolecular protein. Its molecular weight ranges widely from about 10 to over 300 kDa. The sericin protein is made of 18 amino acids most of which have strongly polar side groups such as hydroxyl, carboxyl and amino groups. In addition, the amino acids serine and aspartic acid constitute approximately 33.4% and 16.7% of sericin, respectively. When sericin is dissolved in a polar solvent, hydrolyzed in acid or alkaline solutions, or degraded by a protease, the size of the resulting sericin molecules depends on factors such as temperature, pH and the processing time. Lower molecular weight sericin peptides ($\leq$20 kDa) or sericin hydrolysates are used in cosmetics including skincare and haircare products, health products, and medications. High-molecular weight sericin peptides ($\geq$20 kDa) are mostly used as medical biomaterials, degradable biomaterials, compound polymers, functional biomembranes, hydrogels, and functional fibers and fabrics [70].

Sericin can be classified into three fractions, depending on their solubility as sericin A, sericin B, and sericin C. Sericin A is the outermost layer and insoluble in hot water. Sericin B is the middle layer and on acid hydrolysis it yields amino acid of sericin A, in addition to tryptophan. Sericin C is the innermost layer, which is adjacent to fibroin and is insoluble in hot water and can be removed from fibroin by treatment

with dilute acid or alkali [71]. The γ-ray study shows the three layers in the sericin structure. The outer layer contained some fiber direction filaments, middle layer exhibits cross-fiber direction filaments, and the inner layer shows longitudinal filaments [72]. Sericin contains random coil and β-sheet structure. Random coil structure is soluble in hot water and as the temperature lowers the random coil structure converts to β-sheet structure, which results in gel formation [73-74]. Sericin has sol-gel property as it easily dissolves into water at 50-60 °C and again returns to gel on cooling [75].

Sericin is soluble in hot water and it converts into gel as the time preceding. The conversion of α-random coil to β-sheet structure have been found by Jun et al. 1 wt% aqueous sericin solution generates gel at pH 6-7 at room temperature and gelation speed growing when the concentration of sericin adds.

1.2.2. sericin-hope cocoon

The molecular weight of sericin significantly decreased in the degumming process by the action of alkali solution. Actually it is impossible to get native sericin without decreasing of molecular weight by collecting the sericin from the sericin solution which obtained by the conventional technique. Many gene scientists have been paid a great attention to produce novel silk sericin cocoon by genetically modification and diversification of B. mori silkworm [76-78]. Generally, there are two kinds of sericin silkworms in the market. One is the naked pupa Nd strain, which secretes silk thread at a rate of 30 mg/head, with spinning and cocooning rates of 99%. The other sericin silkworm, the Nd-s strain, which secretes only a few silk threads, with a sericin content as low as 92%, at the cocoon stage. Unfortunately, neither of the existing strains is practical for sericin extraction. In order to effectively produce intact sericin protein, recently a new silkworm race 'Sericin Hope' has been developed by cross breeding an Nd mutant (naked pupa) and a high cocoon yielding strain KCS83 [78]. It secretes silk thread, at the rate of about 80 mg/head, while the spinning and cocooning rates have been improved to 99%. The output of the cocoon layer is over four times that of the Nd strain. Sericin can be very efficiently produced, because the

sericin purity is as high as 98.5% at the cocoon stage. The sericin hope cocoon, named 'Virgin Sericin' can be gelled in water with less hydrolyzing by autoclaving at 110 °C for 10 min. Sericin-hope facilitates mass production of native sericin with high purity.

1.2.3. Application

SS due to its proteinous nature is susceptible to the action of proteolytic enzymes present in body and hence it is digestible. This property makes it a biocompatible and biodegradable material. Because of some additional properties like, gelling ability, moisture retention capacity, and skin adhesion. It has wide applications in medical, pharmaceutical, and cosmetics.

Sericin has been found to possess wound healing property and can be used as wound healing covering material in the form of film [79]. Sericin also has adhesive property due to its chemical composition. It has affinity to keratin [80]. Silk threads obtain from mulberry silkworm can be used for making surgical sutures [81]. SS membranes are good bandage materials and the film has adequate flexibility and tensile strength. Due to its good biocompatibility and infection resistant nature, it is a novel wound coagulant material. Additionally, its flexibility and water absorption properties promote smooth cure for defects in the skin and do not cause any peeling of the skin under regeneration when detached from the skin [82]. SS as a biomaterial has been explained by Kurioka [83]. SS has the potential to find application in the development of contact lenses.

In addition to above-mentioned medical and pharmaceutical uses of sericin, it has been used as component of cosmetics. Sericin alone or in combination with SF has been used in skin, hair, and nail cosmetics. Sericin when used in the form of lotion, cream and ointment shows increased skin elasticity, antiwrinkle and antiaging effects [80, 84-86]. Nail cosmetics, containing 0.02-20 percent sericin are reported to prevent nail from chapping, brittleness, and imparting the inherent gross to nails [87]. Hair and bath preparations, containing 0.02-2 percent sericin and 0.01-1 percent olive oil, fatty acid or their salts showed reducing damage of hair surface by binding of sericin to hair [88]. Sericin hydrolysates with average molecular weight 300-3000 are used as

conditioners for skin and hair [89]. Shampoo containing sericin and pelarogenic acid of pH less than six are useful for the care and cleaning of hairs [90].

1.3. Tussah silk fibroin

While common silk is obtained from domestic silkworm, Bombyx mori, there are many types of wild silkworm producing silk fibroin with wide varieties of primary structure and chemical/physical properties. Because of the widened utilizations of SF as biomedical materials such as wound covers [91-92], enzyme immobilization membrane [93], cell culture medium [94], and soft contact lenses [95], SF from wild silkworms attracts our attention as starting material for providing improved properties over domestic SF.

1.3.1. Structure and properties

Of many wild silkworms, Antheraea pernyi is a fairly common species, being mass-produced in northeast China for silk fiber production. Its SF has been studied for chemical structure, molecular conformation and physical properties [96-98]. The chemical structure of silk proteins both from Bombyx mori and Antheraea pernyi silkworms is dominated by two simple amino acid residues [99], glycine and alanine, whose sum comprises approximately 75 mol% of the protein. In tussah silk, the relative amount of glycine is higher compared with domestic silk, resulting in marking differences in their primary structure.

In contrast to the amino acid composition of domestic SF, the alanine residue content of TSF is higher than that of domestic SF. There are many repeated -(Gly-Ala-Gly-X)n sequences [100], with X=Ser or Tyr, in the crystalline region of domestic SF [101-102]. However, there are mainly -(Ala)n- sequences in the crystalline region of TSF [103-104]. Because tussah silk contains abundant –(Ala)n– sequence in crystalline region, the dissolution of tussah silk fibers is difficult. Additionally, TSF molecule contains the tripeptide sequence Arg-Gly-Asp (RGD) and more amino acids with positive charge which could favour the cells to attach [105-106]. The amorphous regions contain most of the amino acid residues with

bulky and polar side chains and are more abundant in wild SF. The scientific information on the crystalline and amorphous regions is important because the tensile properties of the silk fibers depend mainly on the crystalline structure while physical properties such as moisture regain, dyeablility and chemical resistance depend on the state of amorphous regions.

Several researchers have reported on the molecular conformations of native Antheraea pernyi fibroin film, which is taken from the posterior silk gland of full-grown silkworm larvae. The influences of casting temperature [107], drying rate [108], solvent [109], and heat treatment [110] on the molecular conformation have also been extensively studied. Similar to the domestic silk fibroin, that of A. pernyi can be formed into films by casting the glandular silk. The molecular conformation in this film has been found to be rich in α-helix and random coil. Thermal or aqueous methanol treatment has been found to cause β-sheet formation in this material [111-117]. Since such transformation is known to be effective in improving physical strength and water resistance of the domestic silk fibroin film, similar effects are also expected for that of A. pernyi.

1.3.2. Application

Silkworm silks, including domestic silk and various wild silks, are the valuable candidate materials for biomedical applications for their distinctive biomedical properties including good biocompatibility, blood compatibility, good oxygen and water permeability, biodegradability, non-cytotoxicity and minimal inflammatory reaction [118-119]. The applications of regenerated A. pernyi SF are somewhat restricted due to the difficulties in controlling the shape. Dissolution of SF is often required when nontextile applications are demanded in forms of film, porous membrane, powder, gel, and among others. A. pernyi SF film, containing several basic amino acids and the tripeptide sequence arg-gly-asp, can be highly attractive for several biotechnological and biomedical applications not only on enzyme immobilization and matrix for mammalian cell culture but also on wound covering and artificial skin [120].

SF membrane immobilized antigens can be used as biosensors for disease detection. The antigen contained in SF membranes reacts with an antibody to form an immobilized antigen-antibody complex. This reaction can be monitored using electronic techniques and used for the development of disease-specific biosensors. The basic techniques for this application have been developed by Kanebo Co. Ltd. [121]. The amino acid composition of SF from Bombyx mori is quite different from that of TSF. TSF having a much higher amount of basic amino acids such as Lys, Hist, and Arg compared with Bombyx mori is suitable as a substrate for cell attachment and proliferation, suggesting that cell attachment and growth are acutely sensitive to the primary structure of SF molecules [122]. When phosphate groups are introduced to the silk, the fibroin fiber can adsorb Ca^{2+} ions. It can thus be applied as an artificial tendon, since it can adhere to hydroxyapatite, a major constituent of bones, and form a strong crystalline like interface. Furthermore, these modified silk fibers exhibit excellent tensile properties [123]. Ethylene glycol can be chemically grafted onto the reactive sites of SF amino acid residues, such as Lys, Arg and His. This chemical modification allows to control the degree of cell attachment and growth rate, which are based on the high mobility exhibited by long ethylene glycol chains [124-125]. SF membranes containing pharmaceuticals can be used as a substrate for drug delivery systems for releasing acetylsalicylic acid [126].

1.4. The purpose, method and significance of our research

Until recently, there is few references on production of SS nanofibers with smooth surfaces using SS solution, and there is no literature on preparation of sericin-hope cocoon (SC) nanofibers with smooth surfaces. Among the wild silks, the silk produced by Antheraea pernyi, tussah silk, is the most popular for production and use. TSF is a potential biomaterial because TSF has chemically active amino acids, basic amino acids and acidic amino acids.

We attempted to produce SS nanofibers, SC nanofibers, TSF nanofibers and SC/TSF nanofibers having smaller diameters, narrow diameter distribution, smooth surfaces and bead-free structures via electrospinning in an organic solvent. The effects

of the solution variables and electrospinning process on morphological appearance and average diameter of the as-spun fibers were examined. The structure and physical characteristics of electrospun fibers were also analyzed.

1.5. Organization of this dissertation

This dissertation is organized to provide snapshots of development of electrospun SS, SC, TSF and SC/TSF composite nanofibers.

In chapter 1, I reviewed references and provided brief summary of electrospinning technology, SS, SC and TSF.

In chapter 2, we reported the surface morphologies of electrospun SS nanofibers and analyzed the characteristics.

In chapter 3, we reported the fabrication of silk sericin nanofibers from a silk sericin-hope cocoon with elelctrospinning method.

In chapter 4, we successfully produced the fabrication of electrospun TSF nanofibers and analyzed the physical properties.

In chapter 5, we prepared the fabrication of electrospun SC/TSF composite nanofibers and analyzed the characteristics.

In chapter 6, we did a conclusion of this dissertation.

Reference

[1] E.J.W. Barber, Prehistoric Textiles: the Development of Cloth in the Neolithic and Bronze Ages with Special Reference to the Aegean, Princeton University Press, 31 (1992).

[2] R. Fedic, M. Zurovec, F. Sehnal, Journal of Insect Biotechnology and Sericology, 71(1), 1-15 (2002).

[3] H. Teramoto, M. Miyazawa, Journal of Insect Biotechnology and Sericology, 72, 157-162 (2003).

[4] http://en.wikipedia.org/wiki/Bombyx_mori.

[5] N. Minoura, M. Tsukada, M. Nagura, Polymer, 31, 265-269 (1990).

[6] M.N. Padamwar, A.P. Pawar, Journal of Scientific & Industrial Research, 63, 323-329 (2004).

[7] X. Zhang, M.M.R. Khan, T. Yamamoto, M. Tsukada, H. Morikawa, International Journal of Biological Macromolecules, 50, 337–347 (2012).

[8] T. Yamamoto, K. Mase, T. Miyajima, K. Hara, Japanese Patent No. 3374177.

[9] T. Yamamoto, T. Miyajima, K. Mase, T. Iizuka, National Institute of Agrobiological Sciences, Tsukuba, Japan, 24-25 (2002).

[10] F. Lucas, J.T. Shaw, S.G. Smith, J Mol Biol, 2, 339–349 (1960).

[11] M.D. Pierschbacher, E. Ruoslahti, Nature, 309, 30-33 (1984).

[12] Z. Zhang, Y. Raphael, W. Matthew, B.P.J. Thomas, B. Roy, T. Patrick, Biomaterials, 26, 47–61 (2005).

[13] J. Xie, X. Li, Y. Xia, Macromolecular Rapid Communications, 29, 1775-1792 (2008)

[14] J. Zeleny, J. Phy. Rev., 3, 69–91, (1914).

[15] A. Formhals, U. S. Patent 975 (1934) 504.

[16] A. Formhals, U. S. Patent 160 (1939) 962.

[17] A. Formhals, U. S. Patent 187 (1940) 306.

[18] A. Formhals, U. S. Patent 323 (1943) 025.

[19] A. Formhals, U. S. Patent 349 (1944) 950.

[20] P.K. Baumgarten, J. Colloid Interface Sci., 36, 71–79 (1971).

[21] H.L. Simons, U.S. Patent 280 (1966) 229.

[22] G.I. Taylor, Electrically driven jets, Proc. R. Soc. London 313A, 453–475 (1969).

[23] X. Zhang , R.M. Reagan , D.L. Kaplan, Advanced Drug Delivery Reviews, 61, 988–1006 (2009).

[24] D. Annis, A. Bornat, R.O. Edwards, A. Higham, B. Loveday, J. Wilson, Trans. Am. Soc. Artif. Intern. Organs, 24, 209–214 (1978).

[25] A.C. Fisher, L.D. Cossart, T.V. How, D. Annis, Life Support Syst., 1, 462–465 (1985).

[26] X. Fang, D.H. Reneker, J. Macromol. Sci., Phys. B, 36, 169–173 (1997).

[27] L. Larrondo, R. St. John Manley, J. polym.Sci.: polym. Phys. Ed, 19, 909(1981).

[28] L. Larrondo, R. St. John Manley, J. polym.Sci.: polym. Phys. Ed, 19, 921(1981).

[29] L. Larrondo, R. St. John Manley, J. polym.Sci.: polym. Phys. Ed, 19, 933(1981).

[30] G. I. Taylor, proc. R. Soc. Lond. Ser. A, 280, 383 (1964).

[31] K. Schaefer, H. Thomas, P. Dalton, M. Moeller, Vol 97, Chapter 7, Nano-fibers for Filter Materials, Multifunctional Barriers for Flexible Structure: Textile Leather and Paper (Springer Series in Materials Science).

[32] J.M. Deitzel, J. Kleinmeyer, D. Harrus, N.C. Beck Tan, Polymer, 42, 261–272 (2001).

[33] A.L. Yarin, S. Koombhongse, D.H. Reneker, J. Appl. Phys., 89, 3018–3026 (2001).

[34] D.H. Reneker, A.L. Yarin, H. Fong, S. Koombhongse, J. appl. Phys., 87, 4531–4547 (2000).

[35] J. Doshi, D.H. Reneker, J. Electrostat., 35, 151–160 (1995).

[36] S.Warner, A. Buer, M. Grimler, S. Ugbolue, G. Rutledge, M. Shin, Nano fibers, Natl. Text, Cent. Annu. Rep., 83 (1998).

[37] Y.M. Shin, M.M. Hohman, M.P. Brenner, G.C. Rutledge, Appl. Phys. Lett., 78, 1149–1151 (2001).

[38] S. Ramakrishna, K. Fujihara,W.E. Teo, T. Yong, Z. Ma, R. Ramaseshaa, Materials Today, 9, 40–50 (2006).

[39] T.J. Sill, H.A. von Recum, Biomaterials, 29, 1989–2006 (2008).

[40] Z.M. Huang, Y.Z. Zhang, M. Kotaki, S. Ramakrishna, Compos. Sci. Technol., 63, 2223–2253 (2003).

[41] I. Hayati, A.I. Bailey, T.F. Tadros, J. Colloid Interf. Sci., 117, 205–221 (1987).

[42] J.M. Dietzel, J. Kleinmeyer, D. Harris, N.C. Beck Tan, Polymer, 42, 261–272 (2001).

[43] T. Subbiah, G.S. Bhat, R.W. Tock, S. Parameswaran, S.S. Ramkumar, J. Appl. Polym. Sci., 96, 557–569 (2005).

[44] J. Kameoka, R. Orth, Y. Yang, D. Czaplewski, R. Mathers, G.W. Coates, H.G. Craighead, Nanotechnology, 14, 1124–1129 (2003).

[45] X.H. Zong, K. Kim, D.F. Fang, S.F. Ran, B.S. Hsiao, B. Chu, Polymer, 43,

4403–4412 (2002).

[46] H.S. Kim, K. Kim, H.J. Jin, I.J. Chin, Macromol. Symp., 224, 145–154 (2005).

[47] J.M. Deitzel, J. Kleinmeyer, D. Harris, N.C.B. Tan, Polymer, 42, 261–272 (2001).

[48] W.K. Son, J.H. Youk, T.S. Lee, W.H. Park, Polymer, 45, 2959–2966 (2004).

[49] C.X. Zhang, X.Y. Yuan, L.L. Wu, Y. Han, J. Sheng, Eur. Polym. J., 41, 423–432 (2005).

[50] P. Gupta, C. Elkins, T.E. Long, G.L.Wilkes, Polymer, 46, 4799–4810 (2005).

[51] T. Jarusuwannapoom, W. Hongroijanawiwat, S. Jitjaicham, L. Wannatong, M. Nithitanakul, C. Pattamaprom, P. Koombhongse, R. Rangkupan, P. Supaphol, Eur. Polym. J., 41, 409–421 (2005).

[52] A. Koski, K. Yim, S. Shivkumar, Mater. Lett., 58, 493–497 (2004).

[53] J.S. Lee, K.H. Choi, H. Do Ghim, S.S. Kim, D.H. Chun, H.Y. Kim, W.S. Lyoo, J. Appl. Polym. Sci., 93, 1638–1646 (2004).

[54] J. Magoshi, Y. Magoshi, M.A. Becker, S. Nakamura, Polymeric Materials Encyclopedia, CRC Press Inc, Boca Raton, FL, 667–679 (1996).

[55] C. Lu, P. Chen, J. Li, Y. Zhang, Polymer, 47, 915–921 (2006).

[56] J.S. Choi, S.W. Lee, L. Jeong, S.H. Bae, B.C. Min, J.H. Youk, W.H. Park, Int. J. Biol. Macromol., 34, 249–256 (2004).

[57] D.H. Reneker, I. Chun, Nanotechnology, 7, 216–223 (1996).

[58] C.S. Ki, D.H. Baek, K.D. Gang, K.H. Lee, I.C. Um, Y.H. Park, Polymer, 46, 5094–5102 (2005).

[59] J.S. Lee, K.H. Choi, H. Do Ghim, S.S. Kim, D.H. Chun, H.Y. Kim, W.S. Lyoo, J. Appl. Polym. Sci., 93, 1638–1646 (2004).

[60] M. Schindler, I. Ahmedb, J. Kamalb, A. Nur-E-Kamalb, T.H. Grafec, H.Y. Chungc, S. Meiners, Biomaterials, 26, 5624–5631 (2005).

[61] Z.M. Huang, Y.Z. Zhang, M. Kotaki, S. Ramakrishna, Combust. Sci. Technol., 63, 2223–2253 (2003).

[62] A Weghmann, Schriftenreihe des Deutschen wollforschungsinstitutes, 85, 314 (1981).

[63] K. Schmidt, Melliand Textilber, 61(6), 495 (1980).

[64] D. Luzhansky, INDA/TAPPI, Baltimore, MD, 16-18 September (2003).

[65] http://www.elmarco.cz.

[66] B. Bartow, M.D. Buffalo, J Bone Jt Surg, 2, 217 (1916).

[67] L. Meinel, S. Hofmann, V. Karageorgiou, L. Zichner, R. Langer, D.L. Kaplan, G.V. Novakovic, Biotechnol Bioeng, 88, 379 (2004).

[68] J.P. Rigueiro, C. Viney, J. Llorca, M. Elices, J Appl Polym Sci, 75, 1270 (2000).

[69] J. Vincent , B. Anthony, J Mater Sci, 47, 3082–3088 (2012).

[70] Y.Q. Zhang, Biotechnology Advances, 20(2), 91-100 (2002).

[71] M.N. Padamwar, A.P. Pawar, Journal of Scientific & Industrial Research, 63, 323-329 (2004).

[72] T. Wang, J. Wang, J. Zhou, Fangzhi Xuebao, 6(3), 133-134 (1985).

[73] L.J. Zhu, J. Yao, L. You, Zhejiang Nongye Daxue Xuebao, 24(3), 268-272 (1998).

[74] P.H. Huddar, Ph D Thesis, Summitted to University of Pune, India, 23-75 (1985).

[75] L.J. Zhu, M. Arai, K. Hirabayashi, Nippon Sanshigaku Zasshi, 65(4), 270-274 (1996).

[76] T. Yamamoto, T. Miyajima, K. Mase, T. Iizuka, BRAIN Techno News, Natl. Inst. Agrochiol. Resour. Jpn., 94, 14–17 (2002).

[77] K. Mase, E. Okada, T. Miyazima, T. Yamamoto, Bio Industry, 24(11), 53–59 (2007).

[78] K. Mase, T. Iizuka, E. Okada, T. Miyajima, T. Yamamoto, J. Insect Biotech. Sericol., 75(2), 85–88 (2006).

[79] C. Wu, B. Tian, D. Zhu, X. Yan, W. Cheng, G. Xu, Y. Guo, Y. Wu , S. Jia, Chem Abstr, 130(1996) 100662.

[80] R. Voegeli, J. Meier, R. Blust, Cosmet Toilet, 108, 101-108 (1993).

[81] G.N. Gapurova, Zdravookhr Turkm, 27(7), 15-17 (1983).

[82] K. Tsubouchi, Chem Abstr, 130(4) (1999) 43418.

[83] A. Kuriba, Silk Sci Res Inst Tokyo, Japan, Zairyo Gijutsu, 16(5), 195-201 (1998).

[84] H. Yamada, Y. Fuha, O. Yuri, M. Obayashi, T, Arashima, Chem Abstr, 129(14)

(1998) 179985.

[85] A. Ogawa, H. Yamada, Chem Abstr, 131(7) (1999) 923508.

[86] W. Henne, U. Hoppe, Chem Abstr, 104(6) (1986) 39519.

[87] H. Yamada, K. Yamasaki, K. Zozaki, Chem Abstr, 134(14) (2001) 197888.

[88] U. Hoppe, K. Koerbaecher, M. Roeckl, chem Abstr, 100(1984) 215305.

[89] O. Hata, Chem Abstr, 106(26) (1987) 219374.

[90] W. Engel, U. Hoppe, Chem Abstr, 108(16) (1988) 137689.

[91] C.Y. Wu, B.Z. Tian. 3rd International Silk Conference, Suzhou, China , (1996).

[92] K. Tusbouchi, PCT Int. Appl., WO 9726927.

[93] M. Demura, T. Xomura, T. Asakura. Sen-i Gakkaishi, 46, 391–396 (1990).

[94] N, Minoura, S, Aiba, Y, Gotoh, M, Tsukada, Y. Imai, J. Biomed. Mater. Res., 29,1215–1221 (1995).

[95] N. Minoura, T. Tsuruta, K. Kataoka, K. Ishihara, Y. Kimura, Editors, CRC Press, Boca Raton, FL, 128 (1993).

[96] F. Lucas, J.T.B. Shaw, S.G. Smith, Shirley Inst. Memories, 28, 77 (1955).

[97] F. Lucas, J.T.B. Shaw, S.G. Smith, J. Mol. Biol., 2, 339–349 (1960).

[98] J. Kirimura. Sanshi Shikenjo Houkoku, 17, 447–522 (1962).

[99] M. Tsukada, Y. Gotoh, G. Freddi, M. Matsumura, H. Shiozaki, H. Ishikawa, J. Appl. Polym. Sci., 44, 2203 (1992).

[100] F. Lucas, J.T.B. Shaw, S.G. Smith, Adv. Prot. Chem., 13, 107 (1958).

[101] C.Z. Zhou, F. Confalonieri, M. Jacquet, R. Perasso, Z.G. Li, J. Janin, Protein Struct Funct Genet, 44, 119-122 (2001).

[102] S. Inoue, K. Tanaka, F. Arisaka, S. Kimura, K. Ohtomo, S. Mizuno, J Biol Chem, 275, 40517-40528 (2000).

[103] M.Z. Li, W. Tao, S.Z Lu, C.X. Zhao, Polym Adv Technol, 19, 207-212 (2008).

[104] J.T.B. Shaw, S.G. Smith, Biochim. Biophys. Acta, 52, 305 (1961).

[105] N. Minoura, S. Aiba, M. Higuchi, Y. Gotoh, M. Tsukada, Y. Imai, Biochem Biophys Res Commun, 8, 511-516 (1995).

[106] M.D. Pierschbacher, E. Ruoslahti, Nature, 309, 30-33 (1984).

[107] J. Magoshi, Y. Magoshi, S. Nakamura, J Appl Polym Sci, 21, 2405 (1977).

[108] M. Tsukada, J Polym Sci Part B: Polym Phys, 24, 457 (1986).

[109] M. Tsukada, G. Freddi, P. Monti, A. Bertoluzza, N. Kasai, J Polym Sci Part B: Polym Phys, 33, 1995 (1995).

[110] G. Freddi, P.Monti, M. Nagura, Y. Gotoh, M. Tsukada, J Polym Sci Part B: Polym Phys, 35, 841 (1997).

[111] K. Hirabayashi, Y. Kondo, Y. Go, Sen-i Gakkaishi, 23(5), 199–207 (1967).

[112] Y. Kondo, K. Hirabayashi, E. Iizuka, Y. Go, Sen-i Gakkaishi, 23(7), 311–315 (1967).

[113] K. Hirabayashi, M. Tsukada, J. Sericult. Sci., 45(6), 473–478 (1976).

[114] J. Magoshi, S. Nakamura, J. Polym. Sci. Polym. Phys. Ed., 23, 227 (1985).

[115] M. Tsukada, J. Polym. Sci. Polym. Phys. Ed., 24, 457–460 (1986).

[116] G. Freddi, P. Monti, M. Nagura, Y. Gotoh, M. Tsukada, J. Polym. Sci. B: Polym. Phys., 35, 841–847 (1997).

[117] M. Tsukada, G. Freddi, N. Kasai, P. Monti, J. Polym. Sci. B: Polym. Phys., 36, 2717–2724 (1998).

[118] Q. Wang, L. Qi, Iran Polym J, 18, 663-670 (2009).

[119] K. Wei, Y. Li, K.O. Kim, Y. Nakagawa, B.S. Kim, K. Abe, G.Q. Chen, I.S. Kim, J Biomed Mater Res A, 97, 272-280 (2011).

[120] H.Y. Kweon, I.C. Um, Y.H. Park, Polymer, 41, 7361–7367 (2000).

[121] Kanebo Co. Ltd., Japanese Patent Tokkai Show 60-142259 (1985).

[122] N. Minoura, Polymeric Materials Encyclopedia: Silk (Soft Tissue), 7744 (1996).

[123] Y. Tamada , COE Research Discussion Meeting, (1998).

[124] Y. Gotoh, M. Tsukada, N. Minoura, Y. Imai, Biomaterials, 18, 267 (1997a).

[125] Y. Gotoh, M. Tsukada, T. Baba, N. Minoura,. Polymer, 38, 487 (1997b).

[126] M. Tsukada, G. Freddi, N. Minoura, G. Allara, J. Appl. Polym. Sci., 54, 507 (1994b).

Chapter 2

The surface morphologies of electrospun silk sericin nanofibers and analyzed the characteristics

Chapter 2: The surface morphologies of electrospun silk sericin nanofibers and analyzed the characteristics

2.0. Introduction

Electronspinning is a spinning technique to produce nanofibers with diameters ranging from sub-micron to nano dimension. Ultrathin fibers were produced from a rich variety of materials including polymers, composite, ceramic materials and cellulose acetate via electronspinning which is a simple and versatile method. The electrospun micro/nanofibers possess high-specific surface area and high aspect ratio, so they can be used as the substrate of extracellular matrix (ECM) and find practical applications in industrial fields. Many researchers are really interested in the electrospinning technique [1].

The silkworm was domesticated from the wild silkmoth Bombyx mandarina which has a range from northern India to northern China, Korea, Japan and far the eastern regions of Russia. The domesticated silkworm derives from Chinese rather than Japanese or Korean stock [2-3]. Silkworms were first domesticated during the Han Dynasty in china 2000 years ago. Since then, the silk production capacity of the species has increased nearly tenfold. The cocoon is made of a thread of raw silk from 300 to 900 meters long. The fibers are very fine and lustrous, about 10 micrometers in diameter.

The cocoon filament of the Bombyx mori silkworm is composed of two silk proteins: SF and SS. SS is a family of proteins synthesized exclusively in the middle silk gland of silkworms and stored as an aqueous solution until spinning [4] and ranges in size from 65 to 400 kDa [5-6]. SS content is 20-30 wt% of the cocoon filament. SS envelops fibroin fibers together in a cocoon acting as a protein glue and stuffs the interspace of the fibrous framework to add the cocoon's toughness. SS plays important roles in the spinning process of the silkworm and the construction of a robust cocoon shell. However, SS protein should be removed to get the good luster and hand feel. The removed SS protein is usually abandoned, but there have been many attempts to reuse it as a natural resource [7].

Sericin is mostly discarded in silk processing. If the sericin protein is recovered and recycled, it can represent a significant economic and social benefit. Many applications of sericin were studied by many researchers. Seves et al [8] blended sericin with other resins produced environment-friendly biodegradable polymers. Pure sericin is not easily made into membranes, however, membranes of sericin cross-linked, blended or copolymerized with other substances can be realized readily. A cross-linked thin film made of sericin for water and ethanol separation was prepared by Kensaka et al [9]. Hideyuki and Yorikyo [10] described a membrane from sericin, which was capable of resolving racemic mixtures. Masakazu et al [11] showed a gel material which could separate ether-alcohol mixtures by blending agar or agarose with sericin. Sericin film located on the surface of a liquid crystal made by Yasushi [12] could help the liquid crystal molecules to provide distortion-free high-quality liquid crystal displays uniformly. Li [13] found that sericin protein coated on surfaces of various durable materials improved their functionality. The fine structure and the physical properties of blended films made of sericin and PVA was studied by Ishikawa et al [14]. Fumio et al [15] investigated the mixed hydrogel made of sericin or fibroin and PVA, which had good moisture-adsorbing and -desorbing properties and elasticity. Minoura et al [16] and Tsukada et al [17] studied the attachment and growth of animal cells on films made of sericin and fibroin. Ahn et al [18] produced a novel mucoadhesive polymer by template polymerization of acrylic acid in the presence of silk sericin. Tamada [19] made silk protein into a biomaterial with anticoagulant properties using sulfonation treatment of sericin and fibroin. Coating with natural macromolecules such as chitin, chitosan, fibroin, and sericin can enhance functions of some synthetic fibers. Yamada and Nomura [20] thought sericin-coated fibers could be used to treat abrasive skin injuries and prevented the development of rashes. The chitosan-sericin composite nanofibers were produced by Kensuke [21].

Both naturally derived and synthetic hydrophilic polymeric materials, which have good biocompatibility, have been intensely researched as biomedical materials [22]. SS contains many hydrophilic amino acids including serine ca.35% [23-24],

which lends it high hydrophilicity and sensitivity to chemical modifications [25]. SS is anticipated as a naturally derived biomaterial because of its distinct characteristics, such as induction of heterogeneous nucleation of apatite [26] enhanced attachment of primary cultured human skin fibroblast [27] and affinity to human skin and hair. Cosmetics is the most successful application of SS because of its moisturizing and antioxidative effects. Except for these, there have been some researches to use SS in polymeric fields like SF [7]. However, in most of these researches, SS was incorporated with other polymers [28-29].

Anyway, SS have been made into film, fibers, molded objects, membranes and so on. On the other hand, finding a good solvent for the fabrication of natural polymer is a crucial step for its application. In the case of SF, HFIP or formic acid is used as a solvent [30-31]. Surprisingly, to our knowledge, there have been very few literatures on the production of SS nanofibers with smooth surfaces. In this chapter, the final goal is to produce SS nanofibers with smooth surfaces and bead-free structures via electrospinning techniques, then discussed the electrospinning conditions which affected the morphology of SS nanofibers and analyze the structure of SS nanofibers. Firstly we found that SS can be dissolved in water or TFA, then we tried to find the best conditions for electrospinning techniques and to analyze the structure and properties of SS nanofibers. The results obtained are quite promising as a basis for possible future biomaterials.

2.1. Experiment

2.1.1. Materials

Sericin as the powder form of SS (Lot No. 0704206) were purchased from the Seiren company, Fukui city. Trifluoroacetic Acid (TFA) was used as received.

2.1.2. Sample solution

In 2.2.1., Sericin powder was stirred for 30 min at 85 °C in deionized water. The different concentration of sericin solutions from sericin powder were obtained by dissolving sericin powder in deionized water.

In 2.2.2., sericin powder were dissolved in TFA and stirred at room temperature. Thus different concentration (1.3, 2.6, 3.8, 9.6, 11.7, 14.2, 16.5, 20.9, 22.9 wt%) of sericin powder solution were obtained.

2.1.3. Electrospinning setup and process

Electrospinning of the solutions was conducted under normal atmospheric conditions. The electrospinning setup used in this study consisted of a syringe (SS-05LZ, Terumo Corporation, Tokyo, Japan) and needle (NN-2238N, Terumo Corporation, Tokyo, Japan), a piece of aluminum collecting screen, a syringe pump and a high voltage power supply (Kato tech company, Japan). The spinning speed of the syringe pump was adjusted within the range of 0.003–0.320 cm/min. High voltage power (Kato Tech Company, Japan) was supplied in the range of 0 to 40 kV. The sample solution was placed into the 5 ml syringe, with a stainless 21 gauge needle (inner diameter 0.3 mm) connected the high voltage power supplier. All electrospinning experiments had been done under the same processing conditions. The voltage was applied between the end of the needle and collecting screen. When there was a SS solution droplet at the tip of the needle, a jet was ejected with the voltage increasing. Then SS nanofibers were produced on the aluminum screen.

2.1.4. Characterizations of SS nanofibers

The morphology and diameter of SS nanofibers were examined with a Scanning Electron Microscope (SEM, Hitachi S-3000N, Japan) at room temperature. For SEM measurements, samples were mounted on aluminium plate and sputteringly coated with gold layer to imaging, diameter sizes of beads and nanofibers were acquired from SEM images. The mean diameters and standard deviation (SD) of diameters of SS beads and nanofibers were calculated from measuring the different parts of SS nanoparticles/fibers using the commercial software package, SPSS.

The change of the structure of the SS and SS nanofibers were measured using Fourier Transform Infrared spectroscopy (FTIR, Prestige-21). The spectra of samples were acquired in transmittance mode with a resolution of 4 cm^{-1} and spectral range of

4000–500 cm^{-1}. Infrared spectra were recorded from 16 scans per sample.

Differential Scanning Colorimetry (DSC) curves of samples were measured with a DSC instrument (Thermo Plus DSC 8230, Rigaku Corporation, Japan) under a nitrogen atmospheric condition, at a heating rate of 10 °C/min. The temperature ranged from room temperature to 380 °C and the sample weight was about 3 mg.

Thermogravimetry/differential thermal analysis (TG-DTA) measurements were carried out using a TG-DTA instrument (Thermo Plus TG 8120, Rigaku Corporation, Japan) under a nitrogen atmosphere in the range from room temperature to 380 °C and at a heating rate of 10 °C/min. The sample weight was about 6 mg.

2.2. Results and discussion

2.2.1. Electrospinning of SS from SS-water solution

2.2.1.1. Morphology of SS nanofibers at different concentrations

We attempted to produce SS nanofibers. The spinning distance between the aluminum screen and the tip of the needle was 15 cm. The voltage was 20 kV.

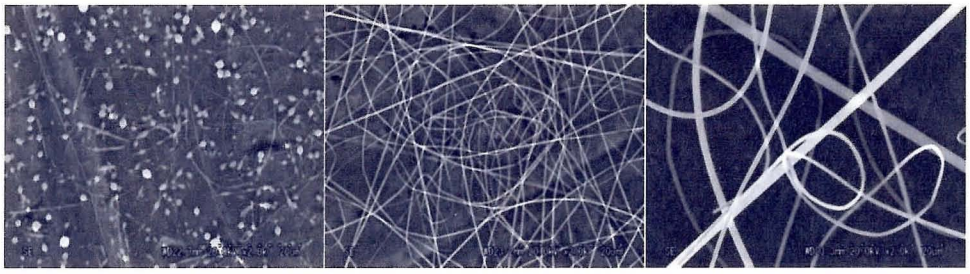

(a) 40% (b) 50% (c) 60%

Fig. 2.1 SEM micrographs of SS nanofibers: (a) 40%; (b) 50% and (c) 60%.

Fig. 2.1(a) shows SEM micrographs of SS nanofibers electrospun at 40 wt%. A number of isolated beads, spindle-like beads, bead-on-string and a few fine fibers were produced at 40 wt%. On the other hand, the as-spun nanofibers exhibited smooth surfaces and bead-free structure at 50 wt% (Fig. 2.1(b)), so did at 60 wt%. However, the fiber mean diameter was thicker and diameter distribution at 60wt% wider than those at 50 wt%. It is evident that the nanofibers with smooth surface can be produced at the concentrations above 50 wt%. The viscosity of SS solution increased with the

increase of concentration, and higher viscosity sustains preparation of smooth fibers with large diameter and without beads [32-35]. The general trend of morphological variations, including the diameter of the fibers, observed in the present study was consistent with the previous literatures. The optimum concentration for the nanofibers with smooth surfaces and narrow diameter distribution was around 50 wt%.

2.2.1.3. Morphology and the diameter distribution of nanofibers with different voltages

From above, we can get best nanofibers from the 50 wt% sericin solution. For this part we electrospun the optimum concentration (50 wt%) with different voltages. The distance between the aluminum foil and the nozzle was 10 cm. The size of the needle was 0.3 mm in diameter. In the electrospinning process, the net charge density carried by the jet was primarily provided by the applied electrostatic field. Higher net charge density not only supply fibers without beads, but also the production of thinner fibers [36].

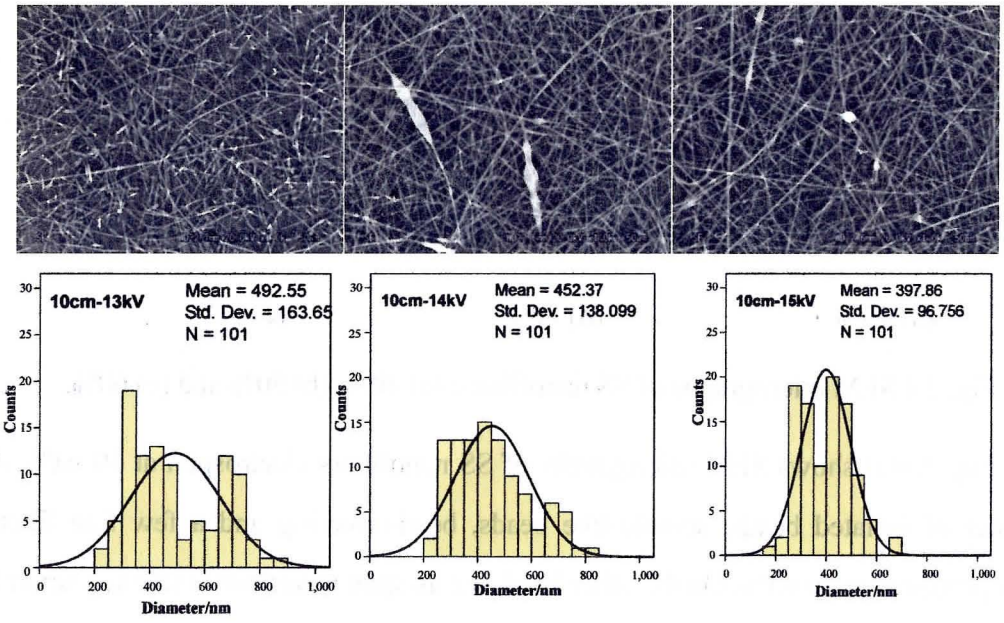

(a) 13 kV (b) 14 kV (c) 15 kV

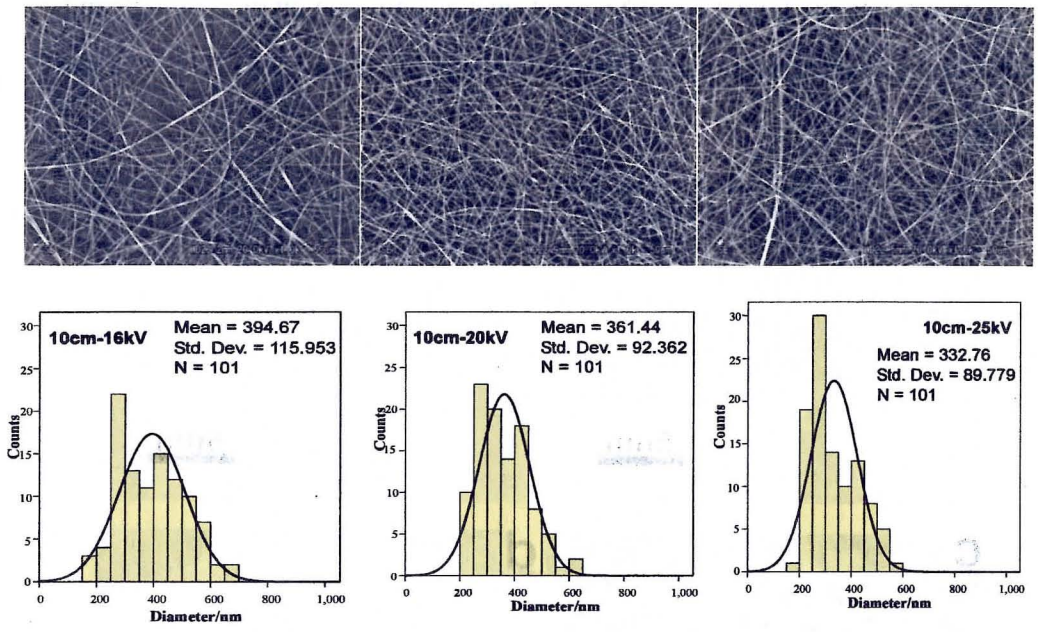

(d) 16 kV (e) 20 kV (f) 25 kV

Fig. 2.2 SEM micrographs and the diameter distributions of SS nanofibers at voltages (kV): (a)13; (b)14; (c)15; (d)16; (e)20 and (f)25.

Fig. 2.2 shows SEM micrographs and diameter distributions of sericin nanofibers. Large number of spindle-like beads and beads along the fibers were produced at the voltage of 13 kV. The mean diameter and the standard deviation of the nanofibers was thicker and wider (Fig. 2.2 (a)). The number of beads decreased with increasing the voltage from 13 kV to 25 kV. It was noted that the nanofibers with smooth surface were made with increasing the voltage up to 25 kV. The diameters size of nanofibers were between 150 and 900 nm. The average diameters of the nanofibers decreased down from 493 to 333 nm and their standard deviation reduced from 164 to 90 with increasing voltage. These results are in agreement with literature [36].

2.2.2. Electrospinning of SS nanofibers from SS TFA solution

The electrospinning was conducted with values of working distance, applied voltage and flow rate at 15 cm, 25 kV, 3.2 ml/h, respectively.

2.2.2.1. SEM images and diameter distribution of the SS beads, beaded fibers and nanofibers

To investigate the founction of SS solution concentration on morphology and diameter of the as-spun nanofibers, SS solutions ranging from 1.3 to 22.9 wt% were electrospun.

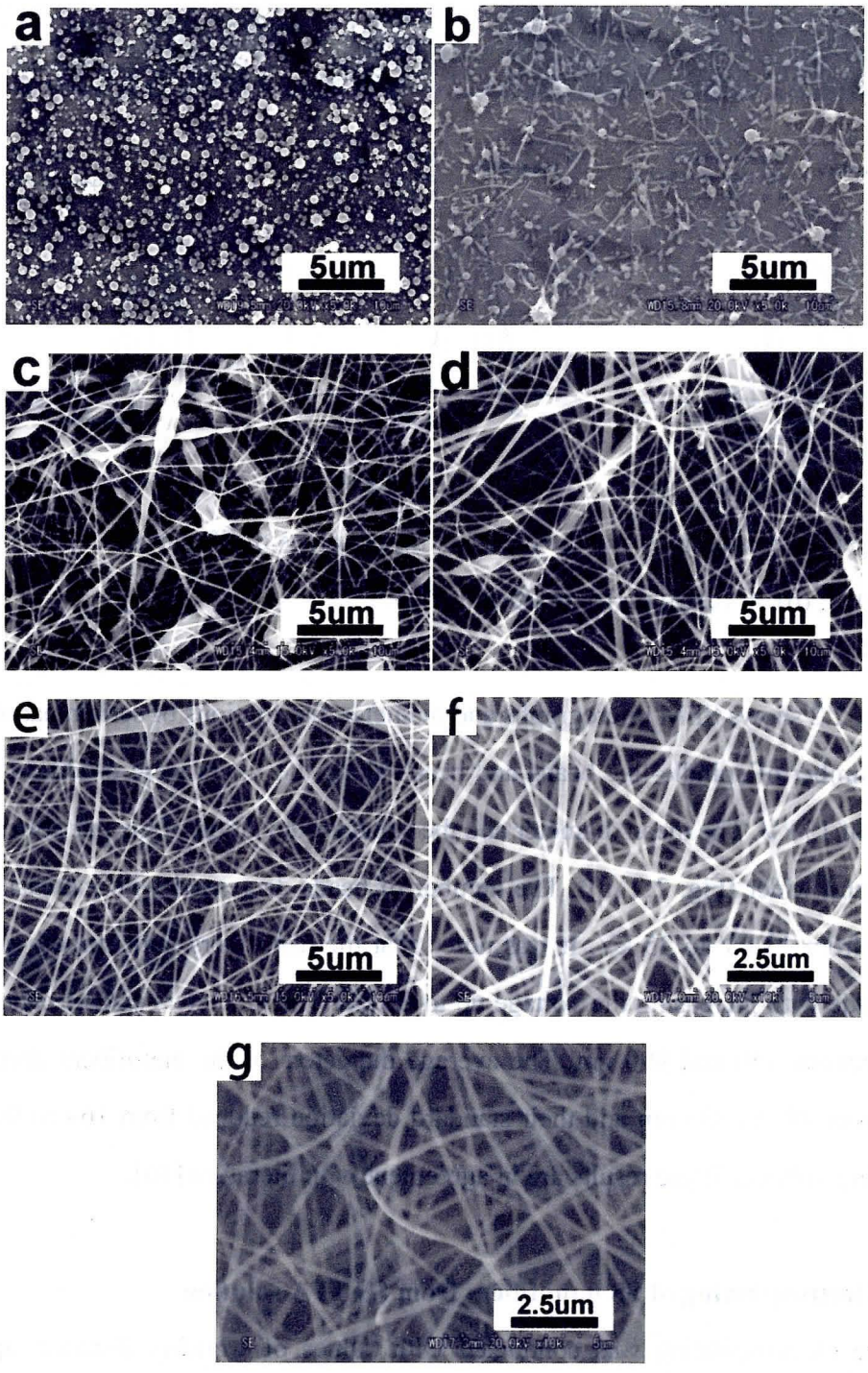

Fig. 2.3 SEM micrographs of SS mats obtained by electrospinning with different weight ratio of SS TFA solution.

wt%: (a) 8.5; (b) 9.6; (c) 11.7; (d) 14.2; (e) 16.5; (f) 20.9 and (g) 22.9.

Fig. 2.3 shows SEM micrographs of SS beads, beaded fibers and nanofibers. From the concentration from 1.3 to 3.8 wt% (the figures were not shown), all SS beads were acquired. There are half-ball holes on the beads, and the number and the size of the half-ball holes decreased with the concentration increasing. When the concentration increased into 6.2 (the figure was not shown) and 8.5 wt% (Fig. 2.3(a)), we abtained all circular beads and no half-ball holes on them. From 9.6 to 16.5 wt% (Fig. 2.3(b-e)), spindle-like beads and beaded fibers were acquired. With the concentrations increasing, the number of the beads decreased and the number of the fibers increased. 20.9 and 22.9 wt% of SS/TFA solution were electrospun (Fig. 1(f-g)), excellent nanofibers with smooth surfaces and round cross section were produced. Due to the imcomplete solvent evaporation and jet split, SS nanofibers'adhesion and bifurcation were observed.

In the low concentration, only beads were acquired and the holes on beads were disappeared with the concentration increasing; in the medium concentration, beaded-fibers were produced; good SS nanaofibers were electrospun using high SS/TFA solution concentration. The optimum concentration for producing SS nanofibers with smooth surfaces was above 20.9 wt%.

2.2.2.2. Diameter distribution of the SS beads, beaded fibers and nanofibers

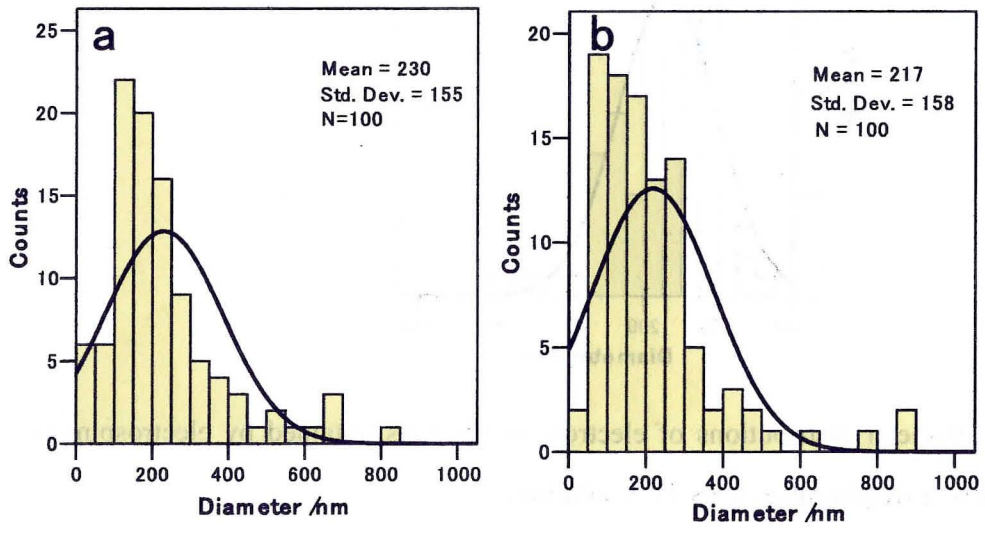

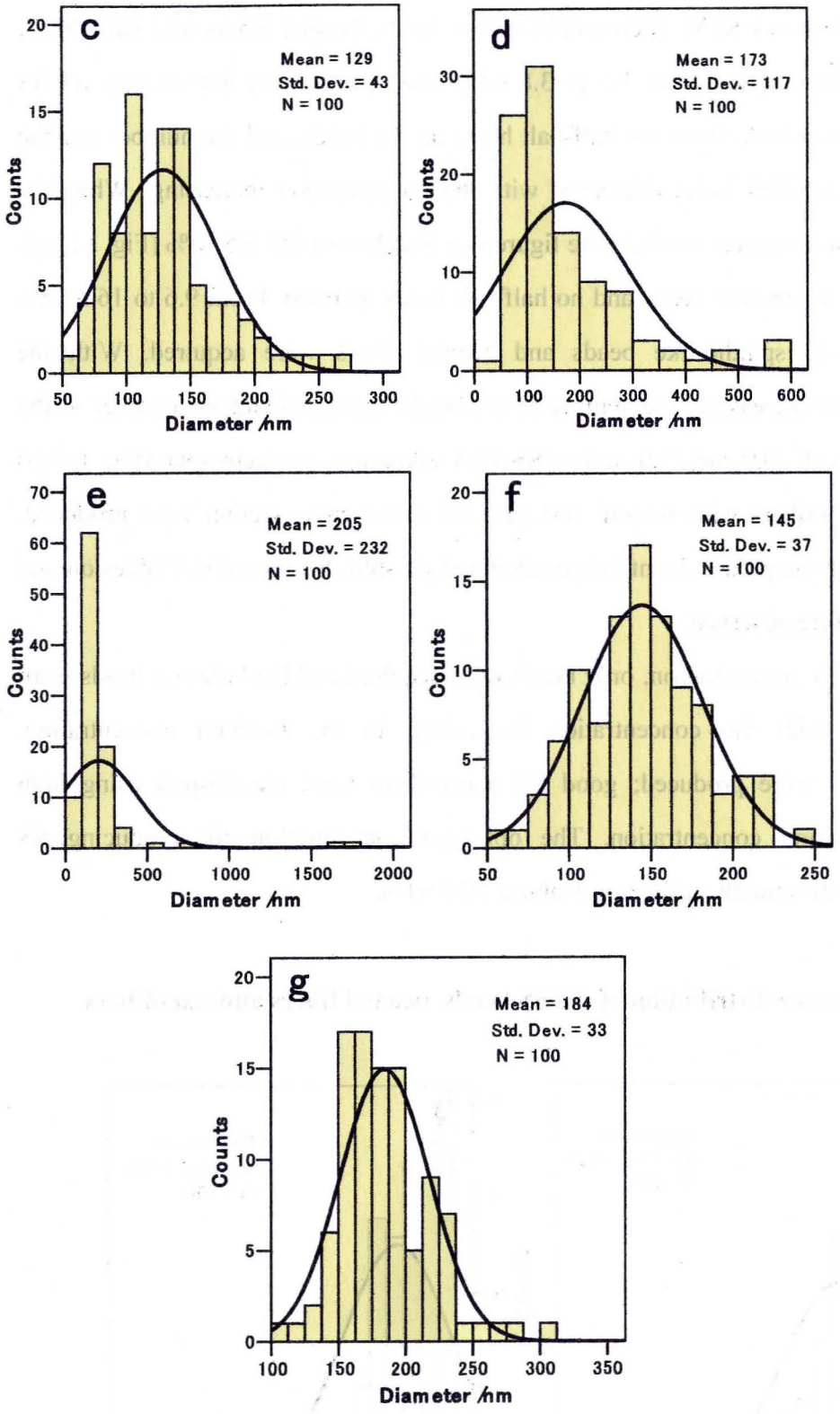

Fig. 2.4 Diameter distributions of electrospun SS mats obtained by electrospinning with different weight ratio of SS TFA solution.

wt%: (a) 8.5; (b) 9.6; (c) 11.7; (d) 14.2; (e) 16.5; (f) 20.9 and (g) 22.9.

Fig. 2.4 and Tab. 2.1 shows diameter distributions of electrospun SS mats obtained by electrospinning with different weight ratio of SS TFA solution. When the concentration from 1.3 to 3.8 wt% (the figures were not shown), The average diameters of SS hole beads were 230, 265 and 311 nm, , the standard dievations were 275, 280 and 335, respectively. In low concentration, the mean diameter of SS beads increased with the concentration increasing. The mean diameter of no hole beads were 254 and 230 nm in responding to the concentration of 6.2 and 8.5 wt%, and the standard deviations were 168 and 155, respectively. In our study, beaded fibers were formed from 9.6 wt%. The average diameters of SS bead-fibers were 129, 173 and 205 nm, respectively. Perfect nanofibers was obtained form 20.9 wt% and 22.9 wt% SS solution, and the average diameters of the SS nanofibers were 145 and 184 nm (Fig. 2.4 f and g), respectively. It is also interesting to note that the average diameters of SS nanofibers increased with increasing SS solution concentration. It is evident that the viscosity of SS solution increased as the function of the concentration increasing and that the viscosity is the major parameter for deciding the fiber diameter, higher viscosity sustain preparation of smooth fibers without beads and lower viscosity favors the thinner fibers [20-23]. The general trend of morphological variations, including the diameter of the fiber, observed in this study was consistent with the previous literatures.

Con wt%	8.5	9.6	11.7	14.2	16.5	20.9	22.9
M.D	230	217	129	173	205	145	184
S.D	155	158	43	117	232	37	33

Tab. 2.1 Mean diameter and diameter distributions of electrospun SS mats obtained by electrospinning with different weight ratios of SS TFA solution.

2.2.2.3. FTIR spectra

Fourier Transform Infrared (FTIR) spectra is a powerful technique to study structure at the molecular level, and reveals typical absorption bands sensitive to

molecular conformation of silk proteins [24]. Fig. 2.5 showed IR spectra of SS, SS nanofibers, heated SS nanofibers and TFA solvent. SS (Fig. 2.5a) exhibited absorption bands at 1641 (I), 1514 (II) and 1233 cm^{-1} (III), which are characteristics of β-sheet structure. SS nanofibers (Fig. 2.5b) exhibited absorption bands at 1653 cm^{-1} (amide I, C=O stretching vibration of the amino group) and 1520 cm^{-1} (II, N-H bending and C-N stretching vibration) which are characteristics of random-coil conformation, whereas Heated SS nanofibers (Fig. 2.5c) revelated 1643 (I) and 1515 cm^{-1} (II), attributed to the β-sheet conformation. The absorption band around 1233 cm^{-1} (III) disappeared in SS nanofibers and heated SS nanofibers.

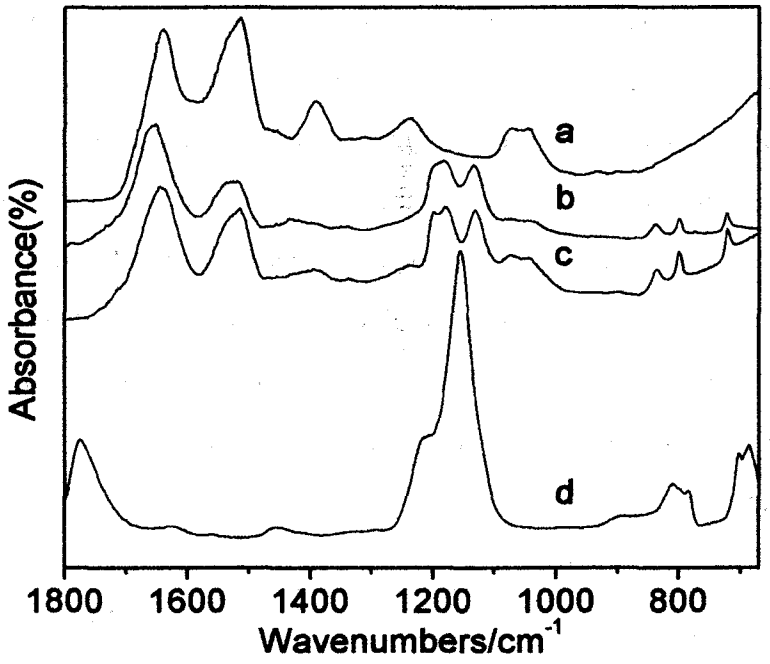

Fig. 2.5 FTIR spectra of the SS, SS nanofibers, heated SS nanofibers and TFA. Sample: a SS; b 22.9 wt% SS nanofibers; c heated SS nanofibers at 160 °C for 1h and d TFA.

The IR spectra of SS nanofibers and heated SS nanofibers (Fig. 2.5b-c) were similar to each other. The minor absorption band at 1787 cm^{-1} did not appear in the SS sample (Fig. 2.5a). It was of interest to note that this absorption band was detected in SS nanofibers (Fig. 2.5b). 1390 (C-H and O-H bending vibrations), 1071 and 1046

cm^{-1} (C-OH stretching vibration), which are also attributable to the abundance of hydroxyl amino acid side chains, were disappeared in SS nanofibers. However, the new bands appeared at 1180, 1133, 837, 801 and 721 cm^{-1} in SS nanofibers (Fig. 2.5b), compared with the spectra of SS (Fig. 2.5a). The heated SS nanofibers (Fig. 2.5c) displayed shoulder absorption band at 1197, 1073 and 1043 cm^{-1} compare with SS nanofibers curve (Fig. 2.5b).

2.2.2.4. DSC curves

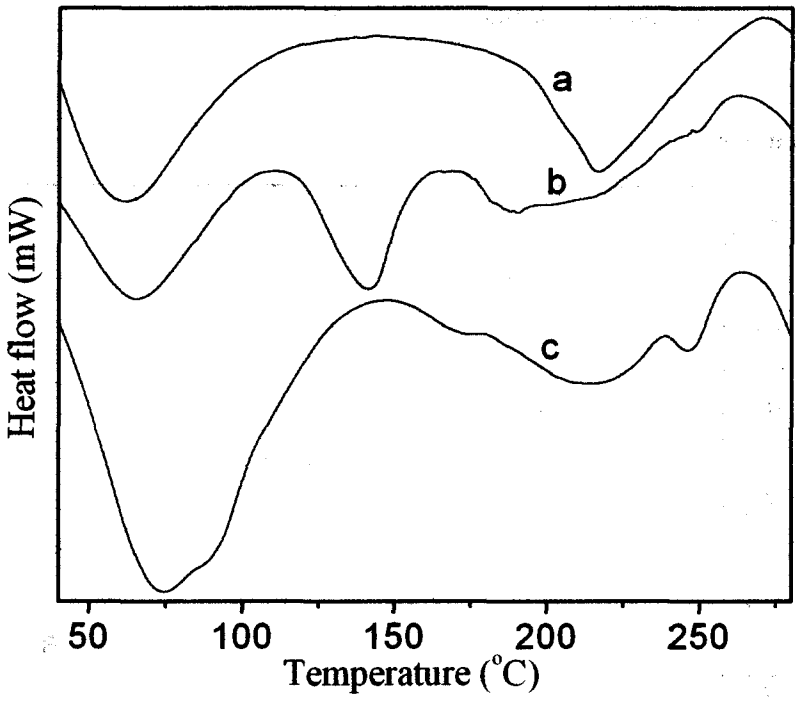

Fig. 2.6 DSC curves of SS, SS nanofibers and heated SS nanofibers.

Sample: a SS; b 22.9 wt% SS nanofibers and c heated nanofibers at 160 °C for 1h.

In order to analyze the thermal behavior of the samples, DSC measurements were conducted. Fig. 2.6 shows the DSC curves for SS, SS nanofibers and heated SS nanofibers. All the curves (Fig. 2.6a-c) showed endothermic peaks under 100 °C, which are attributed to the evaporation of water contained in samples. In addition to this endothermic peak, SS (Fig. 2.6a) showed a major endothermic peak at 217 °C. On the other hand, SS nanofibers (Fig. 2.6b) showed endothermic peak at around 198 °C. However, there is a new endothermic peak at around 142 °C. The

endothermic peak around 217 °C is due to the thermal decomposition of SS. The position of the endothermic peak at 198 °C of SS nanofibers corresponds to the thermal decomposition tempetature (217 °C) of endothermic peak of SS. SS and SF from B. mori silkworm decompose at around 220-230 °C and 320 °C, respectively [25], the decomposition peak in this study coincide to the literature.

The new endothermic peak at around 142 °C disappeared in the heated nanofibers (Fig. 2.6c). It illustrated that TFA can be eliminated by heating. At the same time, endothermic peak at 214 °C and two shoulder endothermic peaks around 172 and 246 °C in the heated nanofibers was shown.

2.2.2.5. TG curves

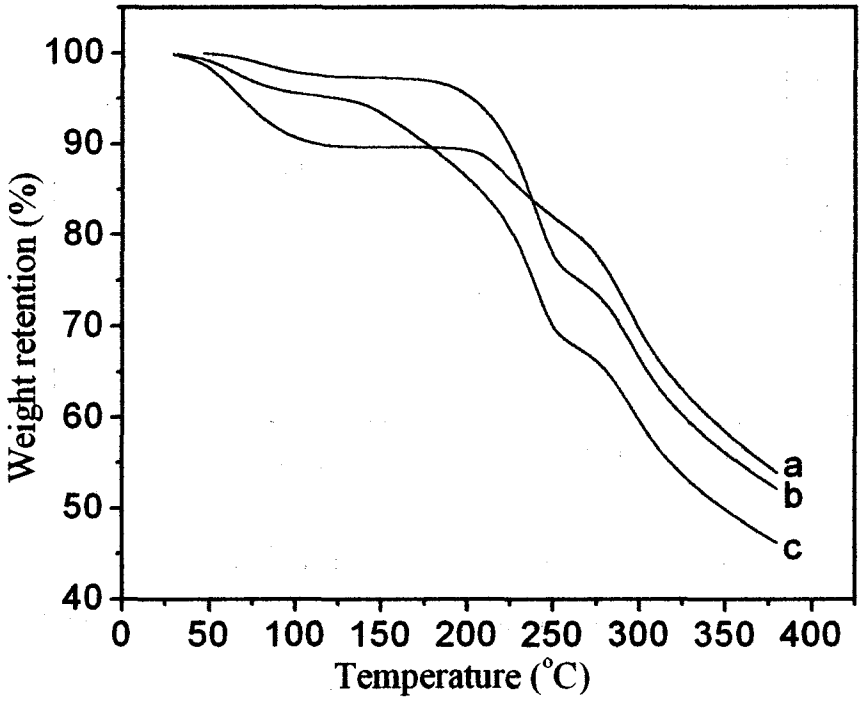

Fig. 2.7 TG curves of SS, heated SS nanofibers and SS nanofibers.

Sample: a SS; b heated nanofibers at 160°C for 1h and c 22.9 wt% SS nanofibers.

The thermal behavior of SS, SS nanofibers and heated SS nanofibers were further studied by means of TG measurements (Fig. 2.7). TG analysis was very useful for the quantitative determination of the SS nanofibers. The weight loss of the samples at less than 100 °C is due to the evaporation of water and solvent contained

in samples.

The slight negative slope of the TG curve marked the onset of weight loss. Fig. 2.7 showed that the weight loss attained 11, 3 and 6% at 208, 183 and 142 °C (Fig. 2.7a-c), respectively, and then the weight loss increased gradually, leading to thermal decomposition at higher temperatures. The weight loss of SS (Fig. 2.7a) was 10% at 100 °C. Before at 142 °C, the weight loss of SS (Fig. 2.7a) was more than SS nanofibers (Fig. 2.7c), after that, slower than SS nanofibers under the same temperature. Before at 234 °C, the weight loss of SS (Fig. 2.7a) was faster than the heated SS nanofibers (Fig. 2.7b), after that, slower than the heated SS nanofibers under the same temperature. In all TG process, the weight loss of SS nanofibers (Fig. 2.7c) was faster than the heated SS nanofibers (Fig. 2.7b). The heated process can remove the solvent TFA.

2.3. Conclusions

Water as the solvent, SS was electrospun at different concentrations. Isolated beads, spindle-like beads, bead-on-string and a few fine fibers were formed at the concentration of 40 wt%. The nanofibers with smooth surfaces and bead-free structures could be made at concentration above 50 wt%. The average diameters of the nanofibers increased with increasing concentration. The optimum concentration was 50 wt%. The number of beads, the average diameters and the standard deviation of SS nanofibers decreased with increasing voltage.

TFA as the solvent, we succeeded in producing SS nanofibers via electrospinning with SS/TFA solution. The morphology, conformational characteristics and thermal property of SS nanofibers were investigated using SEM, FTIR, DSC and TG. In the low concentration, only beads were acquired and the holes on beads were disappeared with the concentration increasing; in the medium concentration, beaded-fibers were produced; good SS nanaofibers were electrospun using high SS/TFA solution concentration. FTIR results showed that the conformation of SS nanofibers change from β-sheet to random coil. The structure of heated SS nanofibers can become β-sheet by heating SS nanofibers for 1h at 160 °C. The results

of DSC and TG illustrated that TFA can be eliminated by heating.

References

[1] Z.M. Huang, Y.Z. Zhang, M. Kotaki, S. Ramakrishna, Composites Science and Technology, 63, 2223–2253 (2003).

[2] K.P. Arunkumar, M. Metta, J. Nagaraju, Molecular Phylogenetics and Evolution, 40, 419–427 (2006).

[3] H. Maekawa, N. Takada, K. Mikitani, T. Ogura, N. Miyajima, H. Fujiwara, M. Kobayashi, O. Ninaki, Chromosoma (Berl.), 96, 263-269 (1988).

[4] T. Gamo, T. Inokuchi, H.Laufer, Insect Biochem, 7, 285-295 (1977).

[5] T. Gamo, Biochemical Genetics, 20, 165-177 (1982).

[6] A. Garel, G. Deleage, J.C. Prudhomme, Insect Biochem. Molec. Biol., 27, 469-477 (1997).

[7] Y.Q. Zhang, Biotechnology Advances, 20, 91-100 (2002).

[8] A. Seves, M. Romano, T. Maifreni, S. Sora, O. Ciferri, Inter. Biodet. Biodeg., 42, 203 (1998).

[9] M. Kensaka, I. Takashi, A. Noboru, JP 03284337A (1991).

[10] Y. Hideyuki, F. Yorikyo, JP 05345117A (1993).

[11] Y. Masakazu, M. Akira, O. Yoji, JP 2001129371A (2001).

[12] N. Yasushi, JP 06018892A (1994).

[13] X.F. Li, CN 1116227 (1996).

[14] H. Ishikawa, M. Nagura, Y. Tsuchiya, Sen'i Gakkaishi 43, 283 (1987).

[15] Y. Fumio, K. Jamikazu, M. Keizo, S. Sohzo, JP 2000169736A (2000).

[16] N. Minoura, S.I. Aiba, Y. Gotoh, M. Tsukada, Y. Imai, J Biomed. Mater. Res, 29, 1215 (1995).

[17] M. Tsukada, A. Hayazaka, K. Inoue, S. Nishikawa, S. Yamamoto, JP 11243948A (1999).

[18] J.S. Ahn, H.K. Choi, K.H. Lee, J.H. Nahm, C.S. Cho, Novel Mucoadhesive Polymer, 80, 274 (2001).

[19] Y. Tamada, JP 09227403A (1997).

[20] H. Yamada, M. Nomura, JP 10001872A (1998).

[21] S. Kensuke, JP 2008163520A (2008).

[22] J.L. Drury, D.J. Mooney, Biomaterials, 24, 4337-4351 (2003).

[23] Y. Takasu, H. Yamada, K.Tsubouchi, Biosci.Biotechnol.Biochem., 66, 2715-2718 (2002).

[24] N. Kato, S. Sato, A. Yamanaka, H.Yamada, N. Fuwa, M.Nomura, Biosci. Biotechnol. Biochem., 62, 145-147 (1998).

[25] H. Teramoto, K.I. Nakajima, C. Takabayashi, Biomacromolecules, 5, 1392-1398 (2004).

[26] A. Takeuchi, C. Ohtsuki, T. Miyazaki, M. Kamitakahara, S.I. Ogata, M. Yamazaki, Y. Furutani, H. Kinoshita, M. Tanihara, J. R. Soc. Interface, 2, 373–378,(2005).

[27] K. Tsubouchi, Y. Igarashi, Y. Takasu, H. Yamada, Biosci.Biotechnol.Biochem., 69, 403-405 (2005).

[28] J.S. Ahn, H.K. Chio, K.H. Lee, J.H. Nahm, C.S.Cho, Journal of Applied Polymer Science, 80, 274-280 (2001).

[29] W. Wu, W.J. Li, L.Q. Wang, K.H. Tu, W.L.Sun, Polymer International, 55, 513-519 (2006).

[30] F. Zhang, B.Q. Zuo, H.X. Zhang, L. Bai, Polymer, 59, 279-285 (2009).

[31] F. Zhang, B.Q. Zuo, L. Bai, J. Mater. Sci., 44, 5682-5687 (2009).

[32] M.E. Helgeson, N.J. Wagner, J. AIChE, 53, 51-55 (2007).

[33] K. Ohkawa, K.I. Minato, G. Kumagai, S. Hayashi, H. Yamamoto, Biomacromolecules, 7, 3291 (2006).

[34] S.L. Shenoy, W.D. Bates, H.L. Frisch, G.E. Wnek, Polymer, 46, 3372 (2005).

[35] C. Wang, C.H. Hsu, J.H. Lin, Biomacromolecules, 39, 7662 (2006).

[36] H. Fong, I. Chun, D.H. Reneker, Polymer, 40, 4585-4592 (1999).

Chapter 3

Fabrication of silk sericin nanofibers from a silk sericin-hope cocoon with electrospinning method

Chapter 3: Fabrication of silk sericin nanofibers from a silk sericin-hope cocoon with electrospinning method

3.0. Introduction

Electrospinning is a spinning technique to generate fibers with diameter ranged from 2 nm to several micrometers, yielding a three-dimensional porous network (a random mat) of nanofibers with high aspect ratio and a large specific surface area by stretching and splitting polymer solution under high-voltage electric field [1].

The sizes of nanofibers with nano scale order primarily depend on the major factors of specifications of solvents, such as viscosity, conductivity and surface tension as well as the electrospinning conditions, including applied voltage, spinning flow rate and working distance [2]. Among them, viscosity and molecular weight of the sample are the most important factors to decide the fibrous nanofiber size. Very smooth, thinner nanofibers without beads can be produced with using sample solvents with low viscosity [3]. Surface tension favors the formation of beads and bead fibers. As for electric field strength, it is illuminated that the jet diameter firstly decreased with the electric field strength increasing, and then increased when the electric field strength increased further. Very low and high flow rate are not preferable to produce very thin nanofibers. Too high flow rates did not produced fibers because the polymer solution was pushed out of the syringe so fast that it did not have time to evaporation. Since the time needed to eject the solution, very low flow rate was also not chosen [4]. The working distance between the needle and collector varies the path length and solvent evaporation, so it greatly influences the mean diameter and uniformity of the fibers [5].

The micro/nanometer scale bears helpful specialties, high aspect ratio, high-specific surface area and high porosity with very small pore size. Therefore, the micro/nanofibers can simulate the extracellular matrix (ECM) and enhance the cell migration and proliferation and be applied in biomedical domain, involving drug delivery, wound dressing, tissue engineering scaffolds, and others [6,7].

Silk fiber derived from silkworm (B. mori) is a natural biopolymer that is mainly composed of two different macromolecular proteins, i.e., fibroin (the inner brins) and sericin (outer coating). SS is a family of adhesive silk proteins synthesized exclusively in the middle silk glands of silkworms, which envelops the fibroin fiber with successive sticky layers that help in the formation of a cocoon [8]. SS constitutes 25–30% of silk protein and ensures the cohesion of the cocoon by gluing silk threads together. Silk sericin consists of 18 kinds of amino acids most of which have strong polar side groups such as hydroxyl, carboxyl, and amino groups, and are characterized by a high serine content, about one third of the total amino acids [9-10], which lends it high hydrophilicity. Abundant hydroxyl groups in sericin are hoped to play a significant role in structural formation.

Recently it has been shown that silk sericin resists oxidation, and is anti-bacterial, biocompatible, UV resistant, absorbs and releases moisture easily, can be cross-linked, copolymerized, and blended with other macromolecular materials [11–13]. Moreover, it exhibits a lot of biological activities, such as, tyrosinase activity inhibition [14], pharmacological functions such as anticoagulation [15], anti-cancer activities [16], promote digestion [17], and nitrogen source for culture medium [18]. Mandal et al. [19] prepared and characterized novel silk sericin/gelatin 3-D scaffolds and 2-D films for potential tissue engineering applications. They showed that blended sericin/gelatin 3-D scaffolds were highly porous with an optimum pore size of 170 ± 20 μm. The scaffolds were robust with enhanced mechanical strength and showed high compressibility. Hence it is anticipated that silk sericin is a promising natural resource for developing novel protein based materials. One important materials option for biomaterials such as, silk sericin is the formation of nanofibers. The nanofibers from SS would be the most attractive materials in view of medical and industrial applications. The silk protein nanofibers with very thin and smooth surface, with smaller diameter and its narrow standard deviation, and with thick bead free nanofibers are important morphological feature for using in industrial fields.

Silk textile materials are composed mainly of silk fibroin and not of sericin,

which can be almost removed by the elevated alkali and enzymatic solution. Thus sericin is the by-product proteins which are produced in the course of reeling process of raw silk fibers. The molecular weight of SS significantly decreased in the degumming process by the action of alkali solution. Actually it is impossible to get native silk sericin without decreasing of molecular weight by collecting silk sericin from the sericin solution which obtained by the conventional technique.

Many gene scientists have been paid a great attention to produce novel silk sericin-hope cocoon (SC) by genetically modification and diversification of B. mori silkworm [20–22]. Generally, there are two kinds of sericin silkworms in the market. One is the naked pupa Nd strain, which secretes silk thread at a rate of 30 mg/head, with spinning and cocooning rates of 99%. The other sericin silkworm, the Nd-s strain, which secretes only a few silk threads, with a sericin content as low as 92%, at the cocoon stage. Unfortunately, neither of the existing strains is practical for sericin extraction. In order to effectively produce intact sericin protein, recently a new silkworm race 'Sericin Hope' has been developed by cross breeding an Nd mutant (naked pupa) and a high cocoon yielding strain KCS83 [22]. It secretes silk thread, at the rate of about 80 mg/head, while the spinning and cocooning rates have been improved to 99%. The output of the cocoon layer is over four times that of the Nd strain. Sericin can be very efficiently produced, because the sericin purity is as high as 98.5% at the cocoon stage. The sericin hope cocoon, named 'Virgin Sericin' can be gelled in water with less hydrolyzing by autoclaving at 110 °C for 10 min. Sericin-hope facilitates mass production of native sericin with high purity. Utilizing the cocoon of the Sericin-hope, there have been some researches about hydrogel, which can be produced via chemical modification and so on [23–26]. Until recently, there is no literature on preparation of SC nanofibers with smooth surfaces using sericin-hope cocoon.

In the present study, we attempted to produce SC nanofibers having smaller diameters, narrow diameter distribution, smooth surfaces and bead-free structures via electrospinning from sericin cocoon solution. The effects of the solution variables and

electrospinning process on morphological appearance and average diameter of the as-spun sericin cocoon fibers were examined. The structure and physical characteristics of electrospun sericin nanofibers were also analyzed.

3.1. Experimental

3.1.1. Materials

Silk cocoon layer from sericin-hope silkworm race, which has been genetically improved by cross breeding an Nd mutant (naked pupa) and a high cocoon yielding strain KCS83 was used as the silk sericin in the experiment.

3.1.2. Preparation of SC solution

Silk sericin-hope cocoon is dissolved in trifluoracetic acid (TFA) to form a uniform dilute polymer solution. The solution is stirred at 25 °C continuously with a magnetic stirrer for 7 days. The concentrations of sericin solution were in the rage of 2 and 12 wt%.

3.1.3. Electrospinning

The electrospinning instrument was Kato Tech Company, Japan. The SC solution was placed into a 5 ml syringe (SS-01T, Terumo Corporation, Tokyo, Japan) with a 21 gauge stainless needle (inner diameter 0.3 mm, 38-mm long, NN-2238N, Terumo Corporation, Tokyo, Japan), which connected the high voltage power supply. The flow rate can be controlled in the range of 0.02–0.320 cm min^{-1} by the syringe pump. A high voltage in the range from 7 kV to 36 kV was applied to the droplet of SC solution at the tip. A grounded aluminum foil was placed at a distance of 15 cm from the capillary tip. When there was a SC solution droplet at the tip of the needle, a jet was ejected with the increasing of electric voltage, the SC nanofibers were produced on the aluminum collecting screen. SC nanofibers were thus placed on aluminum foil.

3.1.4. Characterization

The surface morphologies of the electrospun fibers were examined with scanning electron microscopy (SEM) (S-2380N, Hitachi, Japan). Before placing the samples in the SEM chamber, the samples were mounted onto an aluminum stud and sputter-coated with gold/palladium for 180 s (E-1010 ION SPUTTER, Hitachi, Japan) to prevent charging. The mean diameter and its standard distribution of the SC nanofibers were calculated using a commercial statistical software package, SPSS, from the diameters of SC nanofibers measured from the different parts of SEM images.

Fourier transform infrared (FTIR) spectroscopy was measured with a Shimadzu FTIR-8400S infrared spectrometer by the ATR method in the region of 4000–400 cm^{-1} at room temperature.

Differential scanning calorimetry (DSC) measurement was performed by a Rigaku Denki Co., Ltd. instrumental (model DSC-8230) at a heating rate of 10 °C min^{-1} under N_2 gas atmosphere.

Thermogravimetric (TG) analysis was carried out with a Rigaku Thermo plus TG 8120 under N_2 gas at a heating rate of 10 °C min^{-1}.

3.2. Results and discussion

3.2.1. Electrospinning processing parameters

It has been revealed that the solution properties and processing parameters strongly affect the morphology and diameter of electrospun nanofibers [27]. In order to electrospin the sericin TFA solution properly, the following variables including the concentration of sample solution, the applied electric field, spinning distance between the spinneret and the collector and flow rate of the feedstock solution were examined.

3.2.1.1. Effect of the concentration of SC solution

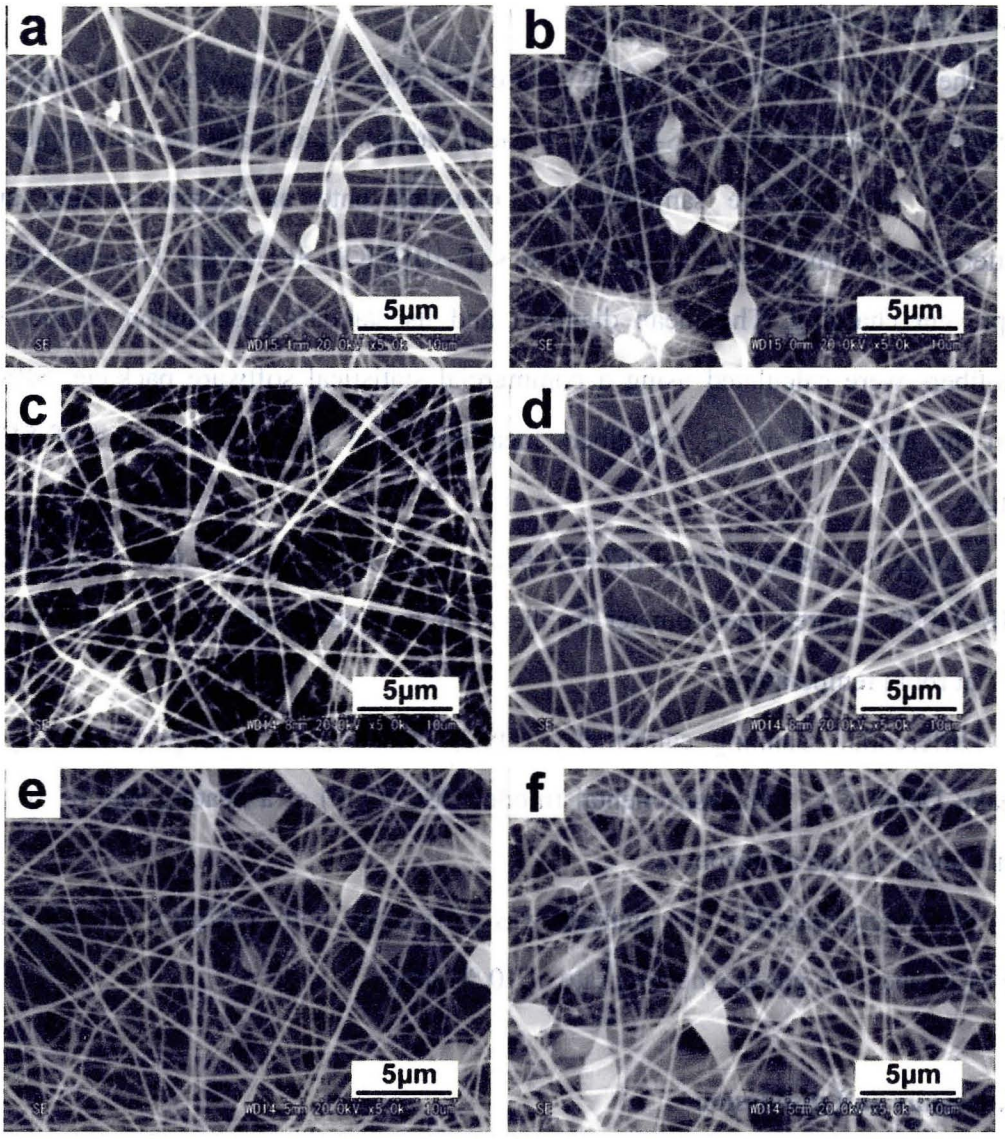

Fig. 3.1 The surface morphology of electrospun SC fibers spun at the voltage of 25 kV with a constant spinning distance of 15 cm at the concentration of solution: (a) 2%; (b) 4%; (c) 6%; (d) 8%; (e) 10% and (f) 12%.

Concentration was found to be the most important parameter among the above major factors to decide the morphologies and the average diameter after the electrospinning process [28]. Fig. 3.1 shows SEM micrographs of SC nanofibers spun from the different concentrations of SC solution at the voltage of 25 kV. From the lower concentration of solution, coarse and thin SC nanofibers with large number of

bead defects and big spindle-like beads were produced due to instability of the jet by effect of surface tension in the presence of electrical forces (Fig. 3.1a and b). The sericin nanofibers (Fig. 3.1d) showed very fine SC nanofiber without the spindle-like beads. It was found that the SC nanofibers can be spun into fibers with the concentration from 6 to 8 wt%. The fibers have smooth surfaces and they have near circular cross-section. The fibers spun with higher solution concentration above 10 wt%, was fine and uniform in size (Fig. 3.1e and f). As shown in Fig. 3.1, the morphologies of the SC nanofiber were influenced by the SS solution concentration. To clarify the influence of solution concentration in more details, we tried to examine the diameter distribution of SC nanofibers. Fig. 3.2 shows the diameter distributions of SC nanofibers. The fiber diameters at each solution concentration followed the normal distribution curve. The trend of mean diameter of SC nanofibers was not directly related with the concentration of solutions. The mean diameter of as spun SC fibers was 227, 114, 172, 231, 173 and 219 nm at the different concentrations of solutions, 2, 4, 6, 8, 10 and 12 wt%, respectively. The standard deviation (SD) of the diameter of nanofibers decreased with increasing the solution concentration. The fibers spun by the solution of 6 and 8 wt% were more homogenous and smooth.

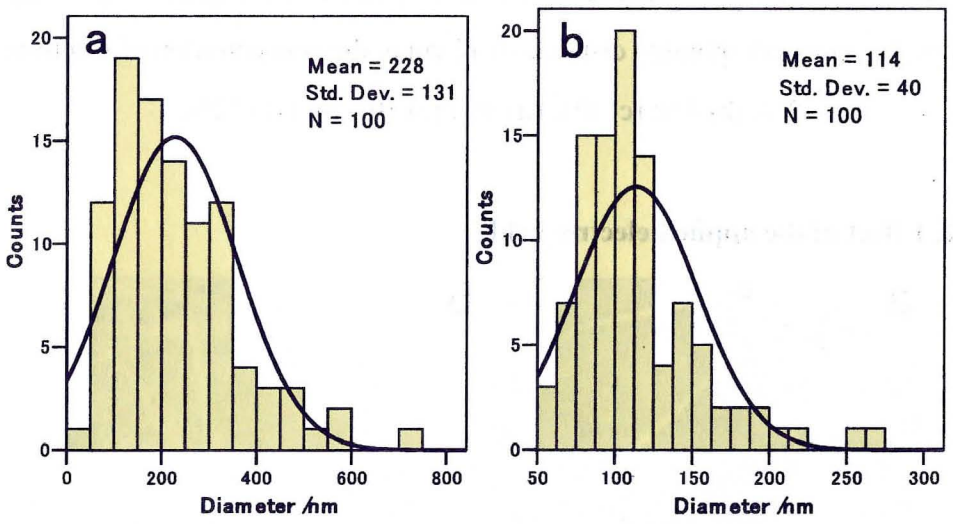

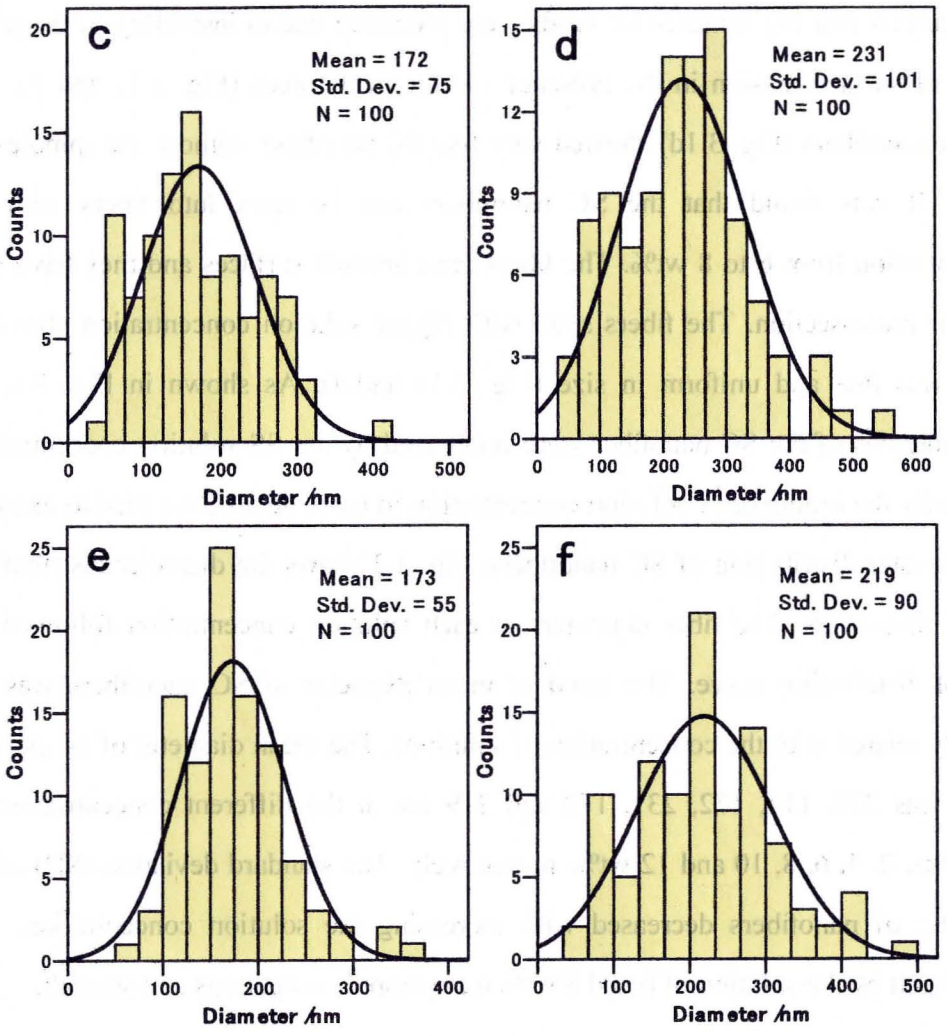

Fig. 3.2 Distribution of fiber diameters of electrospun SC fibers spun at the voltage of 25 kV with a constant spinning distance of 15 cm at the concentration of solution: (a) 2%; (b) 4%; (c) 6%; (d) 8%; (e) 10% and (f) 12%.

3.2.1.2. Effect of the applied electric field

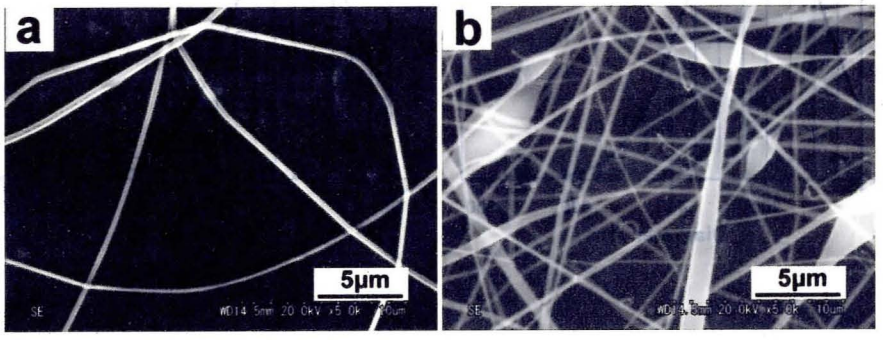

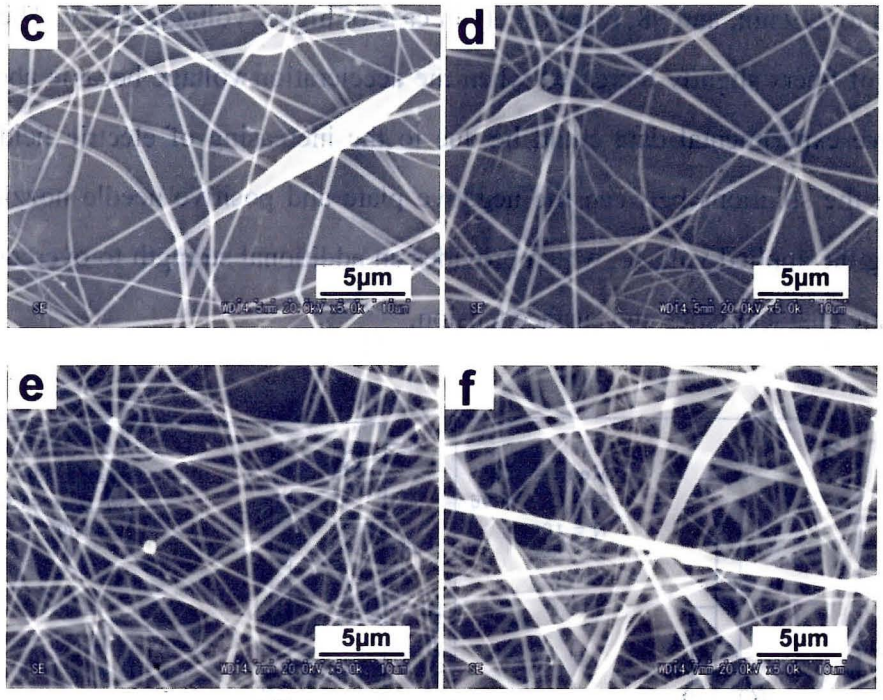

Fig. 3.3 The surface morphology of electrospun SC fibers spun at the solution concentration of 8% with a constant spinning distance of 15 cm at the voltage of: (a) 7 kV; (b) 11 kV; (c) 18 kV; (d) 25 kV; (e) 32 kV and (f) 36 kV.

SC nanofibers were produced by the electrospinning with sericin TFA solution at concentration of 8 wt% at different acceleration voltages ranging from 7 to 36 kV. Fig. 3.3 shows the SEM images of SC nanofibers spun at 8 wt% at different acceleration voltages. It was rarely possible to produce SC nanofibers by electrospinning at the lower acceleration voltage (Fig. 3.3a). The SC nanofibers spun at the voltage above 11 kV were continuous and smooth in the surface except a very few beads (Fig. 3.3b). Spindle-like beads and very thick in size sometimes appeared in the SC nanofibers spun at 11 kV. From the view of nanofibers morphological point, the optimum conditions for the excellent spinnability of SC nanofibers were at the acceleration voltage above 32 kV (Fig. 3.3e). Fig. 3.4 shows the diameter distribution of SC nanofibers spun at different acceleration voltages. It is seemed that the average diameters of SC nanofibers decreased with increasing acceleration voltage. The average fiber diameter and its SD spun at 7 kV was 291 nm and 96, respectively, whereas, those values were

decreased to 229 nm, and 98, respectively in case of higher voltage, 25 kV. The mean diameter of fibers slightly increased when the acceleration voltage became above 32 kV. Above experimental data could be due to the increasing of electric field force acting on the solutions between the negative plate and positive needle nozzle with increasing the applied voltage, which provides an additional strength to overcome the viscoelastic characteristics and surface tension.

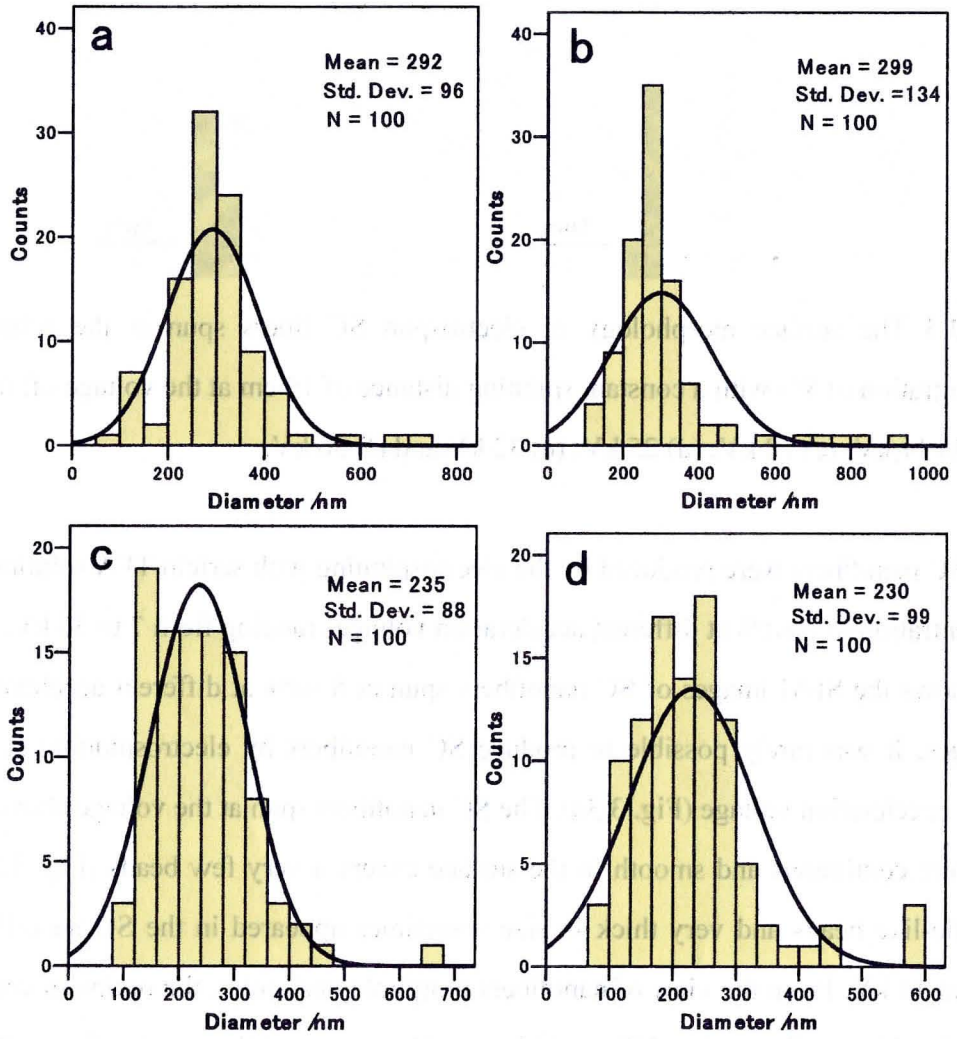

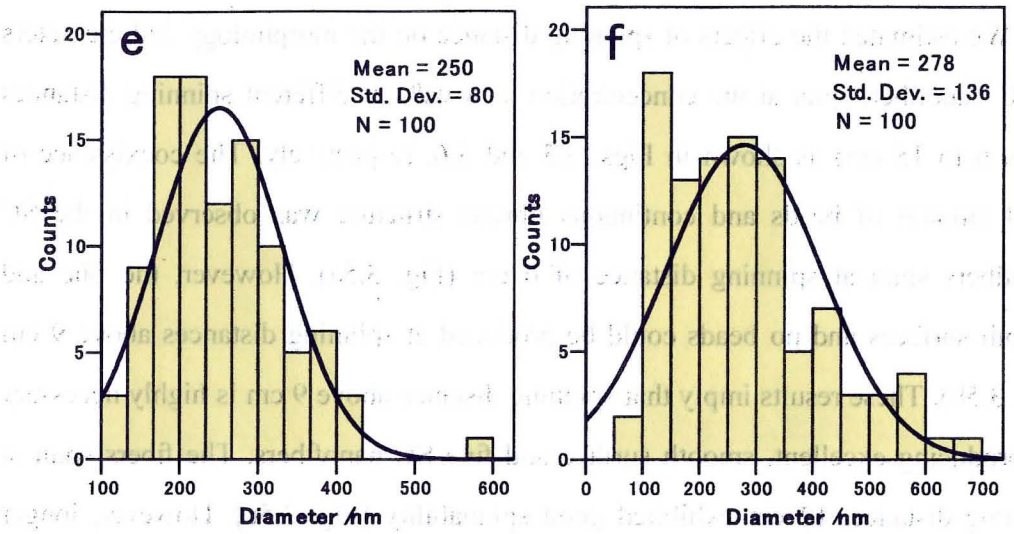

Fig. 3.4 Distribution of fiber diameters of electrospun SC fibers spun at the solution concentration of 8 % with a constant spinning distance of 15 cm at the voltage of: (a) 7 kV; (b) 11 kV; (c) 18 kV; (d) 25 kV; (e) 32kV and (f) 36kV.

3.2.1.3. Effect of spinning distance

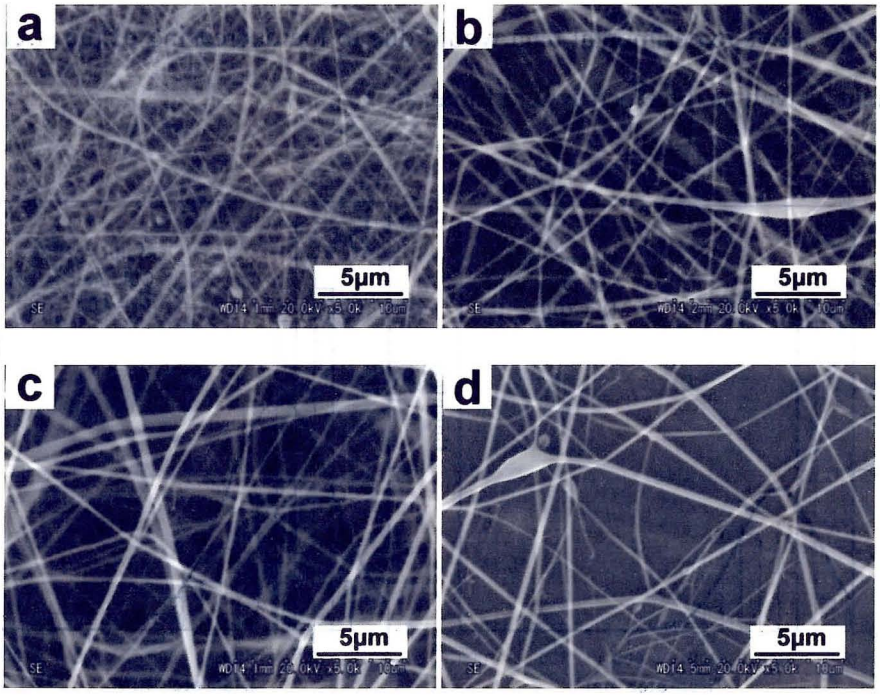

Fig. 3.5 The surface morphology of electrospun SC fibers spun at the solution concentration of 8 % with a constant voltage of 25 kV at spinning distance of: (a) 6 cm; (b) 9 cm; (c) 12 cm and (d) 15 cm.

We estimated the effects of spinning distance on the morphology and diameters of SC nanofiber, spun at the concentration of 8 wt% at different spinning distances (from 6 to 15 cm) as shown in Figs. 3.5 and 3.6, respectively. The coexistence of small amount of beads and continuous fibrous structure was observed in the SC nanofibers spun at spinning distance of 6 cm (Fig. 3.5a). However, the fine and smooth surfaces and no beads could be produced at spinning distances above 9 cm (Fig. 3.5b). These results imply that spinning distance above 9 cm is highly necessary for producing excellent, smooth surface and fine SC nanofibers. The fibers spun at spinning distance, 12 cm exhibited good spinnability [Fig. 3.5c]. However, longer distance (15 cm) was not suitable for fabricating SC nanofibers (Fig. 3.5d). The average fiber diameters were 200 nm ± 113 (SD) and 345 nm ± 147 (SD) at the spinning distance of 6 and 12 cm, respectively (Fig. 3.6). The average diameter of SC fiber slightly increased with increasing spinning distances. At the same time, the variability of diameter of fibers also increased slightly with increasing spinning distance. The above experimental data would due to the decreasing of the strength of electric field as well as the electric field force.

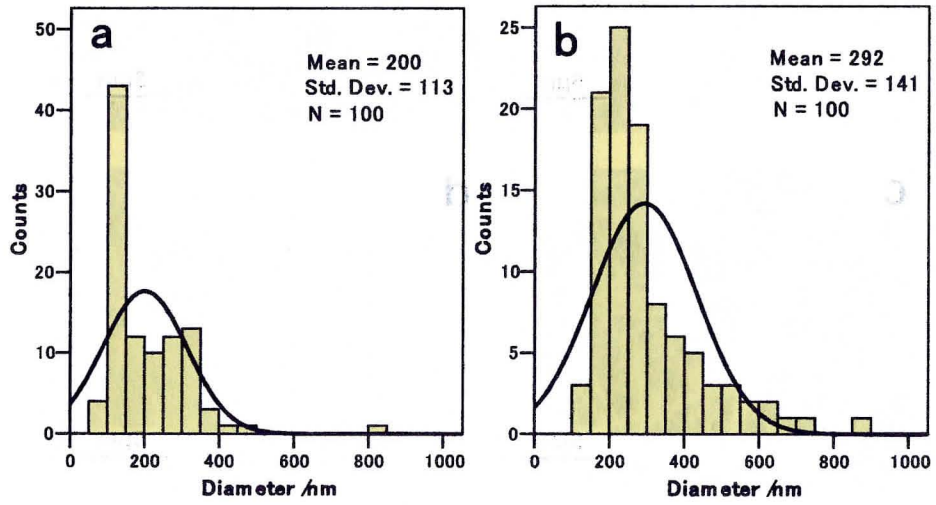

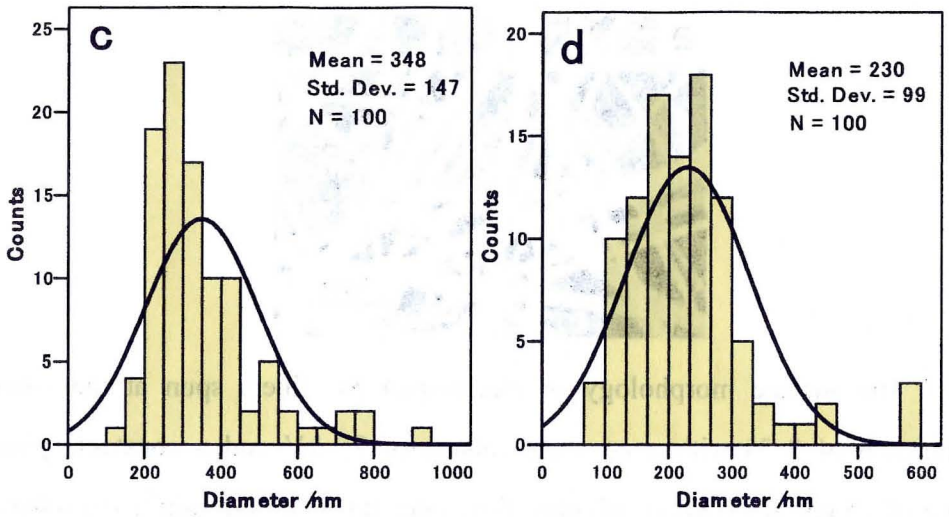

Fig. 3.6 Distribution of fiber diameters of electrospun SC fibers spun at the solution concentration of 8 % with a constant voltage of 25 kV at spinning distance of: (a) 6 cm; (b) 9 cm; (c) 12 cm and (d) 15 cm.

3.2.1.4. Effect of flow rate of spinning solutions

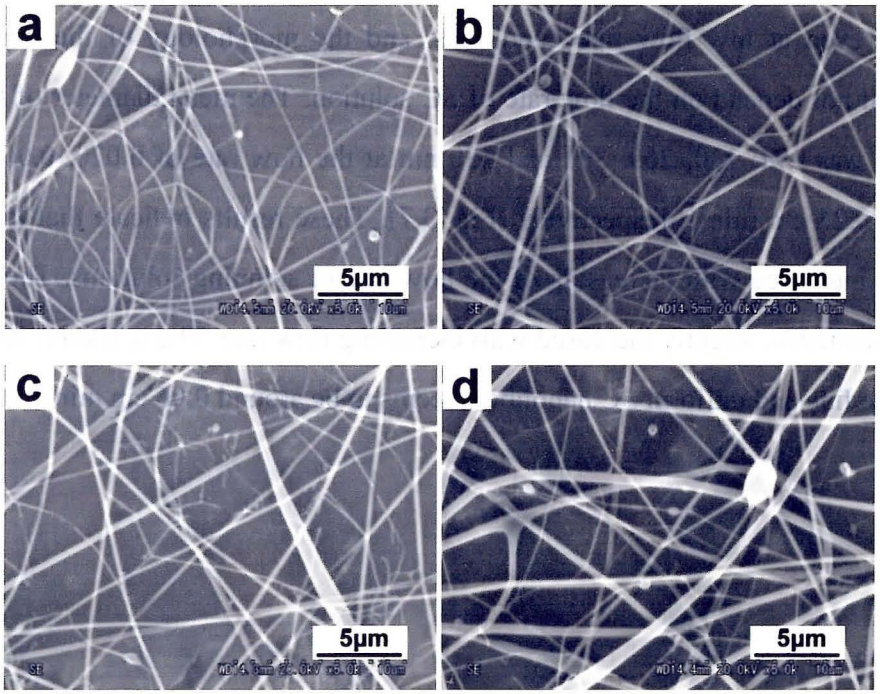

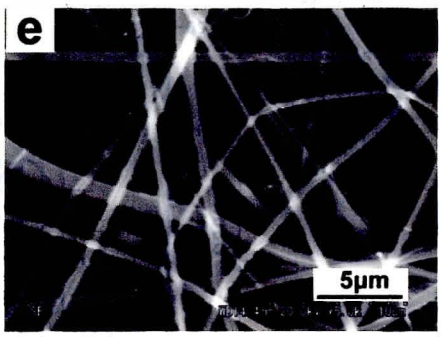

Fig. 3.7 The surface morphology of electrospun SC fibers spun at the solution concentration of 8 % with a constant voltage of 25 kV and a constant spinning distance of 15 cm at different spinning flow rate: (a) 0.020 cm min^{-1}; (b) 0.060 cm min^{-1}; (c) 0.080 cm min^{-1}; (d) 0.150 cm min^{-1} and (f) 0.250 cm min^{-1}.

The ejecting speed of the SS solution from the tip of the syringe was controlled by the syringe pump. The flowing rate of sample solution was adjusted from 0.02 to 0.25 cm min^{-1}. Fig. 3.7 shows the SEM images of SC nanofibers spun at the voltage of 25 kV at different spinning flow rates. Continuous and fine SC nanofibers can be produced even at low flow rate conditions, and the morphology of the deposited sericin did not depend on the flow rate of SC solution. The mean diameter of the SC nanofiber was 194, 230, 269, 301 and 430 nm at the flow rate of 0.020, 0.06, 0.08, 0.15 and 0.25 cm min^{-1}, respectively (Fig. 3.7). These results indicate that the fiber thickness increased with increasing of the flow rate of spinning solutions. The SD of the fiber diameters slightly increased with increasing flow rate. The optimum flow rate to produce fine and uniform SC nanofibers seems to be around 0.06 cm min^{-1}.

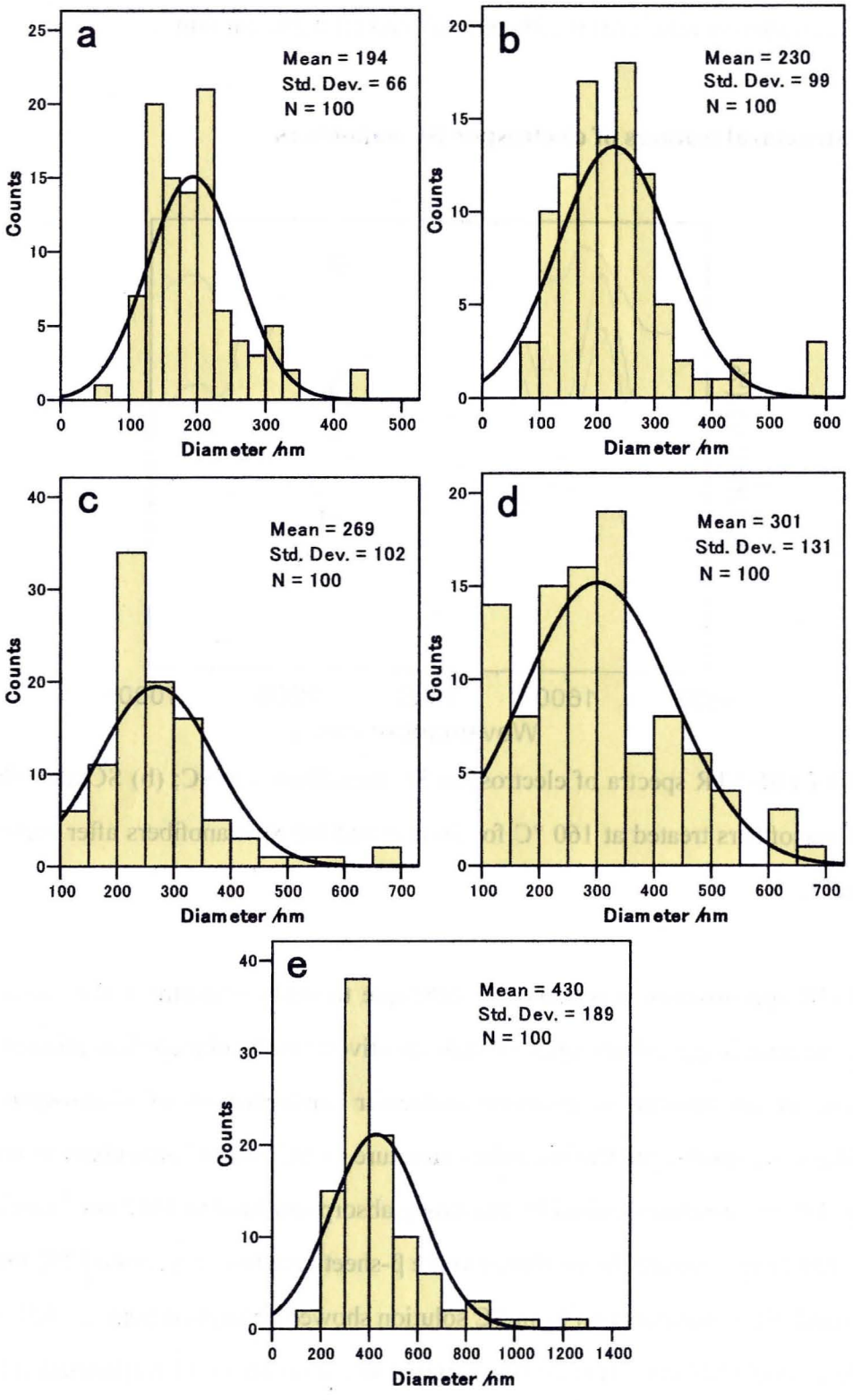

Fig. 3.8 Distribution of fiber diameters of electrospun SC fibers spun at the solution concentration of 8 % with a constant voltage of 25 kV and a constant spinning distance of 15 cm at different spinning flow rate: (a) 0.020 cm min^{-1}; (b) 0.060 cm

min^{-1}; (c) 0.080 cm min^{-1}; (d) 0.150 cm min^{-1} and (f) 0.250 cm min^{-1}.

3.2.2. Structural features of electrospun SC nanofibers

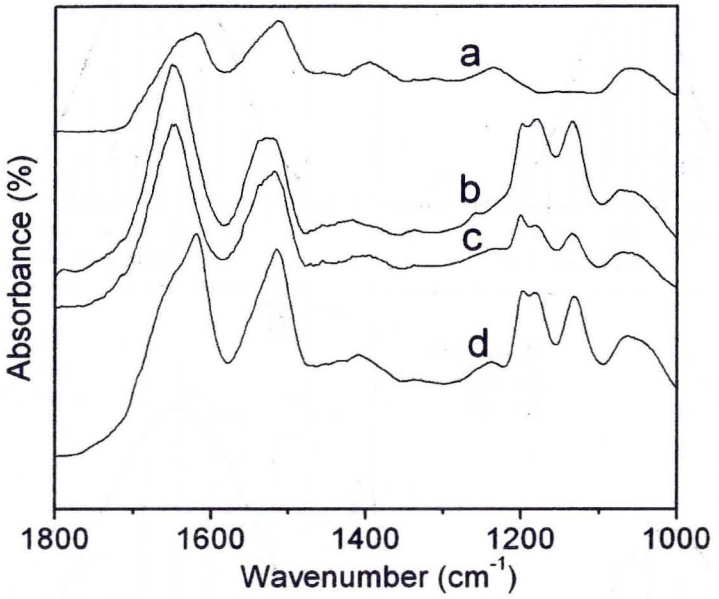

Fig. 3.9 FTIR-ATR spectra of electrospun SC nanofibers: (a) SC; (b) SC nanofibers; (c) SC nanofibers treated at 160 °C for 30 min and (d) SC nanofibers after methanol treatment.

FTIR spectroscopy is a powerful technique to study structure at the molecular level, and reveals typical absorption bands sensitive to molecular conformation of silk proteins. In an attempt to examine molecular conformation of electrospun SC nanofibers, we investigate the secondary structure of SC and SC nanofibers as shown in Fig. 3.9. SC are characterized by the strong absorption band at 1617 cm^{-1} (amide I) and at 1512 cm^{-1} (amide II), attributed to the β-sheet structure (Fig. 3.9a) [29]. On the other hand, SC nanofiber spun from SC solution showed absorption peak at 1651 cm^{-1} (amide I), and 1527 cm^{-1} (amide II), assigned to the random coil conformation (Fig. 3.9b) [30, 31]. In addition, a sharp absorption band exhibited for SC nanofiber at around 1200 cm^{-1} was due to the TFA [32]. After heating fibers at 160 °C for 30 min, the similar random coil conformation was demonstrated, showing the absorption peak

at 1651 cm^{-1} (amide I) and 1527 cm^{-1} (amide II) (Fig. 3.9c). These experimental data suggest that the β-sheet structure of SC breaks in the dissolution process with TFA. It is important to note that the crystallization of SC nanofiber does not occurred by the heat treatment even at elevated temperature. On the contrary, the fibers showed strong β-sheet absorptions at 1618 cm^{-1} (amide I) and 1512 cm^{-1} (amide II) after methanol treatment (Fig. 3.9d).

3.2.3. Thermal behavior of electrospun SC nanofibers

The thermal behavior of SC nanofibers was examined by means of DSC measurement. SC showed the broad and eminent endotherms, one at low temperature (72 °C), due to the evaporation of water, another at high temperature (endo peak at 212 °C), attributed to thermal decomposition of SC with oriented β-sheet configuration (Fig. 3.10a) [33]. The typical endotherm patterns of SC remarkably changed in case of electrospun nanofibers (Fig. 3.10b). The first endotherm became broader and shifted slightly to a lower temperature, 70 °C and the thermal decomposition peak shifted remarkably at a lower temperature, 150 °C. Between two major endotherms, one major exothermic exhibited at 108 °C. These results may cause due to decrease the crystallinity of sericin with conjugation with TFA, occurred according to the following equation:

$$CF_3COOH \rightarrow CO_2 + HCF_3 \qquad (1)$$

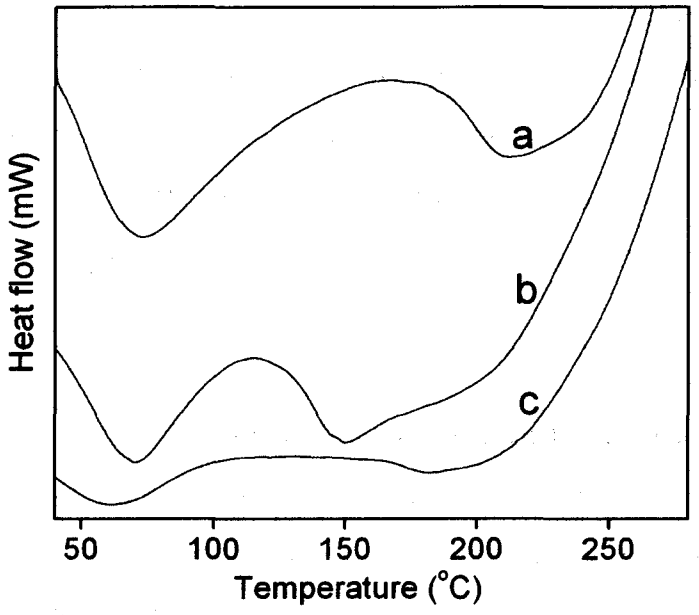

Fig. 3.10 DSC curves of electrospun SC nanofibers: (a) SC; (b) SC nanofibers and (c) nanofibers treated at 160 °C for 30min.

The most interesting feature is that the endothermic peak at 150 °C for SC nanofiber was eliminated after the heat-treatment at 160 °C for 30 min (Fig. 3.10c). As we discussed from the FT-IR spectra, it is assumed that certain amount of TFA presents in SC nanofiber and this small amount of TFA has been removed by the heat-treatment. The disappearance of the endothermic peak at 150 °C is basically due to the removal or evaporation of TFA by the heating at 160 °C.

A TG analysis was very useful to determine quantitatively the degradation behavior and the composition of the fiber. Fig. 3.11 shows TG curves for both the SC and SC nanofibers. For the SC (Fig. 11a), the initial weight loss below 110 °C was attributed to the evaporation of water, and was followed by nearly constant weight from 110 to 190 °C. A second large weight loss took place in the temperature from 215 °C. This was associated with the degradation of side chain groups of amino acid residues and the cleavage of peptide bonds [34]. The weight retention of the SC at 380 °C was 55%. SC nanofiber showed the very rapid and dramatic weight decrease above 120 °C. The position (150 °C) of the major endothermic peak appeared on DSC

curve for SC nanofiber (Fig. 3.10b) coincides with the initiation temperature of TG curves, corresponding to the rapid and dramatic decrease of SC nanofiber (Fig. 3.11b). The weight retention of the sample at 250 and 380 °C was 70% and 42%, respectively. The thermal instability of SC nanofiber was thus observed from basis of TG measurement. After heat treatment, the onset temperature of the second weight loss was shifted to approximately 120 °C (Fig. 3.11c). This may have been related to not only degradation of SC, but also vaporization of the TFA component in the sample. The weight retention of the sample at 250 and 380 °C was about 82% and 49%, respectively.

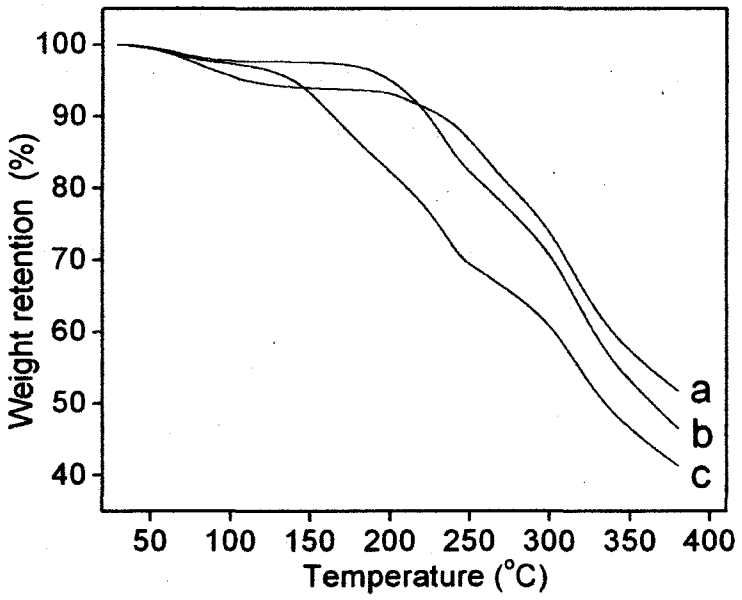

Fig. 3.11 TG curves of electrospun SC nanofibers: (a) SC; (b) SC nanofibers and (c) SC nanofibers treated at 160 °C for 30min.

It has been generally considered that the organic solvent, used in dissolving polymers, can be eliminated during the electrospinning process in the limited distance from the syringe nozzle to the collector target. The experimental results imply that the very little trace of TFA is not eliminated during the electrospinning process, as is obvious from the FTIR spectra of SC nanofiber. However, practical elimination of

TFA could be possible by simple heat-treatment above the position of endothermic peak of 150 °C as described by FTIR, DSC and TG measurements. Since TFA is toxic to the human tissue, simple treatment at 160 °C for 30 min are effective to remove TFA are essentially important, from view of SC nanofiber without TFA for the application in biomedical fields, such as would dressings and scaffolds for tissue engineering.

3.3. Conclusions

The SC were dissolved with TFA, while preserving their polymeric nature. Nano-scale fibers were successfully spun from these solutions by the electrospinning technique. The optimum conditions for producing finely thinner fibrous SC nanofibers without beads were the concentration of SC solution above 6–8 wt%, acceleration voltage ranging from 25 to 32 kV, spinning distance above 9 cm, and flow rate above 0.06 cm min^{-1}. The mean diameter of as spun SC nanofibers varied from 114 to 430 nm at the different spinning conditions. In the as-spun fibers, SC was present in a random coil conformation, while after methanol treatment, the molecular conformation of silk sericin was transformed into a β-sheet containing structure. SC nanofibers demonstrated thermal degradation at lower temperature than SC, which probably due to the randomly coiled rich structure of SC. The availability of SC nanofibers introduces a new set of possible uses of these amazing fibers at a scale not explored before. New uses include small diameter fibers for cell proliferation purposes, nanocomposite reinforcing fibers for nano-technology, wound dressing, scaffolds for tissue engineering and other biomedical applications.

References

[1] S.S. Ojha, D.R. Stevens, T.J. Hoffman, K. Stano, R. Klossner, M.C. Scott, W. Krause, L.I. Clarke, R.E. Gorga, Biomacromolecules, 9, 2523–2529 (2008).

[2] R.R. Klossner, H.A. Queen, A.J. Coughlin, W.E. Krause, Biomacromolecules, 9, 2947–2953 (2008).

[3] H. Fong, I. Chun, D.H. Reneker, Polymer, 40, 4585–4592 (1999).

[4] N. Kattamuri, C. Sung, NSTI-Nanotech, 3, 425–428 (2004).

[5] C.S. Sharma, R. Vasita, D.K. Upadhyay, A. Sharma, D.S. Katti, R. Venkataraghavan, Ind. Eng. Chem. Res., 49, 2731–2739 (2010).

[6] M. Schindler, I. Ahmedb, J. Kamalb, A. Nur-E-Kamalb, T.H. Grafec, H.Y. Chungc, S. Meiners, Biomaterials, 26, 5624–5631 (2005).

[7] Z.M. Huang, Y.Z. Zhang, M. Kotaki, S. Ramakrishna, Combust. Sci. Technol., 63, 2223–2253 (2003).

[8] R. Fedic, M. Zurovec, F. Sehnal, J. Insect Biotech. Sericol., 71, 1–15 (2002).

[9] T. Gamo, T. Inokuchi, H. Laufer, Insect Biochem., 7, 285–295 (1977).

[10] F. Lucas, K.M. Rudall, M. Florkin, K.M. Stotz (Eds.), Comprehensive Biochemistry, 26, 475–558 (1968).

[11] S. Sarovart, B. Sudatis, P. Meesilpa, B.P. Grady, R. Magaraphan, Rev. Adv. Mater. Sci., 5 (3), 193–198 (2003).

[12] K. Komatsu, Nippon Saikingaku Zasshi, 49 (6), 457–465 (1980).

[13] R. Voegeli, J. Meier, R. Blust, Cosmet. Toiletries, 108, 101–108 (1993).

[14] N. Kato, S. Sato, A. Yamanaka, H. Yamada, N. Fuwa, M. Nomura, Biosci. Biotech-nol. Biochem., 62(1), 145–147 (1998).

[15] Y. Tamada, Japan Pat., 09-227402A, 10 (1997).

[16] S. Zhaorigetu, M. Sasaki, H. Watanabe, N. Kato, N. Biosci, Biotechnol. Biochem., 65(10), 2181–2186 (2001).

[17] M. Sasaki, H. Yamada, N. Kato, Nutr. Res., 20(10), 1505–1511 (2000).

[18] Y. Zhang, W. Shen, J. Mao, Y. Ding, Y. Ma, W. Zhou, China Pat., CN 1443840A, 10 (2003).

[19] B.B. Mandal, A.S. Priya, S.C. Kundu, Acta Biomater., 5(8), 3007–3020 (2009).

[20] T. Yamamoto, T. Miyajima, K. Mase, T. Iizuka, BRAIN Techno News, Natl. Inst. Agrochiol. Resour. Jpn., 94, 14–17 (2002).

[21] K. Mase, E. Okada, T. Miyazima, T. Yamamoto, Bio Industry, 24(11), 53–59 (2007).

[22] K. Mase, T. Iizuka, E. Okada, T. Miyajima, T. Yamamoto, J. Insect Biotech. Sericol., 75 (2), 85–88 (2006).

[23] H. Teramoto, K.I. Nakajima, C. Takabayashi, Biomacromolecules, 5, 1392–1398 (2004).

[24] H. Teramoto, A. Kakazu, K. Yamauchi, T. Asakura, Macromolecules, 40, 1562-1569 (2007).

[25] H.Teramoto, T.Kameda, Y. Tamada, Biosci. Biotechnol. Biochem., 72, 3189-3196 (2008).

[26] H. Teramoto, K.I. Nakajima, C. Takabayashi, Biosci. Biotechnol. Biochem., 66, 845–847 (2005).

[27] B. Veleirinho, M.F. Rei, J.A. Lopes-da-Silva, J. Polym. Sci. B: Polym. Phys., 46, 460–471 (2008).

[28] X.H. Zong, K. Kim, D.F. Fang, S.F. Ran, B.S. Hsiao, B. Chu, Polymer, 43, 4403–4412 (2002).

[29] N.V. Bhat, S.M. Ahirrao, J. Polym. Sci. A: Polym. Chem., 21, 1273–1280 (1983).

[30] J. Shao, J. Zheng, J. Liu, C.M. Carr, J. Appl. Polym. Sci., 96, 1999–2004 (2005).

[31] A.B. Mathur, A. Tonelli, T. Rathke, S. Hudson, Biopolymers, 42, 61–74 (1997).

[32] J.C. Yu, W. Ho, J. Yu, S.K. Hark, K. Iu, Langmuir, 19(9), 3889–3896 (2003).

[33] K.Y. Cho, J.Y. Moon, Y.W. Lee, K.G. Lee, J.H. Yeo, H.Y. Kweon, K.H. Kim, C.S. Cho, Int. J. Biol. Macromol., 32, 36–42 (2003).

[34] G. Freddi, M. Tsukada, S. Beretta, J. Appl. Polym. Sci., 71, 1563–1571 (1999).

Chapter 4

Fabrication and physical properties of electrospun tussah silk fibroin nanofibers

Chapter 4: Fabrication and physical properties of electrospun tussah silk fibroin nanofibers

4.0. Introduction

Silk protein polymers that are produced by silkworms are classified into two general groups: wild type (Antheraea pernyi etc.) and domestic type (Bombyx mori) silkworms. Tussah silk, which is produced by Antheraea pernyi, is commercially important, as is silk from Bombyx mori (B. mori). Among the wild silks, the silk produced by Antheraea pernyi (A. pernyi), tussah silk, is the most popular for production and use. The physical properties and chemical reactivity of both B. mori and tussah silk fibroin have been the subject of both fundamental and applied research for textile materials and biotechnological and biomedical applications.

It has been revealed that B. mori silk fibroin has been electrospun with different solvents or blended with other polymers, including chitosan [1], chitin [2] and gelatin [3]. Zhang et al. demonstrated that B. mori silk fibroin/tussah silk fibroin (SF/TSF) nanofibers can be produced with diameters between 300 and 3500 nm using the solvent, hexafluoroisopropanol (HFIP). They demonstrated that the average diameter of the SF/TSF blend fiber increased from 404 to 1977 nm with an increase in the SF content of the blend solution [4]. According to their results, the SF/TSF blend nanofibers are supposed to be an excellent substrate for cell attachment.

The chemical structure of TSF is rather different from that of B. mori silk fibroin. The alanine content of TSF is higher than that of glycine, and furthermore, the amount of basic (lysine, histidine and arginine) and acidic (aspartic and glutamic acid) amino acid residues of TSF is higher than that of B. mori silk fibers [5]. It has been revealed that basic and acidic amino acids, as well as tyrosine, have side groups that are chemically reactive toward agents [6].

TSF fibers are a type of wild silk, and their chemical structure, molecular conformation, as well as physical properties, have been extensively studied [7]. It has been demonstrated that the crystalline structure of the TSF fibers is composed of sequential poly(L-alanine). Because of these physical properties, TSF fibers do not

dissolve in high concentrations of neutral salts, including $CaCl_2$ and LiBr, even at elevated temperatures, while B. mori silk fibers can be dissolve in these neutral salt solutions at lower temperatures. These differences in the solubility of TSF fibers in salt solutions are primarily because of the well organized intermolecular and intramolecular hydrogen bonding properties of poly(L-alanine). Research into structural changes of TSF fibers and the B. mori silk fiber has been conducted to determine structural changes in the silk fibers as a result of heat treatment by taking changes in molecular orientation into account in the amorphous, laterally ordered and crystalline regions [8].

TSF is a potential biomaterial because TSF has chemically active amino acids, basic amino acids and acidic amino acids. He et al. analyzed the structures and properties of novel electrospun TSF/poly(lactic acid) composite nanofibers, which were produced with different composition ratios of TSF and poly(lactic acid) and the solvent (HFIP) [9]. It has been found that TSF/poly(lactic acid) composite nanofibers are potentially important biomaterials for medical applications because of their biodegradable behavior.

Electrospinning is inexpensive and uncomplicated, and can be used to produce polymer nanofibers with diameters from the microscale to the nanoscale range. Our research group has determined the optimum conditions to produce silk sericin/silk fibroin blend nanofibers using the solvent of TFA, and we have determined several physical properties, including their thermal properties and their molecular conformations [10].

The average diameters of the polymer nanofibers are primarily effected by the physical factors of polymer solutions such as surface tension, viscosity and conductivity, as well as the electrospinning conditions such as applied acceleration voltage, flow rate and spinning distance. For industrial application, the important factors for excellent polymer nanofibers are fine and uniform morphologies, which directly determine the surface smoothness of the nanofibers.

The goal of in this chapter is to produce TSF nanofibers with smaller diameters, a narrow diameter distribution, smooth surfaces and bead-free structures by

electrospinning from TSF in an organic solvent. The effects of the solution variables and the electrospinning process on the morphological appearance and average diameter of the as-spun TSF fibers were examined. The structural properties of the TSF nanofibers were examined using fourier transform infrared spectroscopy, differential scanning calorimetry and thermogravimetry.

According to the research result [4] on electrospun composite silk nanofibers made of B. mori and TSF, the obtained results in this chapter studies may allow for better technological applications, and for the exploitation of TSF nanofibers in medical applications, including wound dressings and drug delivery systems [11]. Additionally TSF nanofibers are promising candidate scaffold materials for tissue engineering and can extend our knowledge of the relationship between the structure and functional properties of these natural fibrous fibers.

4.1. Experiments

4.1.1. Materials

TSF fibers from A. pernyi were obtained from the reeling of TSF cocoon threads. TSF fibers were cleaned by an acetone/ethanol mixture system to remove the wax, rinsed in distilled water and dried to constant weight. TSF fibers were degummed in aqueous solutions containing sodium carbonate (3 g/L), sodium metasilicate (3 g/L) and Marseilles soap (2 g/L) at 98-100 °C for 90 min to remove the silk sericin. Finally the degummed TSF fiber was washed thoroughly with running water for 2 h. The TSF fiber was thus obtained after degumming.

4.1.2. Preparation of the TSF solution

TFA purchased from Wako Pure Chemical Industries, Ltd was used without purification. The degummed TSF fiber was dissolved in TFA. The TFA solution containing the TSF fiber was stirred continuously at 25 °C or 40 °C with a magnetic stirrer. A TSF TFA solution was thus prepared. The concentrations of the TSF solution ranged between 2 and 12 wt%.

4.1.3. Electrospinning

The electrospinning instruments were from the Kato Tech. Company, Japan. The TSF solution was drawn into a 1 ml syringe (SS-01T, Terumo Corporation, Tokyo, Japan) using a 21 gauge stainless needle (inner diameter 0.3 mm, 38 mm long, NN-2238N, Terumo Corporation, Tokyo, Japan), which was connected to a high voltage power supply. We adapted the optimum electrospinning conditions throughout the experiment. The flow rate was controlled at 25 μl/min using a syringe pump. A high voltage of around 25 kV was applied to a droplet of the TSF TFA solution at the tip. Ground aluminum foil was placed 15 cm from the capillary tip. When a TSF solution droplet formed at the tip of the needle a jet was ejected with an increase in voltage and TSF nanofibers were produced on the aluminum collection screen.

4.1.4. Characterization

The surface morphologies of the electrospun fibers were examined using scanning electron microscopy (SEM) (S-2380N, Hitachi, Japan). The samples were mounted onto an aluminum stud and sputter-coated with gold/palladium for 180 s (E-1010 ION SPUTTER, Hitachi, Japan) to prevent charging.

The average diameters and the standard distribution of the TSF nanofibers were measured at different 100 places of the samples with downloaded Makijaku soft program (Hiroyoshi Iwata, file version 1.1.0.0) from the internet. Then, histogram and normal distribution curves were drawn with using a commercial statistics software package, SPSS (IBM SPSS Statistics Desktop for Version19.0) soft program.

Fourier transform infrared (FT-IR) spectroscopy was measured with a Shimadzu FT-IR-8400S infrared spectrometer by the ATR method in the region of 4000-400 cm^{-1} at room temperature. The treatment of the TSF nanofibers with methanol solution was performed with a binary system of methanol and water (50 wt%) according to the vapor annealing procedure at room temperature for 3 days using a similar technique to that of Hu et al. [12].

Differential scanning calorimetry (DSC) measurement was performed by a Rigaku Denki Co., Ltd. instrumental (model DSC-8230) at a heating rate of 10 °C

min^{-1} under N_2 gas atmosphere.

Thermogravimetric (TG) analysis was carried out with a Rigaku Thermo plus TG 8120 under N_2 gas at a heating rate of 10 °C min^{-1}.

4.2. Results and discussion

4.2.1. Morphologies and standard deviation of TSF nanofibers

The dissolution parameters, including sample concentration, dissolution temperature, strongly affect the morphology and diameter of the electrospun nanofibers [13-14]. Determining the relationship between the morphology of the polymer nanofibers and the dissolution parameters is an important research theme.

The influence of the TSF TFA concentration on the morphology of the TSF nanofibers was examined after obtaining SEM micrographs of TSF nanofibers.

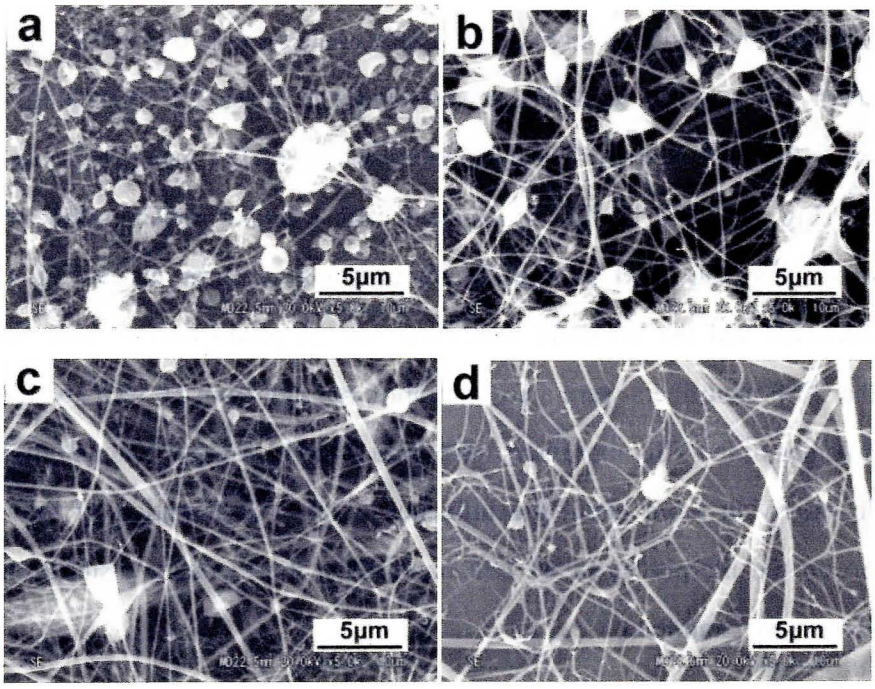

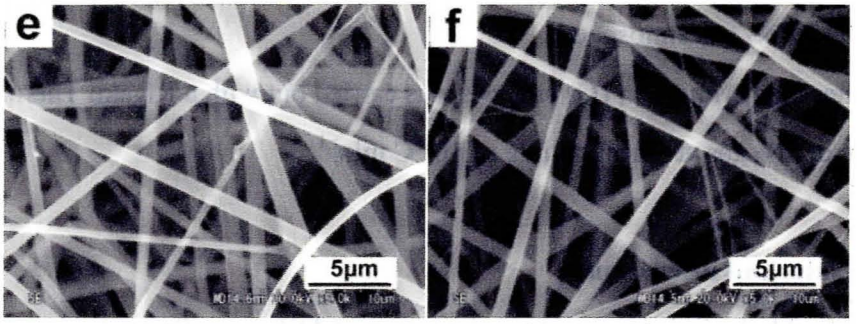

Fig. 4.1 SEM micrographs of TSF nanofibers spun from different concentrations of TSF TFA solution, prepared by dissolving TSF fiber at 25 °C in TFA.
Sample: (a) 2%; (b) 4%; (c) 6%; (d) 8%; (e) 10% and (f) 12%.

After the electrospinning process with a low concentration of less than 6 wt%, thin TSF nanofibers containing a large number of bead defects and big irregular form beads were produced, because of the instability of the jet by the effect of surface tension in the presence of electrical forces (Fig. 4.1a and b). The number of beads gradually decreased with an increase in sample concentration of 6 wt% or 8 wt%. TSF nanofibers with thin and thick fibers were observed in the TSF mats (Fig. 4.1d) that were spun from the 8 wt% TSF TFA solution. These TSF nanofibers have smooth surfaces (Fig. 4.1e and f). The fibers spun from a higher concentration of the TSF solution (higher than 10 wt %) were thinner and more uniform in size (Fig. 4.1e and f). We concluded that the optimum conditions for the production of fine, thinner and smoother TSF nanofibers were a concentration ranging from 10 wt% to 12 wt%. The morphologies of the TSF nanofibers were influenced by sample concentration.

To clarify in more detail the influence of the concentration of the TSF TFA solution on the morphologies of TSF nanofibers, the diameter distribution of TSF nanofibers were examined.

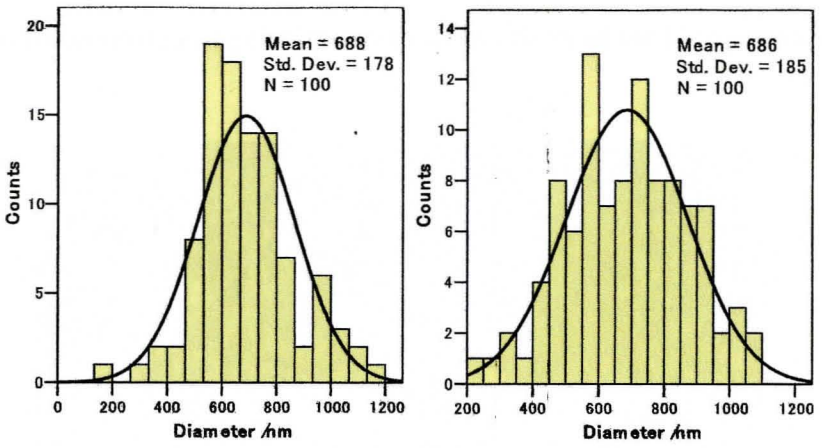

(a) (b)

Fig. 4.2 Average diameters and their distributions of TSF nanofibers spun from different concentrations of TSF TFA solution, prepared by dissolving TSF fiber at 25 °C in TFA. Sample: (a) 10wt% and (b) 12wt%.

Fig. 4.2 shows the diameter distributions of TSF nanofibers obtained from a sample concentration of 10 wt% and 12 wt% and these were prepared by dissolving the TSF fibers at 25 °C in TFA. The fiber diameters for each solution concentration followed the normal distribution curve. The average diameters of TSF nanofibers spun from 10 wt% and 12 wt% were the same about 690 nm. The trend of the mean diameter of TSF nanofibers was independent of the concentration of the solutions, which were 10 wt% and 12 wt%. The standard deviation (SD) of the diameter of TSF nanofibers was almost the same or increased slightly with an increase in the sample concentration.

Fig. 4.3 shows SEM micrographs of TSF nanofibers spun from different concentrations for the TSF TFA solution, which was prepared by dissolving the TSF fiber at 40 °C at a voltage of 25 kV.

A large number of irregular form bead defects and large irregular form bead defects were produced (Fig. 4.3a,b,c) from 2 wt%, 4 wt% and 6 wt% TSF TFA solutions. The number of beads decreased with an increase in the sample concentration up to 6 wt% or 8 wt%, while the number of nanoscale order fine TSF fibers increased when the sample concentration increased to 6 wt%. Fine and thinner

TSF nanofibers could not be produced by electrospinning from lower concentrations

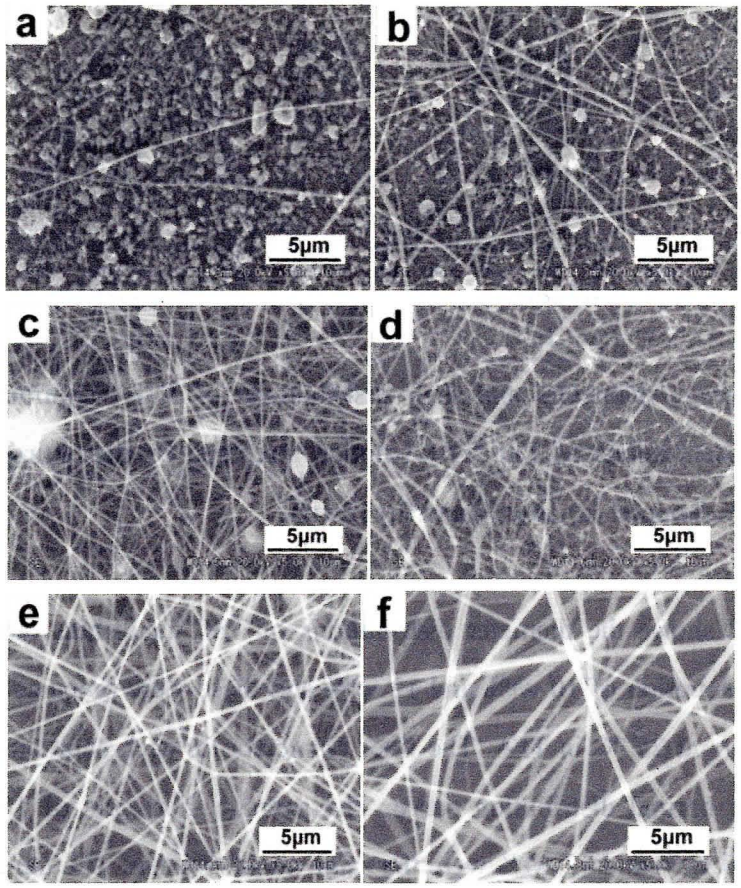

Fig. 4.3 SEM micrographs of TSF nanofibers spun from different concentration of TSF TFA solution, prepared by dissolving TSF fiber at 40°C in TFA.
Sample: (a) 2%; (b) 4%; (c) 6%; (d) 8%; (e) 10% and (f)12%.

of TSF (Fig. 4.3 a,b and c). TSF nanofibers (Fig. 4.3d) without beads were produced from more than 8 wt% TFA solutions. The TSF fibers (Fig. 4.3e and f) have smooth surfaces. Thus, it was assumed that TSF nanofibers can be spun into fine and thinner fibers at concentrations higher than 8 wt%.

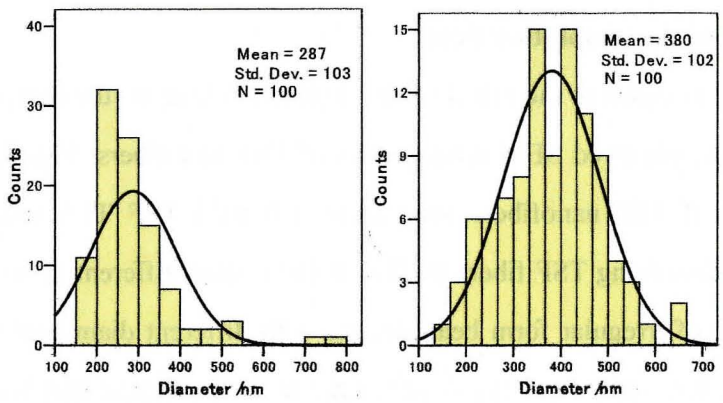

(a) (b)

Fig. 4.4 Average diameters and their distributions of TSF nanofibers spun from different concentrations of TSF TFA solution, prepared by dissolving TSF fiber at 40°C in TFA. Sample: (a) 10wt% and (b) 12wt%.

Fig. 4.4 shows the average diameter distributions of TSF nanofibers obtained from the 10 wt% and 12 wt% sample TFA solutions that were prepared by dissolving TSF fibers in TFA at 40 °C. The fiber diameters at each solution concentration also followed a normal distribution curve. The average diameters of TSF nanofibers spun using 10 wt% and 12 wt% were 287 nm and 380 nm, respectively. The average diameter of TSF nanofibers increased slightly with an increase in sample concentration. The SD of the diameter of the nanofibers was similar regardless of the different sample concentrations.

In order to evaluate the significant of the difference in the mean value between the TSF nanofibers, prepared by dissolving at 25 and 40 °C, t test was performed. After calculation of t values for TSF nanofiber from 10wt% TSF TFS solution, prepared by dissolving at 25 and 40 °C was -19.5, and -14.9, respectively, suggesting that these mean values of TSF nanofibers are significant difference at the 0.01 level between them.

According to the test of the mean values of TSF nanofibers spun from 10wt% and 12wt% solution (Fig. 4.4), the significance of the average mean values are regarded statistically different at the 0.01 level.

4.2.2. Effect of the dissolution time

In order to examine the effect of the dissolution time on the morphology of TSF nanofibers, we observed SEM micrographs of TSF nanofibers. Fig. 4.5 shows SEM micrographs of TSF nanofibers spun from a 6 wt% TSF TFA solution that was prepared by dissolving TSF fibers in TFA at 40 °C over different dissolution times. A large number of irregular form bead defects with different diameters were produced (Fig. 4.5a) when spun from the 6 wt% sample TFA solution that was prepared by dissolving the TSF fiber at 40 °C for 2 d. The number of beads in the TSF nanofibers spun from the 6 wt% TSF TFA solution that was prepared by dissolving the TSF fiber for 3 d decreased slightly compared with that of TSF nanofibers (Fig. 4.5a, b). TSF fibers (Fig. 4.5b) have smooth surfaces. However, irregular form beads without fine TSF nanofibers were dominant in the TSF mats that were spun from the 6 wt% TSF TFA solution, which was prepared by dissolving the TSF fibers at 40 °C over 8 d.

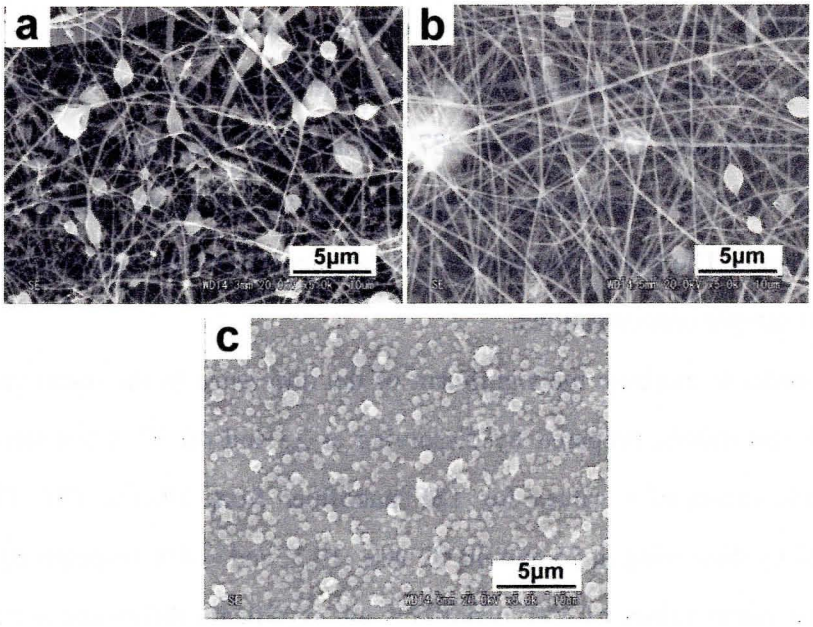

Fig. 4.5 SEM micrographs of TSF nanofibers electrospun from 6 wt% TSF TFA solution, prepared by dissolving TSF fiber at 40°C in TFA. Dissolving time (day): (a) 2; (b) 3 and (c) 8.

From the above SEM images of TSF nanofibers (Fig. 4.5), it is obvious that the

morphologies of TSF nanofibers are greatly influenced by the dissolution time. Fig. 4.6 shows SEM micrographs of TSF nanofibers that were spun from the 12 wt% TSF TFA solution that was prepared by dissolving TSF fibers at 45 °C in TFA over different dissolution times.

The average diameter of TSF nanofibers that were spun from the 12 wt% TSF TFA solution at dissolution times of 24, 32, 36 h were 11,000, 1013, and 596 nm, respectively. The diameter values of TSF nanofibers very markedly differed from the microscale order to the nanoscale order and this was dependent on the dissolution time, even at the same dissolution temperatures. TSF nanofibers were not observed in the TSF mats that were spun from the 12 wt% TSF TFA solution that was prepared by dissolving the TSF fibers at 45 °C in TFA at a dissolution time of 60 h.

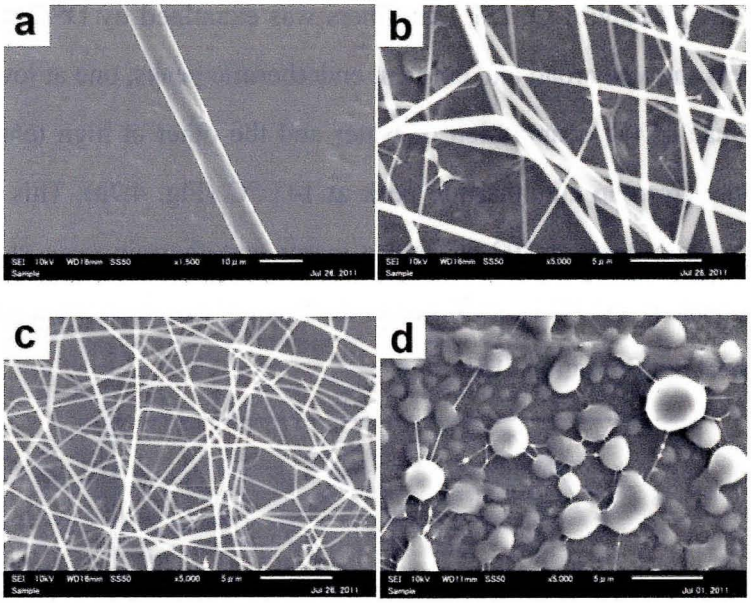

Fig. 4.6 SEM micrographs of TSF nanofibers electrospun from 12 wt% TSF TFA solution, prepared by dissolving TSF fiber at 45 °C in TFA for different period of dissolving time (hr). Dissolving time (hr): (a) 24; (b) 32; (c) 36 and (d) 60.

Assuming that the molecular weight of TSF decreases significantly with an increase in the dissolution time at elevated temperatures, changes in the average diameter and changes in the morphologies of TSF nanofibers occur because of

changes in the molecular weight of TSF during the dissolution process. The SEM micrographs (Fig. 4.6) suggest that the production of dominant beads without fine TSF nanofibers is due to the excessive decrease in molecular weight of the TSF TFA solution if the dissolution time exceeds 60 h at dissolution temperature of 45 °C.

The average diameter of TSF nanofibers spun from a 10 wt% TSF TFA solution at 25 °C for 11 d and at 40 °C for 4 d was 688 and 287 nm, respectively, suggesting that the diameter of the TSF nanofibers are profoundly influenced by a combination of factors such as dissolution temperature and dissolution time (Fig. 4.2, Fig. 4.4). It seems that the dissolution temperature and the dissolution time have an effect on the morphology of TSF nanofibers.

4.2.3. Thermal behavior of electrospun TSF nanofibers

The thermal behavior of TSF nanofibers was examined by DSC measurements. The TSF fibers showed broad and eminent endothermic peaks, one at low temperature (79 °C) because of the evaporation of water and the other at high temperature as a minor shoulder from an endothermic peak at 143 °C (Fig. 4.7a). This sample has a minor endothermic peak at 292 °C and a major endothermic peak at 363 °C. The endothermic peak at 363 °C is attributed to the thermal decomposition of TSF with an oriented β-sheet configuration [15].

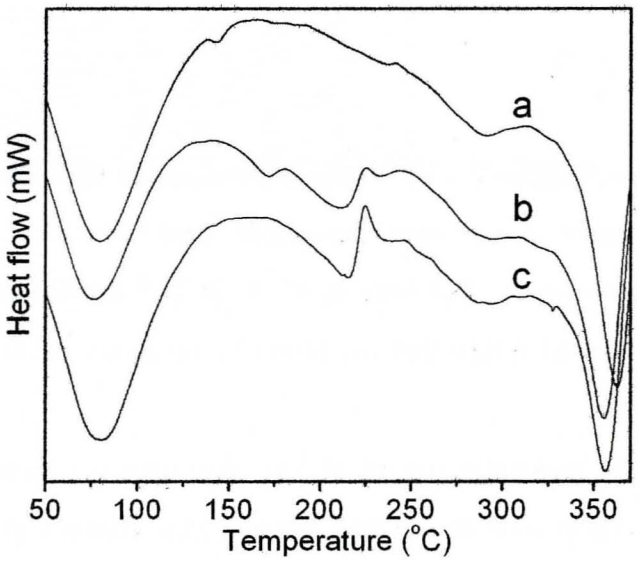

Fig. 4.7 DSC curves of TSF nanofibers spun from 10wt% TSF TFA solution, prepared

by dissolving TSF fiber at 40 °C in TFA. Sample: a TSF fiber; b TSF nanofiber and c TSF nanofiber, heat treated at 160 °C for 1 hr.

On the DSC curve of TSF nanofibers (Fig. 4.7b), the first endothermic peak appeared at around 76 °C. The TSF nanofibers showed new endothermic peaks at 172, 213 and 293 °C. The minor endothermic peak at 172 °C for TSF nanofibers (Fig. 4.7b) disappeared completely after heat-treatment at 160 °C over 1 h. The disappearance of the endothermic peak at 172 °C for TSF nanofibers (Fig. 4.7c) may coincide with the removal of a certain amount of TFA from the sample by heat-treatment. The DSC curves of the sample (Fig. 4.7c) is almost the same as that of TSF nanofibers (Fig. 4.7b) at higher than 180 °C.

The thermal instability of TSF nanofibers was evaluated by TG measurements. TG analysis was very useful for the quantitative determination of the degradation behavior and the composition of the TSF fibers. Fig. 4.8 shows TG curves for both the TSF fiber and TSF nanofibers.

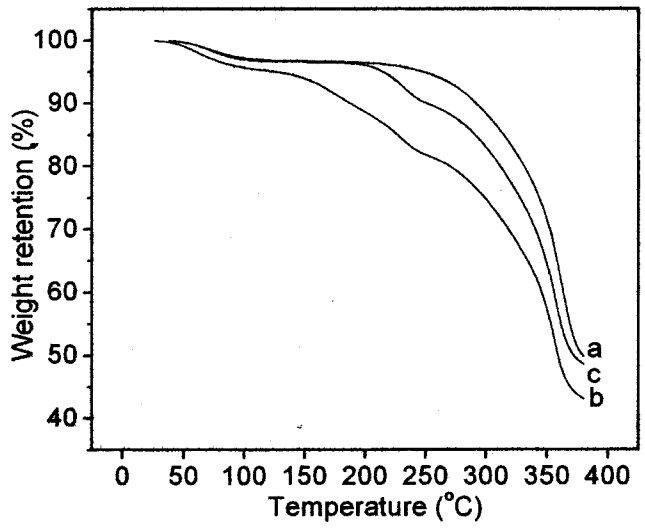

Fig. 4.8 TG curves of TSF nanofibers spun from 10wt% TSF TFA solution, prepared by dissolving TSF fibers at 40°C in TFA. Sample abbreviations are the same that in Fig. 4.7.

The weight loss of the TSF fibers (Fig. 4.8a) at less than 110 °C is attributed to the evaporation of water and this was followed by a near constant weight from110 to 250 °C. A second large weight loss for the TSF fibers was evident above 260 °C. This is associated with the degradation of the side chain groups of the amino acid residues and the cleavage of the peptide bonds [16].

The weight retention of the TSF fiber (Fig. 4.8a) at 380 °C was 50%. The TSF nanofibers (Fig. 4.8b) showed a very rapid and dramatic weight decrease above 120 °C. The position of the minor endothermic peak around 172 °C on the DSC curve of TSF nanofibers (Fig. 4.7b) coincides with the initiation of a rapid and dramatic weight decrease of the TSF nanofibers (Fig. 4.8b). The weight retention of TSF nanofibers(Fig. 4.8b) at 250 and 380 °C was 83% and 45%, respectively. The thermal stability of TSF nanofibers increased significantly by heat treatment at 160 °C for 1 h.

After heat treatment, the onset temperature of the second weight loss was shifted approximately to 200 °C (Fig. 4.8c). The weight retentions of TSF nanofibers at 250 and 380 °C, which had been heat-treated at 160 °C for 1 hr were about 92% and 52%, respectively (Fig. 4.8c). This may be related to the thermal stability because of the removal of TFA, which is present in the sample by thermal treatment at elevated temperatures.

4.2.4. FTIR Spectra of the electrospun TSF nanofibers

To determine the molecular conformation of TSF nanofibers were measured by FTIR (Fig. 4.9). The TSF fibers (Fig. 4.9a) are characterized by the strong absorption bands at 1621 cm^{-1} (Amide I) and at 1511 cm^{-1} (Amide II), which are attributed to the β-sheet structure [17-18] and minor absorption bands were present at 1447, 1221, 1166, 1051 and 964 cm^{-1}. The TSF nanofibers (Fig. 4.9b) that were spun from the TSF TFA solution showed absorption peaks at 1650 cm^{-1} (Amide I) and 1537 cm^{-1} (Amide II), and these can be assigned to the α-helix [17-18] and the random coil conformations [19-20].

The TSF nanofibers (Fig. 4.9b) showed an absorption band at 1519 cm^{-1} (Amide II) and specific absorption bands at 1199, 1175, 1135, 1049 cm^{-1}, while the absorption

peaks are absent for the TSF fiber (Fig. 4.9a). It is assumed that TSF nanofibers spun from the TSF TFA solution possesses an α-helix and a random coiled form, and it does not take on β-sheet structure.

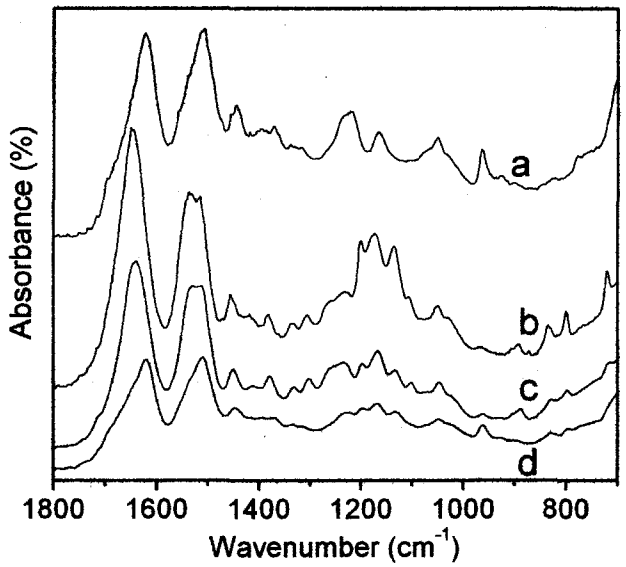

Fig. 4.9 FITR spectra of TSF nanofibers spun from 10wt% TSF TFA solution, prepared by dissolving TSF fiber at 40 °C in TFA.
Sample: a TSF fiber; b TSF nanofiber; c TSF nanofiber, heat treated at 160 °C for 1 hr and d TSF nanofiber, treated with 50% methanol at 25 °C for 3 days.

The FTIR spectrum of TSF nanofibers (Fig. 4.9c) was measured after heat treatment at an elevated temperature of 160 °C. The temperature of 160 °C was selected to determine the cause of the endothermic peak of TSF nanofibers around 170 °C on the DSC curve (Fig. 4.7b).

The TSF nanofibers that were heat-treated at 160 °C for 1 h (Fig. 4.9c) showed almost the same FTIR absorption band as TSF nanofibers (Fig. 4.9b) except for the decrease in intensities of the absorption bands around 1200 cm^{-1} for TSF nanofiber. The above FTIR data indicates that heat-treatment at 160 °C does not induce structural changes in the molecular conformation of TSF nanofibers. The most drastic change in the FTIR spectra occurred for TSF nanofibers, which were treated at room temperature by methanol/water vapor annealing [21]. Actually, the TSF nanofibers,

treated by methanol/water vapor annealing showed absorption bands at 1625 cm^{-1} (Amide I) and 1514 cm^{-1} (Amide II), which can be assigned to the β-sheet structure [17-18]. Therefore, the TSF nanofibers, having α-helix and the random coil conformation were crystallized. Their molecular conformation transformed clearly into a β-sheet structure after methanol/water vapor annealing. It is important to note that the crystallization of TSF nanofibers proceeds effectively by methanol/vapor annealing and not by heat treatment even at elevated temperatures.

To clarify the absorption peaks around 1200 cm^{-1} of TSF nanofibers (Fig. 4.9b), the FTIR spectrum of TFA was measured (Fig. 4.10). The major absorption bands for TFA appeared at 1777 and 1155 cm^{-1} and minor absorption bands at 1459, 812 and 783 cm^{-1}. The wave number of the major absorptions of TSF nanofibers (Fig. 4.9b) at 1199, 1175 cm^{-1} coincides with that of the major absorption at 1155 cm^{-1} of TFA.

These data imply that a trace amount of TFA is present on the molecular level in TSF nanofibers.

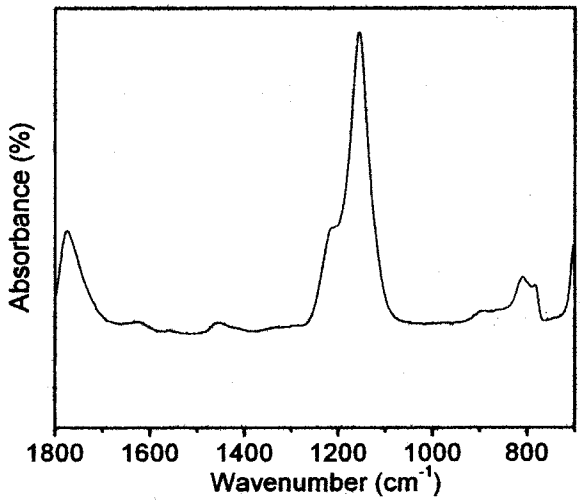

Fig. 4.10 FTIR spectrum of TFA. FTIR measurement was performed by FTIR analysis with an ATR (Atenuated Total Reflectance) accessory.

Many reports have been published [2-3, 9] on silk fibroin nanofibers. However, there is no literatures mentioning the presence of organic solvents in the polymer nanofibers.

It has been considered that the organic solvent used to dissolve polymers can be eliminated and/or evaporated during the electrospinning process over the limited distance from the syringe nozzle to the collector target. However, the experimental data suggests that trace of TFA exists in TSF nanofibers. A trace of TFA might be bound to the polymer molecules could not be eliminated in the electrospinning process.

To apply TSF nanofibers to the biomedical field as the substrate wound dressings and scaffolds for tissue engineering, the complete removal of TFA is preferable, since TFA is toxic to human body and living cells. The combination of heat-treatment at elevated temperature and immersion treatment in methanol could be possible to remove the TFA contained in TSF nanofibers.

The TSF nanofibers become insoluble in water after the methanol/water vapor annealing can be applied in the tissue engineering field, such as the candidate of scaffold materials and would recovery systems.

TSF possesses a large number of chemically reactive amino acides, such as basic amino acids, lysine, arginine and histidine. These chemically reactive sites could be the reactive sites for chemical modification with epoxide compounds and dibasic acid anhydrides etc. Chemically modified TSF nanofibers may be useful protein materials, which can be used in the application in biomedical fields.

4.3. Conclusions

TSF can be dissolved in TFA, while preserving their polymeric nature. Nano-scale fibers were successfully spun from these solutions by the electrospinning technique. The optimum conditions for producing finely thinner TSF nanofibers without beads were the concentration of TSF solution above 10 wt%. In the as-spun fibers, TSF nanofibers was present in a random coil conformation, while after methanol treatment, the molecular conformation of TSF was transformed into a β-sheet containing structure.

References

[1] W.H. Park, L. Jeong, D.I. Yoo, S. Hudson, Polymer, 45(21), 7151-7157 (2004).

[2] K.E. Park, S.Y. Jung, S.J. Lee, B.M. Min, W.H. Park, Int J. Biol Macromol., 38, 165-173 (2006).

[3] G. Yin, Y. Zhang, W. Bao, J. Wu, D. Shi, Z. Dong, W. Fu, J. Appl. Polym Sci, 111, 1471-1477 (2009).

[4] F. Zhang, B. Zuo, H. Zhang, L. Bai, Polymer, 50, 279-285 (2009).

[5] G. Freddi, H. Shiozaki, G. Allara, Y. Goto, H. Yasui, M. Tsukada, Journal of the Society of dyers and colourists, 112, 88-94 (1996).

[6] H. Mori, M. Tsukada, Review in Molecular Biotechnology, 74, 95-103 (2000).

[7] G. Freddi, M. Tsukada, Current Trends in Polymer Science, 5, 53-62 (2000).

[8] M. Tsukada, G. Freddi, M. Nagura, H. Ishikawa, N. Kasai, J. Appl. Polym. Sci, 46, 1945-1953 (1992).

[9] J. He, Y. Qin, S. Cui, Y. Gao, S. Wang, J. Mater. Sci, 46, 2938-2946 (2011).

[10] X. Zhang, M. Tsukada, H. Morikawa, K. Aomima, G. Zhang, M. Miura, Nanoscale Research Letters, 6, 510-517 (2011).

[11] N. Tretinnikov, Y. Tamada, Langmuir, 17, 7406-7413 (2001).

[12] X. Hu, K. Shmelev, L. Sun, E.S. Gil, S.H. Park, P. Cebe, D.L. Kaplan Biomacromolecules, 12, 1686-1696 (2011).

[13] S.H. Tan, R. Inai, M. Kotaki, S. Ramakrishna, Polymer, 46, 6128-6134 (2005).

[14] B. Veleirinho, M.F. Rei, J.A. Lopes-da-Silva, J. Polym. Sci. Part B Polym. Phys., 46, 460-471 (2008).

[15] M. Tsukada, G. Freddi, M. Nagura, H. Ishikawa, N. Kasai, J. Appl. Polym. Sci, 46, 1945-1953 (1992).

[16] A. Theron, E. Zussman, A.L. Yarin, Nanotechnology, 12, 384-390 (2001).

[17] M. Tsukada, M. Nagura, H. Ishikawa, J. Polym. Science: Part B: Polym. Physics, 25, 1325-1329 (1987).

[18] M. Tsukada, J. Polym. Science: Part B: Polym. Physics, 26, 949-952 (1988).

[19] B. Veleirinho, M.F. Rei, J.A. Lopes-da-Silva, J. Polym. Sci. Part B Polym. Phys., 46, 460-471 (2008).

[20] X.H. Zong, K. Kim, D.F. Fang, S.F. Ran, B.S. Hsiao, B. Chu, polymer, 43, 4403-4412 (2002).

[21] X. Hu, K. Shmelev, L. Sun, E.S. Gil, S.H. Park, P. Cebe, D.L. Kaplan, Biomacromolecules, 12, 1686-1696 (2011).

Chapter 5

Preparation and characterization of ultrafine composite SC/TSF fibers

Chapter 5: Preparation and characterization of ultrafine composite SC/TSF fibers

5.0. Introduction

Electrospinning is an effective and inexpensive technique, which can be used to generate polymer nanofibers with diameter ranged from several micrometers down to 2 nanometers, yielding a three-dimensinal nanofibrous membrane of nanoscale fibers bearing high aspect ratio, high-specific surface area and high porosity with small pore size [1]. The three-dimensinal nanofibrous membrane prepared via electrospinning technique are deem as an ideal materials for tissue engineering due to not only imitate the nanoscale dimension of the natural extracellular matrix (ECM) but also take shape an established architecture to direct cell growth and development [2].

Sericin is a class of silk protein contained 18 amino acids including essential amino acids and is characteristical of 32 percent of serine. The hydroxy amino acids in sericin is 45.8 percent. There are 12.2 percent of nonpolar amino acid and and 42.3 percent of polar amino acid residues [3]. Due to these unique amino acid composition and sequence [4], sericin is anticipated to be a promising natural resource giving specific properties for developing novel protein-based materials. But the native SS without decreasing molecular weight can't be obtained from the SS solution acquired from the conventional technique. A great interest have been paid by many gene scientists to prepare novel SS cocoon named sericin-hope cocoon (SC) using genetically modification and diversification of B. mori silkworm [5-6]. The productivity of SC is approximately four times Nd strain, and it generated thin cocoons containing approximately exclusively of 98.5% sericin. Sericin-hope facilitates mass yield of native sericin with high purity. About the usage of Sericin-hope, there have been some researches about hydrogel prepared by chemical modication and so on [7-10].

Tussah silk is produced by A. pernyi. The chemical structure of TSF is rather different from that of B. mori silk fibroin. Compared to B. mori silk, its amino acid is traited by more Ala, Asp, and Arg and less Gly contents. In addition, it is well known

that the presence of the tripeptide sequence Arg-Gly-Asp (RGD) may act as a biological recognition signal, promoting cell adhesion and consequently, make TSF suitable for biomedical application [11]. TSF is a class of wild silk and the chemical structure, molecular conformation as well as physical properties have been extensively studied [12]. Due to the sequential $-(Ala)_n-$ was involved in crystalline region of the TSF fibers, TSF fibers is difficultly dissolved. In our previous work, the smooth and fine SC nanofibers and TSF nanofibers have been fabricated via electrospiinning, respectively [13-15].

In the present study, we attempted to yield the SC/TSF composite nanofibers which has smaller diameters, narrow standard deviation and perfect surfaces with bead-free structures by electrospinning from the SC/TSF blene solution. The function of different weight ratios and the dissolution time on morphological appearance and mean diameter of the as-spun SC/TSF composite nanofibers were examined. The morphology, secondary structure and thermal tests were also analyzed.

5.1. Experiment

5.1.1. Solution preparation

Sericin source was the same as in our previous study [13]. TSF were prepared according to the previous procedures [14]. Different weights of SC layers (0.0, 0.25, 0.50, 0.75, 0.1 g) were added into 0.928g TFA respectively with different TSF (0.1, 0.75, 0.50, 0.25, 0.0 g), the mixtures were stirred in TFA at 40 °C continuously with a magnetic stirrer. Then the spinning solutions with different weight ratios (SC/TSF: 100/0, 75/25, 50/50, 25/75 and 0/100) were prepared.

5.1.2. Electrospinning setup and process

Electrospinning of the solutions was conducted in the air atmosphere. The electrospinning apparatus were composed of syringe (SS-01T, Terumo Corporation, Tokyo, Japan), needle (NN-2238N, Terumo Corporation, Tokyo, Japan), aluminum collecting screen, and syringe pump. The spinning speed of the syringe pump was adjusted in the speed range of 0.003~0.320 cm/min. The high voltage power (Kato

tech company, Japan) was supplied in the voltage range from 0 to 40 kV. The sample solution was placed into the 1 ml syringe, with 21 gauge needle (inner diameter 0.3 mm). All the air is rid of from the needle by hand. Then the 1 ml syringe is fixed in the syringe pump. The high voltage was supplied between the end of the needled and collecting screen. When there was a spinning solution droplet at the tip of the needle, a jet was ejected with the voltage increasing. Then the composite nanofibers were produced on the aluminum collecting screen. The electrospinning was conducted with the working distence, applied voltage and flow rate, 15cm, 25kV, 0.06cm/min, respectively.

5.1.3. Characterization

Scanning electron microscopy (SEM, Hitachi S-3000N, Japan) is served to detect the quality of the electrospun membrane and ensure the diameter of the resulting nanofibers at room temperature. Samples were placed on aluminium circular plate and coated using gold layer to imaging, diameter sizes of the composite nanofibers were acquired from SEM images. The mean diameters and fiber diameter distribution were obtained using a commercial software package, SPSS.

The infrared spectra of samples were measured with a FTIR (FTIR, Prestige-21). Every spectrum of samples was acquired in transmittance mode with a resolution of 4 cm^{-1} and spectral range of 4000-500 cm^{-1}. Infrared spectra were recorded from 16 scans per sample.

DSC curves of samples were monitored with DSC instrument (Thermo Plus DSC 8230, Rigaku Corporation, Japan) under nitrogen atmosphere, at a heating rate of 10 °C/min. Temperature range was from room temperature to 300 °C. The sample weight was about 3 mg.

TG measurement was carried out by TG-DTA instrument (Thermo Plus TG 8120, Rigaku Corporation, Japan) under nitrogen atmosphere in the temperature range from room temperature to 300 °C at heating rate of 10 °C/min. The sample weight was about 6 mg.

5.2. Results and discussion

5.2.1. Morphologies of SC/TSF composite nanofibers

The SC/T composite nanofibers were produced by electrospinning with SC/T blend solution stirred in TFA at 40 °C for 4 days.

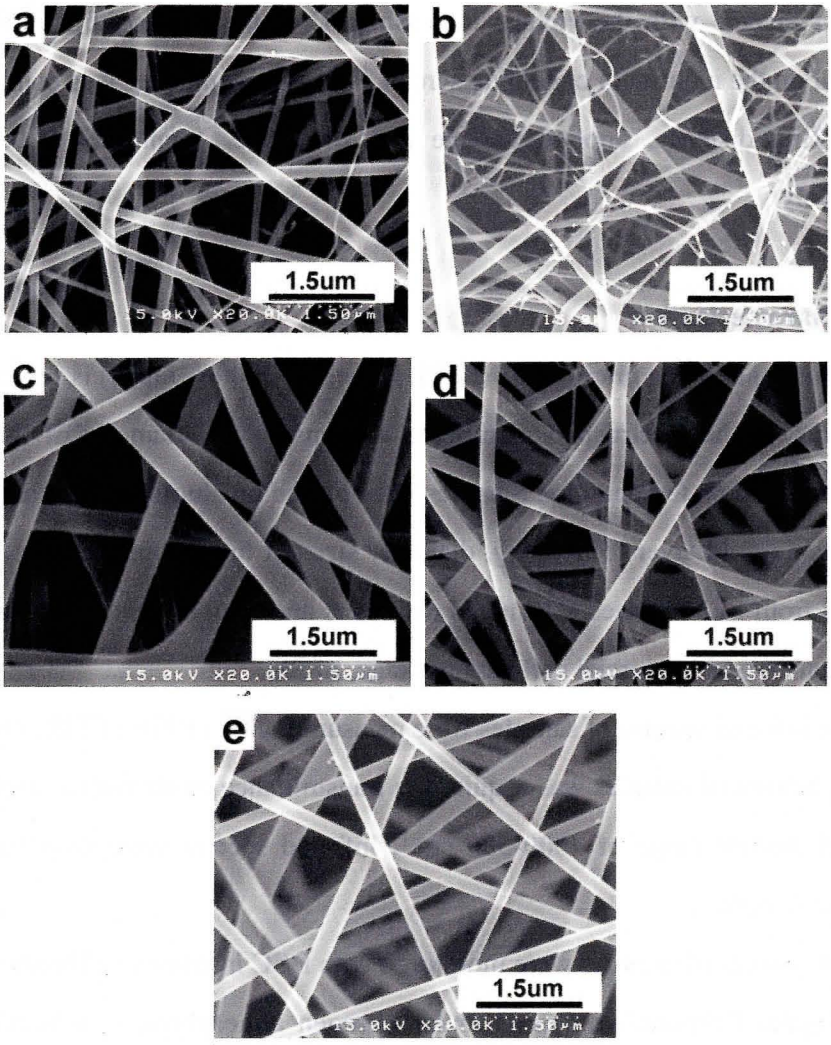

Fig. 5.1 SEM micrographs of the SC/TSF composite nanofibers.
SC/T (w/w): (a) 100/0; (b) 75/25; (c) 50/50; (d) 25/75 and (e) 0/100.

Fig. 5.1 shows SEM micrographs of the SC/TSF composite nanofibers spun from the different composition under the same spinning conditions. In our previous experiments, the smooth and fine pure SC nanofiers have been obtained under different electrospining conditions [13]. In this study, the pure as-spun nanofibers (Fig.

5.1(a)) had a round cross section and smooth surface. He et al. demonstrated that TSF nanofibers present a poor spinnability in electrospinning [16]. The pure TSF nanofibers (Fig. 5.1(e)) showed smooth fibers with few spindle-like beads, and fibers' adhesion and bifurcation were also observed because of the incomplete TFA solvent evaporation and jet split. The SC/TSF (Fig. 5.1(b)) composite nanofibers displayed thick and thin diameter with huge difference, maybe due to the uniformity of the SC/TSF solution. Compared to the SC/TSF (Fig. 5.1(b)) composite nanofibers, the SC/TSF (Fig. 5.1(b) and (c)) composite nanofibers presented more uniformal and better surfaces.

5.2.2. Distribution of SC/TSF composite nanofibers

To clarify the founction of weight ratios in more details, we tried to examine the diameter distribution of SC/TSF composite nanofibers.

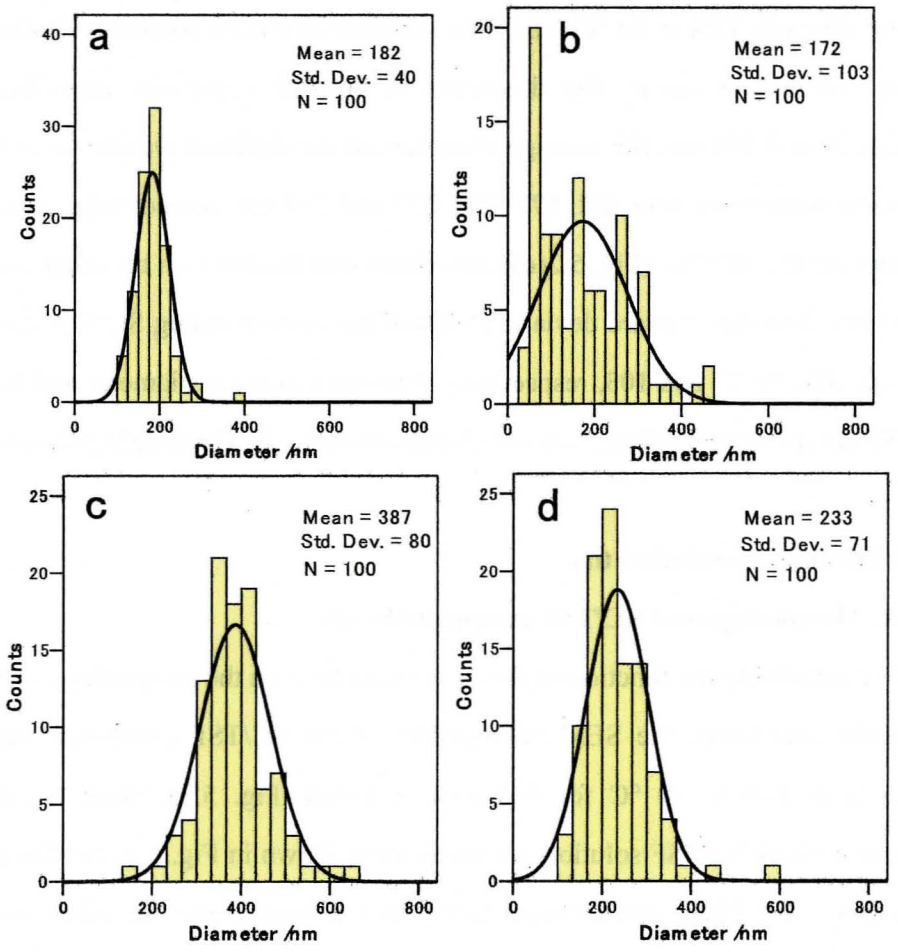

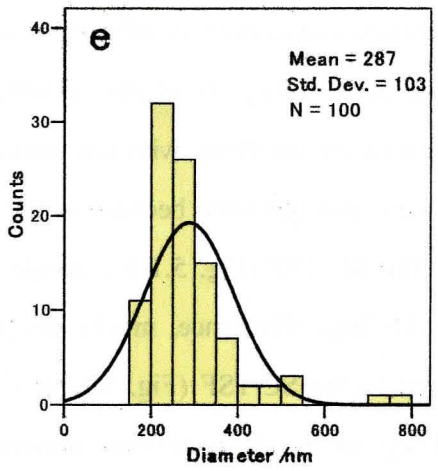

Fig. 5.2 Average diameters and SD of SC/TSF composite nanofibers. SC/TSF(wt/wt): (a) 100/0; (b) 75/25; (c) 50/50; (d) 25/75 and (e) 0/100.

Fig. 5.2 shows the diameter distributions of SC/TSF composite nanofibers obtained from the SC/TSF TFA solution, and these were prepared by dissolving SC/TSF fibers in TFA at 40 °C. The fiber diameters for each proportion followed the normal distribution curve. The diameters of SC/TSF composite nanofibers were between 36 and 768 nm, the average diameters of the different weight ratios SC/TSF composite nanofibers were 182, 172, 387, 233 and 287 nm, respectively. The average diameters of the SC/TSF (Fig. 5.2(c)) nanofibers was thicker than the other composite nanofibers. And the standard deviation (SD) of the corresponding SC/TSF nanofibers were 40, 103, 80, 71 and 103, respectively. The trend of mean diameter and SD of the SC/TSF composite nanofibers was not directly related with the weight proportion.

5.2.3. Effect on dissolution time

5.2.3.1. Morphologies of SC/TSF composite beads

For examining the function of the dissolution time on the morphology of SC/TSF composite nanofibers, the SEM micrographs of the SC/TSF composite nanofibers dissolved in TFA at 40 °C for 15d were detected (Fig. 5.3). From the different proportion blend SC/TSF solution, all beads were shown in Fig. 5.3. For the pure SC beads (Fig. 3a), There are half-ball holes on the beads; and the other composite particles (Fig. 3b, c, d and e), all circular beads and no half-ball holes on them were

obtained.

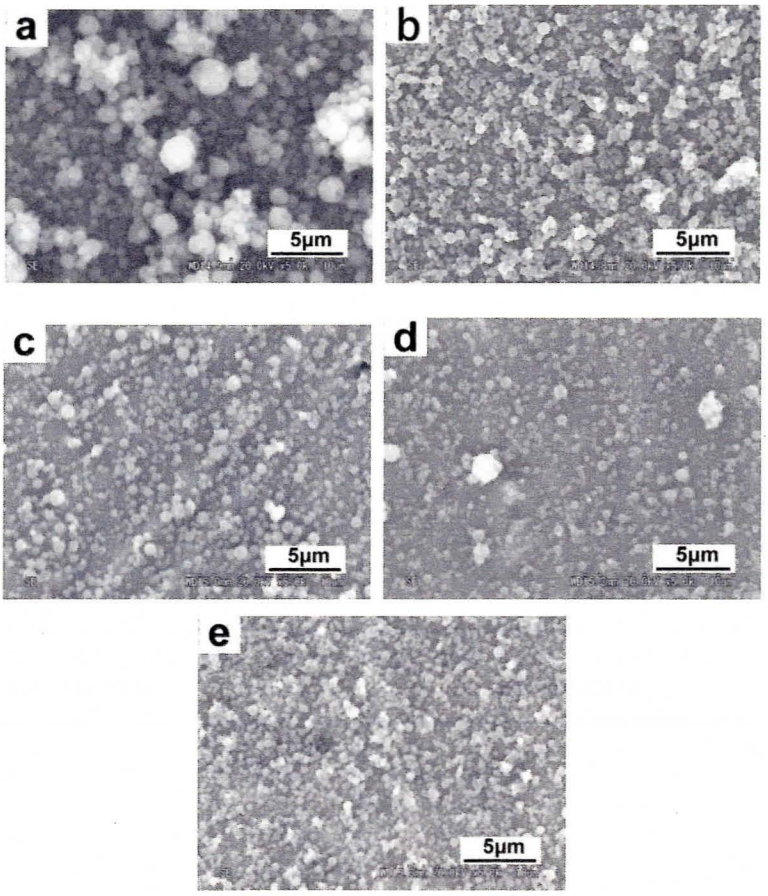

Fig. 5.3 SEM micrograph of the SC/TSF composite nanofibers, prepared by dissolving the blend SC/TSF fibers at 40 °C in TFA for 15d. SC/T (w/w): (a) 100/0; (b) 75/25; (c) 50/50; (d) 25/75 and (e) 0/100.

5.2.3.2. Diameter distribution of SC/TSF composite beads

Fig. 5.4 shows diameter distributions of the electrospun SC/TSF composite mats obtained by electrospinning with different corporation SC/TSF TFA solution. The SC/TSF composite mats changed from smooth nanofibers from beaded structures as dissolving time was prolonged to 15 d. The diameters of the SC/TSF composite nanofibers were between 72 and 2490 nm, The average diameters of the pure SC hole beads was 586 nm, and SD was 33 (Fig. 5.4(a)). The average diameters of the different weight proportion SC/TSF (Fig. 5.4(b), (c), (d) and (e)) composite circular particles were 348, 433, 360 and 356 nm, respectively. And SD of the SC/TSF

particles (Fig. 5.4(b), (c), (d) and (e)) were 155, 204, 165, and 142, respectively. The trend of mean diameter and SD of the SC/TSF composite particles was not directly related with the weight proportion.

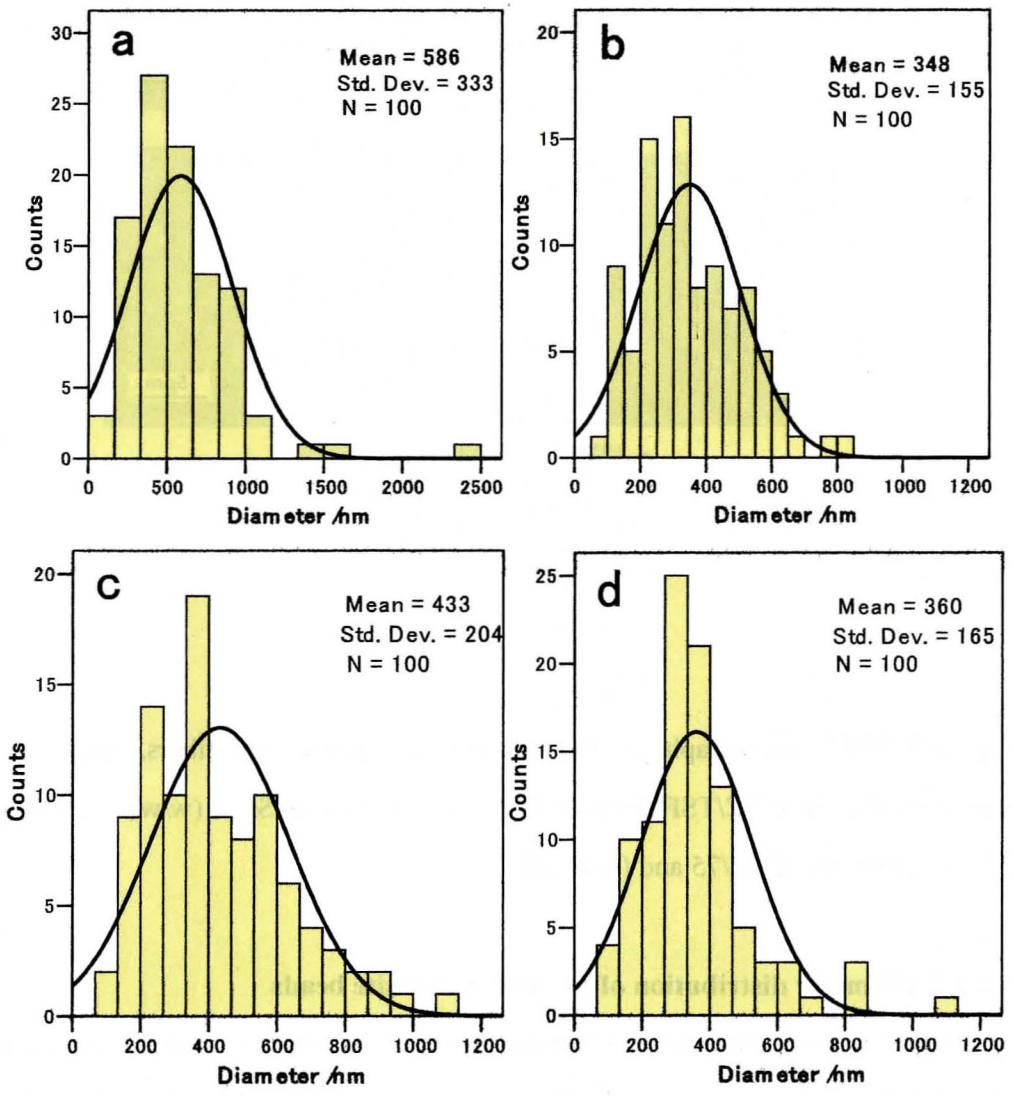

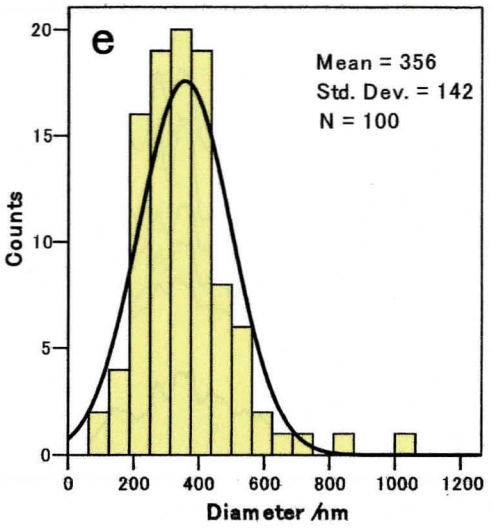

Fig. 5.4 Average diameters and SD of the SC/TSF composite nanofibers spun from the SC/TSF TFA solution, prepared by dissolving the SC/TSF fibers at 40 °C in TFA for 15d. SC/TSF (wt/wt): (a) 100/0; (b) 75/25; (c) 50/50; (d) 25/75 and (e) 0/100.

5.2.4. Structural features of SC/T composite nanofibers

FTIR spectroscopy is a common and powerful measurement for detecting the molecular conformation of silk protein due to the typical absorption bands sensitive to the molecular structure of silk protein. The similar absorption peaks were displayed in the IR spectra of six SC/TSF composite nanofibers (Fig. 5.5). The absorption bands of SC/TSF composite nanofibers were characterized approximately at 1647 cm^{-1} (amide I) attributed to the random coil conformation. The SC/TSF (100/0 and 75/25) composite nanofibers showed absorption peak at around 1527 cm^{-1} (amide II) assigned to the random coil conformation, while SC/TSF (50/50, 25/75, 0/100 and heated 50/50) composite nanofibers displayed at 1538 and 1517 cm^{-1} (amide II), attributed to the random coil and β-sheet structure. However, the intensity of the absorption peak at around 1517 cm^{-1} in the SC/TSF (0/100 and heated 50/50) composite nanofibers was stronger than the corresponding absorption peak in the SC/TSF (50/50 and 25/75) composite nanofibers.

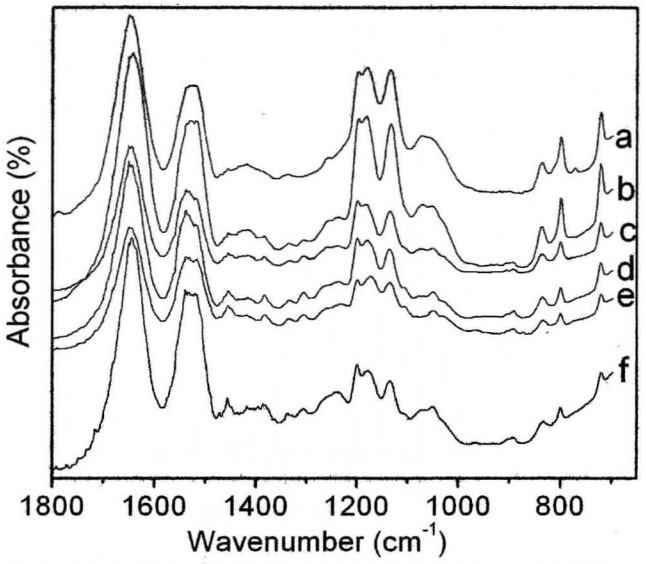

Fig. 5.5 FTIR-ATR spectra of SC/TSF composite nanofibers and heated SC/TSF (50/50) composite nanofibers. SC/TSF (wt/wt): a100/0, b 75/25, c 50/50, d 25/75, e 0/100 and f SC/TSF (50/50) composite nanofibers, heat treated at 160 °C for 1 hr.

All SC/TSF composite nanofibers had the absorption bands around 1200, 1186, 1050, 839, 800 and 724 cm^{-1}. For these absorption bands, SC/TSF composite nanofibers showed absorption band characteristics of both SC and TSF pure components overlapping in the corresponding absorption region. The intensity of these absorption bands decreased with decreasing TSF content. The SC/TSF (100/0, 75/25 and 50/50) composite nanofibers possessed a minor absorption band at 1071 cm^{-1}, however, this peak was disappeared in the SC/TSF (25/75 and 0/100) composite nanofibers'spectra (Fig. 5.5d,e). Around 1200, 1186, 1050, and 724 cm^{-1}, the intensity of these absorption peaks of the heated SC/TSF (50/50) composite nanofibers (Fig. 5.5f), became minor compared with those of the SC/TSF (50/50) composite nanofibers (Fig. 5.5c).

5.2.5. Thermal behavior

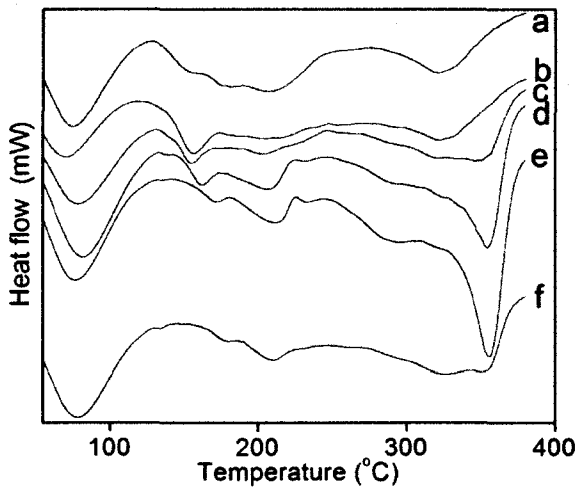

Fig. 5.6 DSC curves of SC/TSF composite nanofibers and the heated SC/TSF (50/50) composite nanofibers. Sample abbreviation was the same in Fig. 5.5

DSC measurements were conducted to analyze the thermal behavior of SC/TSF composite nanofibers. The DSC curves of SC/TSF composite nanofibers and the heated SC/TSF (50/50) composite nanofibers was showed in Fig. 5.6. All the samples (a-f) presented endothermic peaks approximately at 80 °C, maybe attributed to the evaporation of water or solvent remaining in composite nanofibers. Electrospun pure SC nanofibers displayed a broad complex endothermic peak from 150 to 216 °C and an apparent peak at about 320 °C (fig. 5.6a), while SC/T (75/25) composite nanofibers showed an obvious endothermic peak at around 156 °C and a broad endothermic peak at 207 °C. As increasing TSF content, the endothermic peak intensity at around 156 °C decreased, and the endothermic peak intensity at 207 °C increased and this peak became sharper. After the endothermic peak at 250 °C, the pure TSF nanofibers exhibited a weak peak at around 290 °C and a sharp peak at around 355 °C, while pure SC nanofibers displayed one peak at about 320 °C. For the peaks at around 320 and 355 °C, the composite nanofibers had the two decomposition peaks corresponding to pure SC and TSF.

The decomposition peak at around 154 °C in SC/TSF (50/50) composite nanofibers shifted to 178 °C in heated SC/TSF (50/50) composite nanofibers and the intensity decreased, it is assumed that certain amount of TFA presents in SC/TSF

composite nanofibers and this small amount of TFA has been removed by the heat treatment at 160 °C for 1 hr.

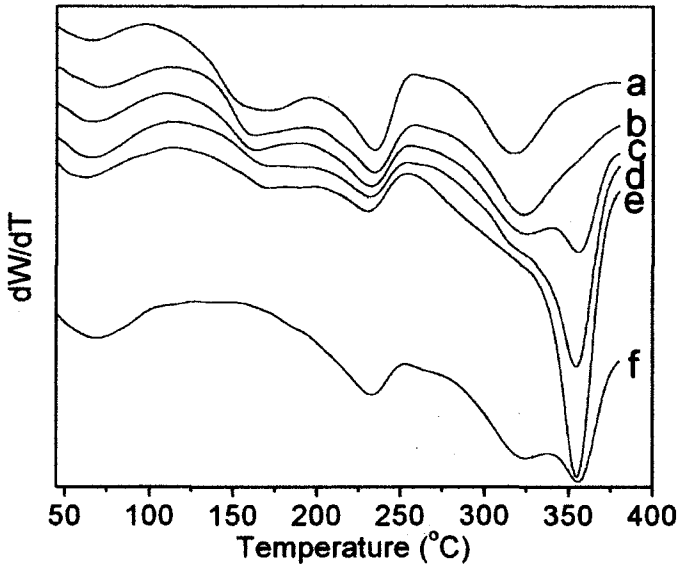

Fig. 5.7 DTG curves of SC/TSF composite nanofibers and the heated SC/TSF (50/50) blend nanofibers. Sample abbreviation in the same in Fig. 5.5.

The DTG patterns of electrospun SC/TSF composite nanofibers were shown in Fig. 5.7. Obviously, at the first peak between 60 and 100 °C in these DTG curves, the weight loss was probably due to water or solvent evaporation. Electrospun pure SC fibers presented a broad decomposition peaks at 161 °C and two obvious decomposition peaks 234 and 316 °C, while pure TSF exhibited three major decomposition peaks at 168, 231 and 354 °C. The broad decomposition peak at around 161 °C of SC nanofibers, which decreased at peak intensity but shifted to higher temperature with the increase of TSF content. As increasing the temperature to 234 °C, the decomposition peak decreased at peak intensity and shifted to lower temperature with the increase of TSF content. At the last decomposition peak at around 316 °C (pure SC) and 354 °C (pure TSF), the blend nanofibers had the two decomposition peaks corresponding to pure SC and TSF. It desmostrated that SC and TSF can not form co-crystal structure and the two crystal region coexisted in composite nanofibers.

The decomposition peak at around 163 °C in SC/TSF (50/50) composite nanofibers disappeared in the heated SC/TSF (50/50) composite nanofibers, it is assumed that certain amount of TFA presents in SC/TSF composite nanofibers and this small amount of TFA has been removed by the heat treatment at 160 °C for 1 hr.

5.3. Conclusions

In this chapter, the SC and TSF dissolved in TFA were electrospun into nanofibers with the blend ratios of 100/0, 75/25, 50/50, 25/75 and 0/100. The average diameter of as spun composite fibers varied from 172 to 387 nm at the different blend ratios. In the as-spun fibers, SC/TSF (100/0 and 75/25) composite fibers was present in random coil conformation, and the random coil and β-sheet structure co-exist in SC/TSF (50/50, 25/75 and 0/100) composite fibers.

Reference

[1] S.S. Ojha, D.R. Stevens, T.J. Hoffman, K. Stano, R. Klossner, M.C. Scott, W. Krayse, L.I. Clarke, R.E. Gorga, Biomacromolecules, 9, 2523-2529 (2008).

[2] W.J. Li, C.T. Laurencin, E.J. Caterson, R.S. Tuan, F.K. Ko, J Biomed Mater Res, 60, 613-621 (2002).

[3] J.T.B. SHAW, S.G. SMITH, nature, 4278, 745 (1951).

[4] R. Voegeli, J. Meier, R. Blust, R. Hofsteter, Cosmetics & Toiletries, 108, 101-108 (1993).

[5] K. Mase, E. Okada, T. Miyazima, T. Yamamoto, Bio Industry, 24(11), 53-59 (2007).

[6] K. Mase, T. Lizuka, E. Okada, T. Miyajima, T. Yamamoto, Journal of Insect Biotechnology and Sericology, 75, 85-88 (2006).

[7] H. Teramoto, K. Nakajima, C. Takabayashi, Biomacromolecules, 5, 1392-1398 (2004).

[8] H. Teramoto, A. Kakazu, K. Yamauchi, T. Asakura, Biomacromolecules, 40, 1562-1569 (2007).

[9] H. Teramoto, T. Kameda, Y. Tamada, Biosci. Biotechnol. Biochem., 72(12), 3189-3196 (2008).

[10] H. Teramoto, K. Nakajima, C. Takabayashi, Biosci. Biotechnol. Biochem., 69(4), 845-847 (2005).

[11] M.D. Pierschbacher, E. Ruoslahti, Nature, 309, 30-33 (1984).

[12] G. Freddi, M. Tsukada, Current Trends in Polymer Science, 5, 53-62 (2000).

[13] X. Zhang, M.R. Khan, T. Yamamoto, M. Tsukada, H. Morikawa, International Journal of Biological Macromolecules, 50, 337-347 (2012).

[14] X. Zhang, K. Aojima, M. Miura, M. Tsukada, H. Morikawa, J. Silk Sci. Tech. Jpn., 20, 61-67 (2012).

[15] X. Zhang, K. Aojima, M. Tsukada, H. Morikawa, J. Silk Sci. Tech. Jpn., 20, 69-76 (2012).

[16] J. He, Y. Qin, S. Cui, Y. Gao, S. Wang, J Mater Sci, 46, 2938-2946 (2011).

Chapter 6

Conclusions

Chapter 6: Conclusions

The dissertation has investigated the characteristic and preparation of silk protein nanofibers from different origins of silkworms and their physical properties.

In chapter 1, I reviewed references and provided brief summary of electrospinning technology and the properties of SS and TSF.

In chapter 2, silk sericin powder was obtained from the raw silk fiber of B. mori silkworm. The solution was prepared by dissolving silk sericin powder in water at 85 °C for 30 minutes. In the electrospinning process, voltage 20 kV was applied and the inner diameter of the syringe needle was 0.3 mm. The distance from the syringe tip to the target was 15 cm. The SS nanofibers with smooth surfaces can not be produced at 40 wt%. However, fine nanofibers were produced at the concentrations of 50 wt% and 60 wt%. It was suggested that the average diameters of the nanofibers increased with increasing solution concentration and the optimum concentration was 50 wt% for best nanofibers. TFA as the solvent, all beads were acquired from electrospinning 1.3 to 8.5 wt% of SS solution; Beaded fibers were produced from 9.6, 11.7, 14.2 and 16.5 wt% of SS solution; And perfect nanofibers were fabricated from 20.9 and 22.9 wt% of SS solution. The average diameter of nanofibers are 145 and 184 nm, respectively. Results from Fourier Transform Infrared (FTIR) showed that the conformation of SS nanofibers changed from β-sheet to random coil and the structure of heated SS nanofibers was β-sheet. Differential Thermal Analysis (DSC) and Thermogravimetry (TG) illustrated that TFA can be mostly eliminated by heating. These results suggested that SS nanofibers are quite promising as a basis for possible future biomaterials.

In chapter 3, SC nanofibers from sericin hope-silkworm, whose cocoons consist almost exclusively of sericin were successfully prepared by electrospinning method. Scanning electron microscopy (SEM) was used to observe the morphology of the fibers. The effect of spinning conditions, including the concentration of SC solution, acceleration voltage, spinning distance and flow rate on the fiber morphologies and the size distribution of SC nanofibers were examined. The structure and physical

properties were also observed by FTIR, DSC and TG. The optimum conditions for producing finely thinner fibrous SC nanofibers without beads were the concentration of SC solution above 6–8 wt%, acceleration voltage ranging from 25 to 32 kV, spinning distance above 9 cm, and flow rate above 0.06 cm min^{-1}. The mean diameter of as spun SC fibers varied from 114 to 430 nm at the different spinning conditions. The as-spun fibers was present in a random coil conformation, while after methanol treatment, the molecular structure of SC nanofibers was transformed into a β-sheet containing structure. SC nanofibers demonstrated thermal degradation at lower temperature than SC, which probably due to the randomly coiled rich structure of the SC nanofibers.

In chapter 4, tussah silk fibroin (TSF) nanofibers from the A. pernyi silkworm were successfully produced by electrospinning from a TSF TFA solution. The optimum concentration for the production of very thin and smooth surfaced TSF nanofibers ranged from 10 wt% to 12 wt%. The average diameter of TSF nanofibers spun from 10 wt% TSF TFA solutions and prepared by dissolving TSF fibers at 25 °C was 688±178 nm; that at 40 °C was 287±103 nm. The average diameters of the TSF nanofibers spun from 12 wt% TSF TFA solutions and prepared by dissolving fibers 25 °C was 686±185nm; that at 40 °C was 380±102 nm. In both cases the mean diameters of the TSF nanofibers differed significantly ($P<0.01$) between the two preparation temperatures. We used SEM, FTIR, DSC and TG to examine the physical properties of TSF nanofibers. TSF nanofibers spun from the TSF TFA solution possessed an α-helix and random coil conformations, and did not take on a β-sheet structure. The TSF nanofibers showed specific FTIR absorption bands at 1199, 1175, 1135, and 1049 cm^{-1}, presumably because of the trace of TFA present in the sample nanofibers at a molecular level. TSF nanofibers showed no clear molecular structural changes upon heat treatment at around 160 °C for 1 h. however, methanol/water vapor annealing crystallized the TSF nanofibers, which clearly changed from randomly coiled conformation to a β-sheet structure. A minor endothermic peak around 172 °C on the DSC curve for the TSF nanofibers is attributable to the removal of TFA from the nanofibers; this peak disappeared after heat-treatment at 160 °C for 1 h.

In chapter 5, the SC/TSF composite nanofibers from the sericin-hope silkworm and A. pernyi silkworm, respectively, with different blend ratios were produced via electrospinning with TFA as the solvent. The morphology, secondary structure and thermal tests of the fibers were detected using SEM, FTIR, DSC and TG. The diameters of the different weight ratios SC/TSF composite nanofibers were between 36 and 768 nm, and the average diameters were 182, 172, 387, 233 and 287 nm, respectively. The trend of mean diameter and the standard deviation (SD) of SC/TSF composite nanofibers was not directly related with the weight proportion. Electrospun SC/TSF composite mats changed from smooth nanofibers to beaded structures as dissolving time was prolonged to 15 d. In the as-spun fibers, SC/TSF (100/0 and 75/25) composite fibers was present in random coil conformation, and the random coil and β-sheet structure co-exist in SC/TSF (50/50, 25/75 and 0/100) composite fibers.

List of publications

1. **Xianhua Zhang**, Md. Majibur Rahman Khan, Toshio Yamamoto, Masuhiro Tsukada and Hideaki Morikawa; Fabrication of silk sericin nanofibers from a silk sericin-hope cocoon with Electrospinning method. International Journal of Biological Macromolecules; Vol.50, pp.337-347, 2012.

2.**Xianhua Zhang**, Kazuki Aojima, Mikihiko Miura, Masuhiro Tsukada and Hideaki Morikawa; Fabrication of electrospun Tussah silk fibroin nanofibers; Nippon Silk Gakkaishi, J. Silk Sci. Tech. Jpn. Vol.20, pp.61-67, 2012.

3. **Xianhua Zhang**, Kazuki Aojima, Masuhiro Tsukada and Hideaki Morikawa; Physical properties of electrospun Tussah silk fibroin nanofibers; Nippon Silk Gakkaishi, J. Silk Sci. Tech. Jpn. Vol.20, pp.69-76, 2012.

4. **Xianhua Zhang**, Masuhiro Tsukada, Hideaki Morikawa, Kazuki Aojima, Guangyu Zhang and Mikihiko Miura; Production of silk sericin/silk fibroin blend nanofibers; Nanoscale Research Letters; Vol.6, pp.510(1-8), 2011.

Acknowledgments

It is my pleasure to write this message and express my gratitude to all those who have directly or indirectly contributed to the creation of this thesis. First of all I would like to thank my supervisor Prof. Hideaki Morikawa and vice-supervisor Prof. Masuhiro Tsukada and Mikihiko Miura for giving me the opportunity to study in this group and for always keeping me motivated and supporting me with a lot of useful advice.

I would like to express my sincere thanks to Global COE of Shinshu University for financial support.

I thank Mr. Mitsuo Ueno, Ms. Miho Nakamura, and Ms. Etsuko Adachi in Shinshu University for sharing their extensive knowledge of experimental equipment and offering their guidance, and valuable insight to my study.

Thanks also go to my group mats (Mr. Guangyu Zhang, Mr. Yuji Satoh, Ms. Mariko Yamaguchi, Mr. Kazuki Aojima, Mr. Noriyoshi Oka, Mr. Yuki Kishimoto) of their general advice and input on various things related to research, as well as things not related.

Special thanks to Prof. Baoqi Zuo, and Dr. Feng Zhang at Soochow University (Suzhou, Jiangsu).

I also want to express my thanks to the oversea students Ms. Chunxia Gao, Mr. Qiang Gao, Mr. Jinxing Shi, Mr. Yi Wang, Mr. Yaofeng Zhu, and Ms. Xiaowen Lei et al., who gave me many different helps and encourage me to finish this work in my depressed periods.

Finally, I dedicate this work to my family; I am grateful for being able to say that I have a great family that has always set a good example and provide me with unlimited support.